GEOLOGICAL SURVEY OF FINLAND

Guide 53

2007

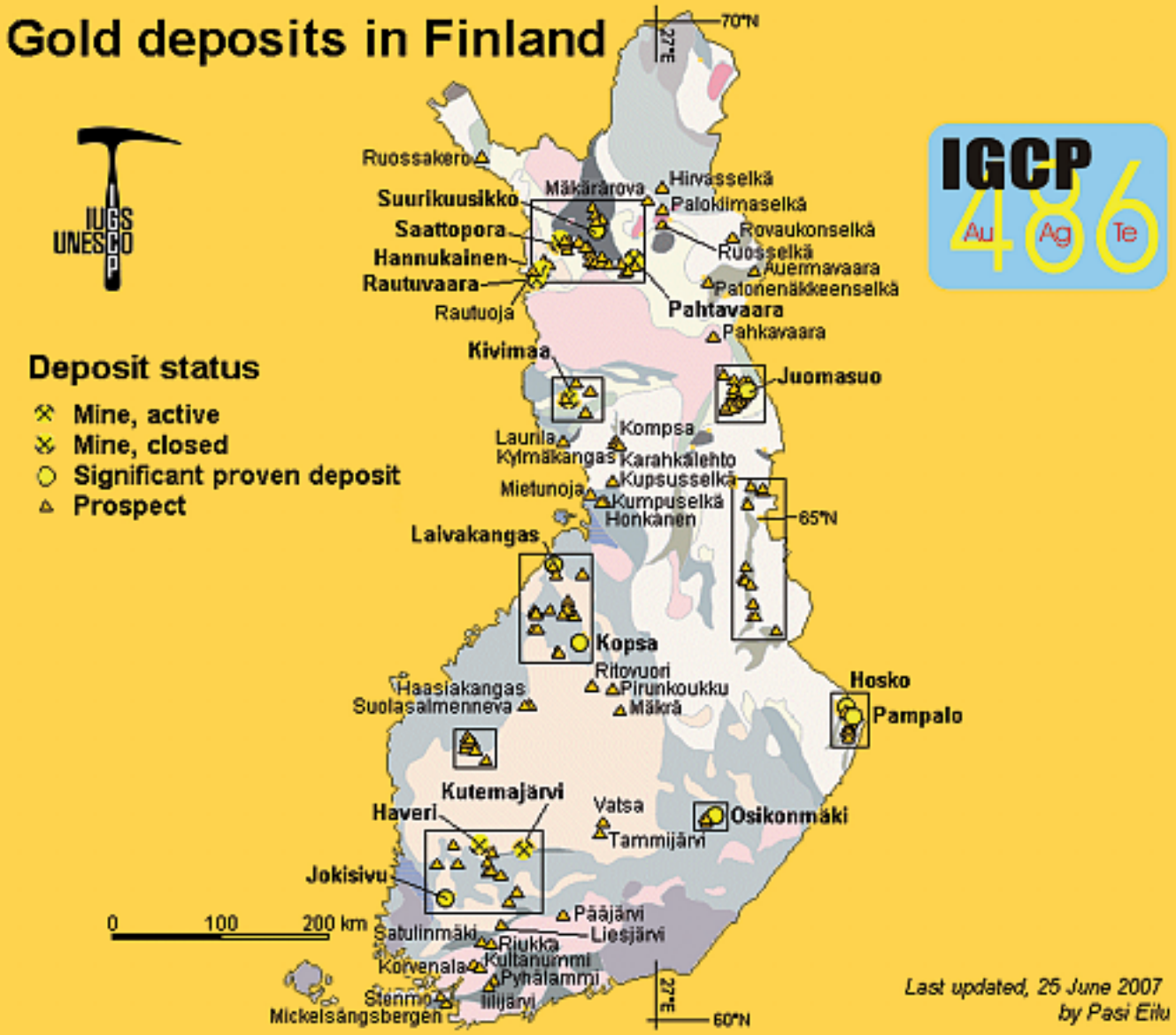

http://en.gtk.fi/ExplorationFinland/Commodities/Gold/gtk_gold_map.html

Au-Ag telluride-selenide deposits
Field Workshop Espoo, Finland, August 26-31, 2007

GTK

Kari K. Kojonen, Nigel J. Cook & V. Juhani Ojala (eds.)

GEOLOGIAN TUTKIMUSKESKUS **GEOLOGICAL SURVEY OF FINLAND**

Opas 53 Guide 53

Au-Ag telluride-selenide deposits

Field Workshop of IGCP-486, Espoo, Finland
26-31st August 2007

Proceedings volume

Edited by

Kari K. Kojonen, Nigel J. Cook and V. Juhani Ojala

Espoo 2007

Field Workshop of IGCP-486, Espoo, Finland
26-31st August 2007

Kojonen, Kari, K., Cook, Nigel, J. & Ojala, V. Juhani (ed.) 2007: Au-Ag telluride-selenide deposits. *Geological Survey of Finland, Guide 53*. 94 pages, 62 figures and 14 tables.

Proceedings volume

This volume contains papers presented during the IGCP-486 Field Workshop at Geological Survey of Finland, August 30-31, 2007, in Espoo, Finland. The workshop consisted of three days of field excursions to Au-Ag-Te-Se ore deposits and mines in southwestern Finland and two days of scientific sessions at GTK.

International Geoscience Project 486 focuses on studies of all types of Au-Ag-telluride-selenide mineralizations and their ore deposits and attempts to bridge the gap between scientists working in the laboratory and those working in the field from the microscopic- to orogen-scales. During the project we have aimed to understand geological processes causing accumulations of Au (± Ag) with Te and Se over space and time, the mineralogy of these deposits and the internal and external controls on metal and mineral distributions. Comparison and analogy between productive and potential regions in Europe, Asia and other continents has had an important role in the project.

The present field workshop is the fourth organized annually since the project started. The present volume contains a total of 13 extended abstracts describing the mode of occurrence, ore mineralogy, structural geology and geochemistry of Au-Ag deposits from 12 countries in Europe, Australia, North America and Japan.

The first two papers, by **Ciobanu et al.** are experimental studies made on Musariu Au-Ag telluride ore, Romania and the Oya gold deposit in Japan. The authors have used melting experiments and LA-ICP-MS analysis to define the trace gold contents in tellurobismuthite. The results indicate higher temperature ranges as previously reported formation temperatures from fluid inclusions, causing the authors to propose that the assemblages reflect eutectic cooling paths in the systems Au-Bi-Te and Au-Pb-Te, respectively.

LA-ICP-MS analytical techniques have been also used in the paper of **Cook et al.** to define the trace the Au contents in Bi-chalcogenides from Au-Ag telluride deposits in Finland, Sweden and Norway. The results suggest that Bi-chalcogenides may, in some instances, be considered as gold carriers and could contain gold at comparable concentrations as pyrite. A similar approach has been made by **Cook et al.** in a second paper, in which measurements have been made on Bi-(sulpho)tellurides from the CLY Group gold prospect, B.C., Canada. Preserved textures in the ores are interpreted to reflect a primary Au-Bi-Te assemblage that may have been deposited in the molten state and overprinting during a later orogenic episode that led to significant recrystallization and redistribution of gold.

The paper by **Dimitrova et al.** describes minerals of the tennantite-tetrahedrite and polybasite-pearceite series from the Chiprovtsi Ag-Pb deposit in Bulgaria. The paper also includes a fluid inclusion study of the quartz crystals. The fahlores contain high Ag contents in their crystal structures. The fluid inclusion studies point to formation temperatures of 160-170ºC, but the primary fahlores are considered to have formed at 200-250ºC. Formation mechanisms for the tennantite-tetrahedrite series are highly relevant to the project since the mineral group may incorporate Te, and is not uncommonly associated with tellurides.

Howard describes the geological setting, geochemistry and excellent economic potential of the CLY Group prospect, southeastern British Colombia, Canada, in which gold is tied paragenetically to a range of

Bi-tellurides and sulphotellurides. The base-metal poor mineralization has the characteristics of a reduced intrusion-related gold (RIRG) deposit and can readily be compared with other RIRG systems, notably in the Tintina Belt, of Alaska-Yukon.
In their paper, **Ivashchenko et al.** describe Au-Ag-Bi-Se-Te vein mineralization at Roikonkoski, Karelia. A total of 41 ore minerals have been discovered from the quartz-carbonate veins, 14 of which are tellurides. The ore mineralization has formed in the temperature range 550- <170ºC concluded from the ore mineral paragenesis and the published experimental results. The deposit is considered as either xenothermal or orogenic mesothermal.

Kesler at al. have analyzed trace Se and Te in arsenian pyrite from Carlin type and low-sulphidation type epithermal deposits. The strongest correlations observed are between Te and both Au and Ag in Carlin type deposits, and between Te and Ag in epithermal deposits; correlations of Au and Ag with Se are uniformly poor. The results suggest that Se complexes are not present and that Te complexes are of secondary importance as agents of metal transport.

Kojonen describes the Au-Ag tellurides and selenides systematically and has collected data about their diagnostic features. Both tellurides and selenides are often very difficult to identify, and electron probe microanalysis is ultimately needed to confirm their correct identification.

Sparks et al. have studied sulphide melts experimentally by heating ore samples up to 820ºC. They noticed that the melt already appears at 500ºC in many cases. During differentiation, Sb, As, Ag, and Au become enriched and Zn, Pb and S depleted. The experiments were made on samples from Broken Hill, NSW, Australia, but the authors consider that the results are applicable to all polymetallic deposits with high temperature or high metamorphic grade, with implications for telluride-bearing deposits in equivalent terranes.

Talikka describes the volcano-sedimentary Tampere Belt, Finland, which consists mainly of turbiditic sedimentary rocks, volcanic rocks of island-arc type and synorogenic granitoids. The range of isotopic ages of the volcanic rocks and the synorogenic granitoids is ca. 25 Ma, and the main regional metamorphic and deformational phase lasted ca. 10 Ma. Accordingly, the tectonic evolution of the Tampere Belt during the Svecofennian orogeny has been a rapid, continuous process. The Kutemajärvi area is located in the northern flank of the TB and is in contact with the subvolcanic Pukala intrusion, which was emplaced within the metavolcanic rocks before or during the early stages of the Svecofennian orogeny. The Kutemajärvi hydrothermally-altered domain hosts an economic gold deposit. It is suggested that magmatic fluids from the Pukala intrusion caused the pervasive alteration including sericitisation and silicification observed at Kutemajärvi. The pervasive alteration preceded the main regional deformation and metamorphic processes that led to changes in geometry and mineralogy of the gold deposit.

Voudoris at al. describe the Perama Hill Au-Ag telluride quartz-barite base metal veins deposit, Greece, which has overprinted an earlier pyrite-enargite-bearing mineralization hosted in an advanced argillic altered andesitic breccia. Tellurides were deposited from intermediate-high sulphidation fluids under $\log f S_2$ values between -9.7 and -11.2 and at $\log f Te_2$ values between -7.3 and 10.5 (at 275ºC). The authors suggest that the Perama Hill deposit was developed at the transition between a shallow submarine to subaerial environment, showing thus considerable similarities with mineralization in the western part of Milos Island.

In a second paper, **Voudoris at al.** have studied the telluride- and bismuth-sulphosalt-bearing gold deposits of Greece. The deposits studied can be sub-divided into three groups based on their association with gold: (a) deposits which lack tellurides but include Bi-sulphosalts and native gold; (b) the second category includes mineralization where Bi-tellurides of reduced-type (joséite-A, joséite-B, pilsenite, where Bi:X>1, X=Te,S,Se), accompanied by Bi-sulphosalts, native bismuth and native gold, (c) the third category includes deposits/prospects where Au-Ag-tellurides are abundant but Bi-tellurides and Bi-sulphosalts are absent.

Key words: gold ores, silver ores, mineralogy, tellurides, selenides, geochemistry, IGCP-486, symposia

Kari K. Kojonen
Geological Survey of Finland
PL 96
FIN-02151 ESPOO, FNLAND
E-mail: kari.kojonen@gtk.fi

ISBN 978-952-217-002-6
ISSN 0781-643X

CONTENTS

Preface

ABSTRACTS

(Au)-Pb-Te melts: Annealing-Quenching experiments on Samples from the Musariu deposit, Brad district, Romania
Cristiana L. CIOBANU, Nigel J. COOK, John MAVROGENES, Gheorghe DAMIAN and Florica DAMIAN.....5

Au-Bi-Te melts: Annealing-quenching experiments on material from the Oya gold deposit (Japan)
Cristiana L. CIOBANU, John MAVROGENES, Nigel J. COOK, Masaaki SHIMIZU.....15

LA-ICP-MS determination of gold in Bi-chalcogenides from four deposits in the Fennoscandian Shield
Nigel J. COOK, Cristiana L. CIOBANU, Leonid DANUSHEVSKIY, CODES 23

Bi-tellurides in gold veins, BiTel Knoll (CLY prospect), southeastern British Columbia, Canada
Nigel J. COOK, Cristiana L. CIOBANU, William R. HOWARD.....31

Compositional variations in the tetrahedrite-tennantite fahlores and polybasite-pearceite series from the Chiprovtsi Ag-Pb deposit, northwestern Bulgaria
Dimitrina DIMITROVA, Thomas KERESTEDJIAN, Maria PETROVA, Tsvetoslav ILIEEV 39

Structural setting and geochemical correlations in bismuth (sulfo) telluride - native gold–bearing veins, Cly group, British Columbia, Canada: A reduced intrusion-related gold system
William (Bill) R. HOWARD.....45

Au-Ag-Bi-Te-Se vein mineralization at Roikonkoski, Karelia, northern Lake Ladoga region
V.I. IVASHCHENKO, O.B. LAVROV, K. SUNDBLAD, A.N. TORITSIN.....51

Geochemistry of Se and Te in arsenian pyrite: new evidence for the role of Se and Te hydrothermal complexes in Carlin and epithermal-type deposits
Stephen E. KESLER· Artur P. DEDITIUS, Stephen CHRYSSOULIS 57

Au-Ag telluride-selenide minerals and their diagnostic features
Kari K. KOJONEN 61

The secret lives of immiscible metal-rich melts: two liquid immiscibility in the sulfide-antimony system
Heather A. SPARKS, John A. MAVROGENES, B. Ron FROST 65

Tectonic evolution of the Paleoprotezoic Tampere Belt during the Svecofennian orogeny, with reference to hydrothermal alteration at Kutemajärvi
Matti TALIKKA.....71

Gold-silver tellurides and bismuth sulfosalts in the high-intermediate sulfidation Perama Hill deposit, western Thrace (NE Greece)
Panagiotis VOUDOURIS, Constantinos PAPAVASSILIOU, Dimitrios, George FALALAKIS 77

Tellurides and bismuth sulfosalts in gold occurrences of Greece: mineralogical and genetic considerations
P. VOUDOURIS, P.G. SPRY, V. MELFOS, D. ALFIERIS 85

(Au)-Pb-Te melts: Annealing-Quenching experiments on Samples from the Musariu deposit, Brad district, Romania

Cristiana L. CIOBANU, Mineralogy Group, South Australian Museum, North Terrace, Adelaide, S.A., 5000 Australia, and Department of Earth and Environmental Sciences, University of Adelaide, S.A., 5005, Australia

Nigel J. COOK, Natural History Museum, University of Oslo, Boks 1172 Blindern, NO-0318 Oslo, Norway

John MAVROGENES, Department of Geology and Research School of Earth Sciences, Australian National University, Canberra, ACT 0200 Australia

Gheorghe DAMIAN and Florica DAMIAN, North University of Baia Mare, RO-4800 Baia Mare, Romania

Summary: To test the hypothesis that samples composed of native tellurium and altaite, with abundant inclusions of Bi- and Au-Ag-tellurides from the Musariu gold deposit may have resulted from (Au)-Pb-Te melts, annealing-quenching experiments and LA-ICP-MS microanalysis was carried out. Almost complete homogenisation of the samples took place at 420ºC and the quenched materials are used to interpret cooling paths in the system Au-Pb-Te. The diverse mineralogy of this occurrence can be interpreted as the result of crystallization of molten Te-(Pb)-rich precipitates that incorporated minor amounts of other elements. The range of Au scavenged by such melts is from ppm levels ($Pb_{0.1}Te_{0.9}$) up to 6 wt.% [$(AuAg)_{0.08}Pb_{0.11}Te_{0.81}$], as measured by LA-ICP-MS analysis of quenched products resulting from melting of samples with and without Au-Ag-tellurides, respectively. Temperatures of ca. 400ºC are plausible during the porphyry-epithermal transition envisaged for this occurrence.

Key words: gold ores, tellurides, altaite, tellurium, lead, gold, melts, annealing, quenching, experimental studies, Musariu, Romania

1. INTRODUCTION

Six of the ten eutectics within the Au-Pb-Te phase diagram are placed in the Te-rich part of this system, in a temperature interval between 388 and 447ºC (Legendre and Souleau, 1972; Prince et al., 1990). Five of these include native gold and/or $AuTe_2$, a phase known as the mineral calaverite. The other phases involved in these eutectics are also known as minerals, i.e., altaite (PbTe) and native tellurium. All these minerals are commonly found, in variable amounts, within gold ores. The above temperature range for the Te-rich part of the system Au-Pb-Te overlaps with the temperatures estimated for several types of Au deposits, e.g., skarns, porphyry, intrusion-related, orogenic Au, but is too high for what is currently considered for deposits belonging to an epithermal environment, especially those of low sulphidation type (<300C; Cooke and Simmons, 2000).

Musariu is one of eight deposits in the Brad district within the Golden Quadrilateral (GQ), Romania (Fig. 1), a volcano-magmatic province of Neogene age that hosts some 60 epithermal Au deposits (Ciobanu et al., 2004 and references therein). This district is not as rich in tellurides as others in the GQ, even though several occurrences have been reported (Cook et al., 2004 and references therein). Although we do not know the exact location of the present samples, this occurrence is very similar to the one described from Musariu Nou by Berbeleac (1980) and Berbeleac and David (1982). The mineral assemblage features native tellurium, altaite and other tellurides, among which Au-Ag-tellurides are the most diverse. Fluid inclusion studies on quartz from veins in several major deposits from the GQ, including Musariu, have shown that the upper temperatures for early sulphide stages (in deeper parts of the veins where base metal sulphides are predominant over the Au mineralization) are in excess of 300ºC (e.g., Borcos, 1968). Temperatures in excess of 450ºC are also inferred from other features observed in

the sulphide ores, e.g., the presence of Cu-Fe-S *intermediate solid solution* in pyrite and/or sphalerite (Udubasa et al., 1976; Ciobanu et al., 2004 and references therein). Such temperatures are considered, in particular, for those epithermal systems that form as kin-veins on top of immature porphyry roots (e.g., Larga; Cook and Ciobanu, 2004). Although no analogous data is available for Musariu Nou, temperatures around 400ºC may be considered realistic for the tellurium occurrence presented here, to which all the arguments presented above apply.

The phase relationships between diverse telluride species encountered together with native gold and/or Au-bearing minerals often show eutectic associations in one or another Te-bearing system. Can this be a consequence of their crystallisation from molten precipitates that are exsolved from hydrothermal fluids, as discussed by Ciobanu et al. (2005) for Bi-tellurides? If so, such melts would provide a powerful mechanism to scavenge gold from fluids that otherwise might not necessarily be saturated in Au at the time of melt precipitation.

The concept of polymetallic melts assisting formation of gold deposits during high-grade metamorphism was tested for Challenger deposit, Australia (Tomkins and Mavrogenes, 2002) by a series of annealing-quenching experiments on samples that contained blebs of native gold in association with sulphides, maldonite and native bismuth. In this case, the conditions of annealing (p, T) were estimated from peak metamorphic parameters and the quenched textures indicated homogenisation of Au-bearing blebs via melting.

We undertook the same type of experiments to test if the Pb-Te melt scavenger may have operated during vein formation in Musariu. We complemented this by measuring the Au content (by LA-ICP-MS) in the quenched products that do not contain Au-minerals.

2. THE MUSARIU DEPOSIT

The veins in the Musariu deposit, hosted by various lithologies (andesite and basalts), have a NW-SE strike of some 2 km, and were exploited across a depth interval of some 350-450 m. The veins feature common pinch-and-swell morphologies and characteristically contain base metal sulphides in association with native gold. Highest-grade Au is, however, associated with argillic alteration. Individual vein systems are branched and conjugated with secondary, perpendicular systems. The deposit is placed between several sub-volcanic stocks, in an area of intense hydrothermal alteration. The Te-bearing occurrence presented here is located at the SE end of the deposit, Musariu Nou, where the veins are centred onto a buried porphyry stock (intersected by drilling at 1200 m beneath surface and explored in deeper mining levels, i.e., 450 m beneath the upper veins). The deposit, for which tonnage, reserves and average grade are still not publicly available data, is nonetheless famous for spectacular bonanza ores found at vein junctions. The mine was closed in 2006 for economic reasons.

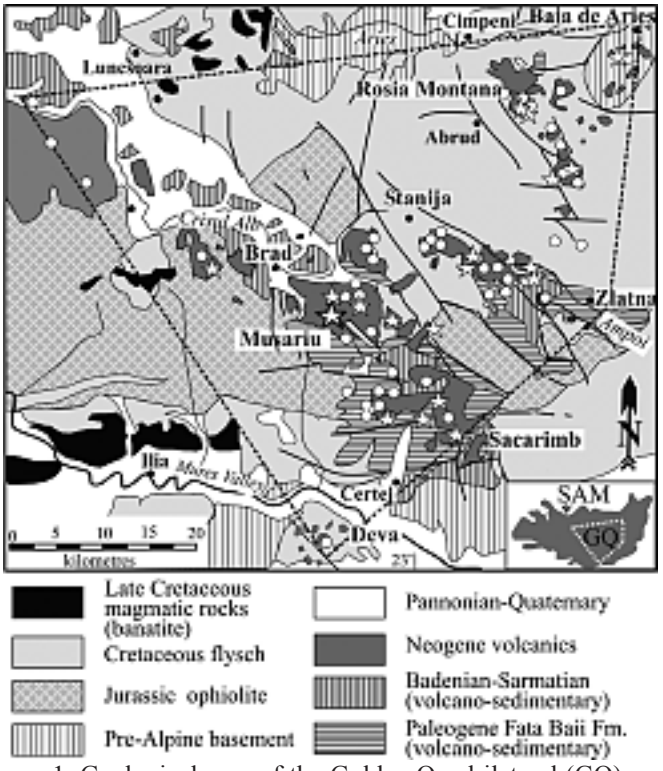

Figure 1. Geological map of the Golden Quadrilateral (GQ), showing the location of the main deposits, including Musariu. Inset shows the position of the GQ in the South Apuseni Mts. (SAM), Western Romania.

3. MINERAL ASSEMBLAGES AND PETROGENETIC ASSESMENT FOR THE EXPERIMENT

The analysed specimens consist of irregular mm- to cm- size patches of *native tellurium* and *altaite* (Alt) that occur within quartz and/or altered andesite (sericite+chlorite). The two minerals are also present as blebs within sulphide grains (e.g., pyrite, rare chalcopyrite and sphalerite) and rutile, which are disseminated throughout the host andesite. In turn, the sulphides are also present within the patches of native tellurium and Alt. The latter is segregated towards the margins of native tellurium patches and is also ubiquitously present inside these patches as small inclusions (5-10 μm; the shapes of such inclusions are either euhedral or scalloped. Altaite inclusions are often associated with Bi-tellurides, *tellurobismuthite* (Tbs) and *rucklidgeite* (Fig. 2a, b). Both Bi-tellurides contain variable amounts of Sb, but concentrations are higher in Tbs (Fig. 2c; Table 1); *tellurantimony* occurs occasionally. Several Au(Ag)- and Ag-tellurides (*sylvanite*, *nagyagite*, *empressite* and *stützite*; Table 1) are observed in some patches, in more abundance in Alt (Fig. 2d). Two-component inclusions consisting of native tellurium and stützite in Alt are also noted (Fig. 2e). *Frohbergite* is irregularly present within the native tellurium as single, euhedral and scalloped grains (Fig. 2f) or as brecciated aggregates (Fig. 2g).

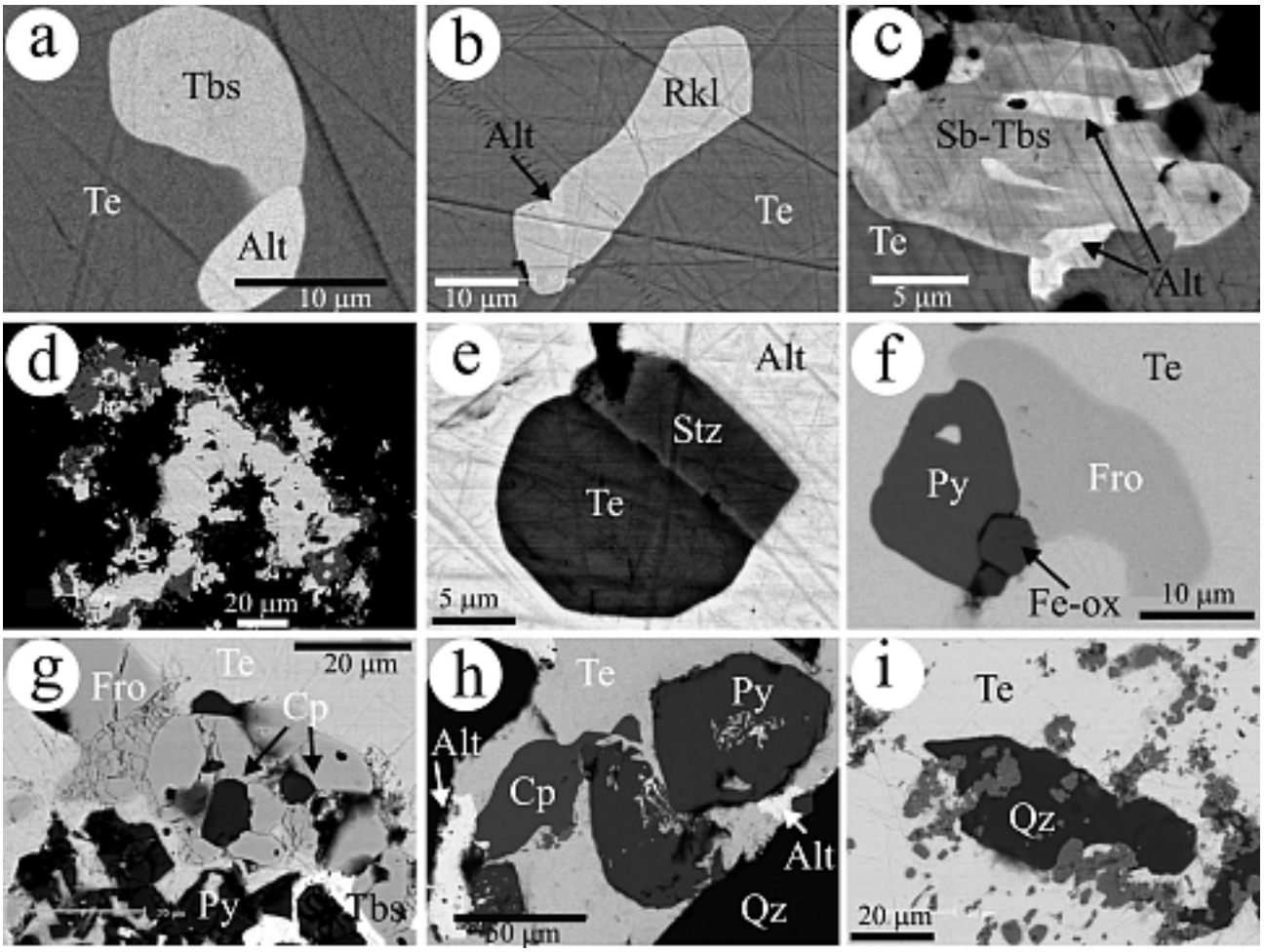

Figure 2. Back-scatted electron images showing aspects of the diverse telluride associations in native tellurium (a-c, f-i) and altaite (d and e). (a), (b) and (c) Typical inclusions of Bi-tellurides and altaite, (d) Characteristic occurrence of Au-Ag-tellurides (empressite, stützite, sylvanite) at the margin of altaite patches that are connected to native tellurium (not shown in picture. (e) Two-component inclusions (native tellurium and stützite) in altaite. (f) Scalloped inclusions of frohbergite associated with pyrite and Fe-oxides. (g) Brecciated aggregate of frohbergite and sulphides, cemented by tellurobismuthite. (h) Coarse pyrite brecciated and replaced by host native tellurium and altaite. (i) Swarms of fine-grained pyrite crosscutting quartz inclusions. Abbreviations: Alt, altaite; Cp, chalcopyrite; Fe-ox, Fe-oxides; Fro, frohbergite, Py, pyrite; Qz, quartz; Rkl, rucklidgeite; Sb-tbs, Sb-bearing tellurobismuthite; Stz, stützite; Tbs, tellurobismuthite; Te, native tellurium.

Table 1. Mean compositions of telluride minerals (Alt, altaite; Tbs, tellurobismuthite; Rkl, rucklidgeite; Sz, stützite; Emp, empressite; Syl, sylvanite). Performed at Adelaide Microscopy; Cameca SX-51 microprobe, 20 kV, 20 na, standards: Au (Au), Ag_2Te (Ag, Te), PbS (Pb, S), Bi_2Se_3 (Bi, Se), As (CoAsS), Sb (Sb_2S_3). na=not analyzed.

wt. %	Alt	Tbs			Rkl	Sz	Emp	Syl
	3	1 (min)	1 (max)	19 (mean)	26	7	5	1
Au	na	na	na	na	na	0.00	0.00	24.67
Ag	0.42	0.10	0.05	0.11	1.31	54.75	42.93	13.56
Pb	58.67	0.44	0.43	0.59	13.49	0.18	0.33	0.00
Bi	1.40	42.83	32.54	38.48	36.45	0.06	0.07	0.00
Sb	0.32	6.14	14.03	9.33	2.46	0.27	0.42	0.48
Te	40.13	50.51	53.57	51.88	45.93	43.24	56.77	63.51
Se	0.02	0.38	0.06	0.13	0.85	0.00	0.01	0.00
S	0.00	0.00	0.01	0.01	0.00	0.01	0.01	0.00
Total	101.0	100.4	100.7	100.5	100.5	98.5	100.5	102.2
apfu	2	5	5	5	7	8	2	6.00
Au						0.00	0.00	1.00
Ag	0.01	0.01	0.00	0.01	0.13	4.78	0.94	1.00
Au+Ag								2.00
Pb	0.93	0.02	0.02	0.02	0.71	0.01	0.00	0.00
Sb	0.01	0.38	0.83	0.57	0.22	0.02	0.01	0.03
Bi	0.02	1.55	1.12	1.37	1.90	0.00	0.00	0.00
Total M	0.97	1.96	1.97	1.97	2.96	4.81	0.95	2.03
Te	1.03	3.00	3.02	3.02	3.92	3.19	1.05	3.97
Se	0.00	0.04	0.01	0.01	0.12	0.00	0.00	0.00
S	0.00	0.00	0.00	0.00	0.00	0.00	0.00	0.00
Te(Se,S)	1.03	3.04	3.03	3.03	4.04	3.19	1.05	3.97

In such aggregates pyrite is also noted. The sulphide is also brecciated, and the entire assemblage is cemented by Tbs. Pyrite appears either as larger brecciated grains, replaced by the host native tellurium ± altaite (Fig. 2h), or as swarms of small, euhedral grains crosscutting any of the other inclusions (altaite, quartz, etc.), within the patches of native tellurium (Fig. 2i).

The above assemblage features several relationships supporting the presumption of formation from melts. All eight observed tellurides are tied to the native Te and/or Alt patches; these two phases are always present together, even though each of them may be dominant in one patch or another. Their mutual relationships preserve, in places, curvilinear boundaries indicative of formation from molten precipitates. The range of contained inclusions indicates that this melt also included small quantities (a few wt.%) of several other metals (Bi, Sb, Fe), as well as higher, yet variable amounts of Au and Ag. The upper temperature for melt exsolution from fluids can be estimated from the two mineral assemblages involving native tellurium and corresponding to eutectics formed at the same temperature, yet from two different phase systems, i.e., native Te and Alt (410ºC in the Pb-Te; Lin et al., 1986) and native Te-Tbs (412ºC, in the Bi-Te system; Gather and Blachnik, 1974).

4. EXPERIMENTAL

The annealing temperature was set at ~10ºC above the eutectics mentioned above (420ºC). The aim was to obtain homogenisation via melting and to observe the resulting textures in the quench products. Two slices, representing the native Te-Alt association with and without Au-Ag-tellurides, were cut through two samples. They were placed into a graphite crucible and heated in a furnace up to 420ºC. The samples were taken out after 15 minutes and quenched in water. The two slices, as well as melt blebs formed on the surface of the samples, were mounted separately into resin and polished for investigation by scanning electron microscopy and microprobe.

Both samples show quenching textures indicating extensive to almost complete melting. The melts appear interstitial to quartz and spread as irregular patches into the altered andesite (Fig. 3a), resembling the geometry in the initial material. Few areas of Alt, found towards the edges of both slices, remained unmelted (Fig. 3b). Grains of pyrite enclosed within the quenched material show advanced skeletal morphologies indicating corrosion by the melts formed during annealing (Fig. 3c).

Each sample is represented by quenched products that consist of (i) two components - native Te and Alt, and (ii) three components - native Te, Alt and a Au-Ag-telluride: the latter is too small to allow definitive identification - however we consider it as ‘sylvanite’ (Syl) given the Au:Ag atomic ratio of 1 corresponding to this mineral (see below). Native tellurium is the first crystallisation product in (i) and is the dominant primary product of the larger melted areas in (ii). In the smaller areas, however, Alt and/or Syl+Alt (e.g., Fig. 3b) crystallise at the onset of cooling. In the first case, native tellurium most typically forms dendrites throughout the fine groundmass (Fig. 3c,d). This is the kind of texture observed in the larger masses of quenched melts in both

samples, as well as in the droplets. The size of such dendrites throughout a given patch can vary. Generally, the margins have coarser textures relatively to the inner parts. The textures observed in the blebs are comparable with those from the patches in each respective sample, even though they are commonly finer in grain size. The smaller patches, especially those hosted by the andesite, are characterized instead by a cellular texture consisting of a network of Alt or Alt+Syl (brighter on BSE images) on a background of native tellurium (darker on BSE images: Fig. 3e). Another feature is that the quenched material shows domains that are equivalent in terms of constituents, but where one of the constituents has variable grain size. This is illustrated in Fig. 3f, where the two constituents are (i) rounded areas of native Te and (ii) symplectite intergrowths of the same minerals. The symplectites are fine and coarse in the two constituents and we note the continuity between the native Te in the rounded areas and in the symplectites. Such domain separation may result from faster cooling. The interstitial area between dendrites of native Te

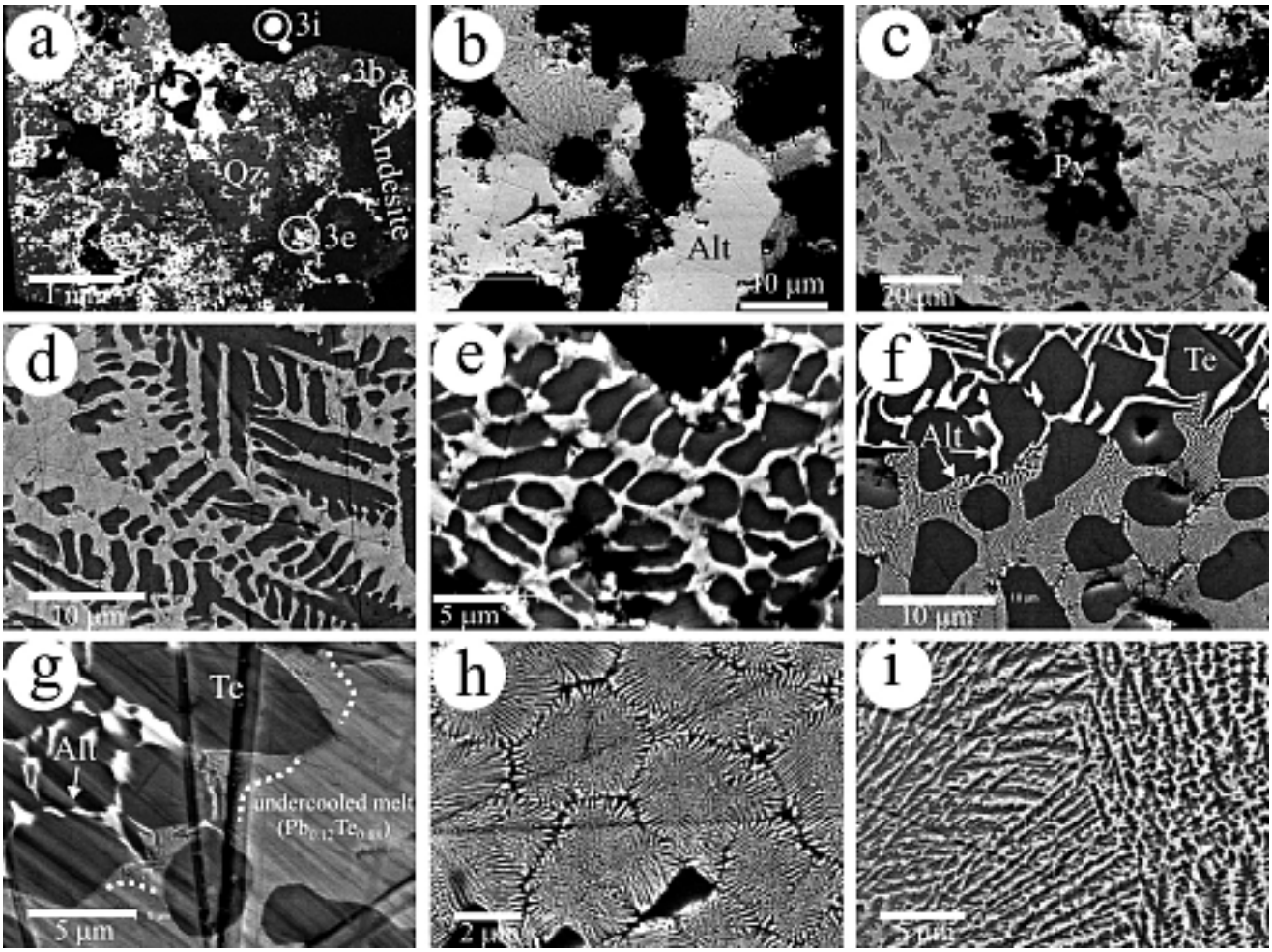

Figure 3. Back-scatted electron images showing aspects of the quenched products. (a) Melts from the Au-Ag-bearing sample interstitial to quartz and spreading into the altered andesite. The black circle indicates an area of dendrites analysed by microprobe. (b) Unmelted altaite and typical quenched product (upper part of image) consisting of first-formed laths of sylvanite. (c) Skeletal pyrite within quenched melt consisting of dendritic native tellurium (darker) and fine-grained native tellurium – altaite symplectite (brighter), (d) Typical appearance of coarse dendrites of native tellurium (darker) within symplectites (native tellurium - altaite, brighter). (e) Cellular texture consisting of an oval-shaped net of altaite and sylvanite (bright) within native tellurium (dark). (f) Segregations of domains with different grain size within quenched melt composed of two constituents (i) native tellurium and (ii) symplectites of native tellurium and altaite. (g) Undercooled melt in contact with crystallized native tellurium with interstitial symplectites of native tellurium and altaite. Note appearance of fine symplectites of the same type at the boundary of the undercooled melt (marked by dashed line). (h) Segregation of hexagonal domains within a mass of symplectites, representing the native tellurium – altaite eutectic. (i) Domain segregation within quenched melt with mottled textures between native tellurium (dark) and altaite/sylvanite (brighter). Abbreviations as in Fig. 2.

appears homogenous (supercooled melt; Fig. 3g); fine native Te-Alt symplectites appear towards the boundary between the two domains. The textures within the fine-grained groundmass to the native Te also display segregation of symplectite domains domains with a hexagonal pattern (Fig. 3h); this represents the native Te-Alt eutectic in the Pb-Te system. In some of the three-component blebs, domain separation may start prior to the crystallisation of native Te. The three phases (native Te, Alt and Syl) form a mottled texture within such domains (Fig. 3i).

Using a defocused electron microprobe beam (size 10 μm), we measured the averaged 'bulk' composition of patches and blebs representative for the main types of quenched textures; mean analyses are given in Table 2. The analytical data was obtained on areas of the sample in which the grain size of all components in the intergrowths is relatively even, so as to avoid a nugget effect caused by coarser dendrites. In the two-component sample, the composition of areas with supercooled melt shows slightly higher Pb and lower Te than the bulk composition of the 'dendritic' textures (17 wt.% / 82 wt.% and 15 wt.% / 83 wt.%, respectively). In the Au-Ag-bearing, three-component sample, the composition of the 'dendritic' textures has the same Pb content as the texturally equivalent areas from the other sample, but incorporation of Au (6 wt.%) and Ag (3 wt.%) lowers the Te content (76 wt.%).

Table 2. Mean compositions of representative quenched products obtained in the two samples. Conditions as Table 1.

	Pb-Te		Pb-Te-Au(Ag)		
wt. %	supercooled melt	dendritic	dendritic and mottled	cellular	patches adjacent to unmelted Alt
	Fig. 3g	Fig. 3c, d	Fig. 3i	Fig. 3e	Fig. 3b (upper)
No. an.	2	5	13	5	10
Au	0.00	0.02	5.88	1.67	15.95
Ag	0.21	0.24	2.82	1.10	9.86
Pb	16.95	14.92	15.47	7.86	14.49
Bi	0.23	0.19	0.10	0.16	0.11
Sb	0.62	0.60	0.51	0.60	0.38
Te	81.92	83.47	75.61	88.18	58.51
Se	0.06	0.05	0.01	0.05	0.03
S	0.00	na	na	na	na
Total	100.0	99.5	100.4	99.6	99.3
1 apfu					
Au	0.000	0.000	0.041	0.011	0.115
Ag	0.003	0.003	0.036	0.014	0.130
Au+Ag	0.003	0.003	0.077	0.025	0.245
Pb	0.112	0.098	0.102	0.050	0.099
Sb	0.007	0.007	0.006	0.007	0.004
Bi	0.001	0.001	0.001	0.001	0.001
Te(Se, S)	0.877	0.891	0.814	0.917	0.651

One of the areas with cellular textures has the highest Te content (88 wt.%) and lowest Pb (8 wt.%); the Au and Ag contents are 2 wt.% and 1 wt.%, respectively. The patches richest in Au (16 wt. %) and Ag (10 wt. %) are those associated with unmelted altaite. They have the same Pb content as the patches with Te dendrites, but much lower Te (59 wt.%).

The plot of analytical points (obtained from both patches and blebs) on the Au-Pb-Te solvus diagram (Fig. 4; Prince et al., 1990), ignoring Ag, show that the two-component quenched products form a tight cluster along the Pb-Te tieline, with a small offset from the eutectic at 410ºC (Alt+native Te) towards the Te apex. The analytical points obtained from the three-component quenched products form three distinct clusters. Areas with dendritic Te and mottled textures plot above the cotectic line between the eutectics at 410ºC and 388ºC (Alt+native Te+$AuTe_2$), whereas the cluster representing the composition of quenched material adjacent to unmelted Alt (Fig. 3b) plots below the same line, close to the eutectic at 388ºC (PbTe+Te+$AuTe_2$).

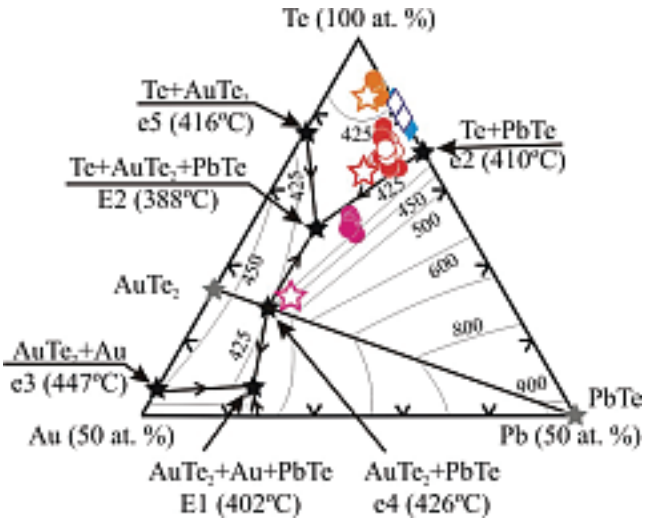

Figure 4. Compositions of quenched melts plotted on the liquidus surface in the system Au-Pb-Te (after Prince et al., 1990). Blue rhombs represent the two-component quenched melts, open symbols for supercooled melt in Fig. 3g. Circles represent compositions of three-component quenched melts. Orange: cellular textures, red: dendritic/mottled textures; purple, patch adjacent to unmelted altaite (Fig. 3b). Open symbols for blebs. Stars of same colour represent calculated mean compositions for each cluster with Ag included (Table 2). This shows their position relative to eutectics (E, e) and isotherms (ºC). See text for explanation.

The above-mentioned clusters all lie within the field defined by isotherms at 425ºC in the Au-Pb-Te phase diagram. A further cluster, representing one of the areas with cellular textures, is placed outside this field, above the 425ºC isotherm, i.e., towards the Te corner. The mean compositions of each cluster obtained from the three-component sample are also plotted (open stars) on the same diagram, with the Ag content included. The shift in the position of two of these clusters (cellular and dendritic) is small and does not modify their geometry relative to the phase boundaries. The position of the third cluster, the richest in Ag, however, is significantly changed and plots close to the eutectic at 426ºC ($AuTe_2$+PbTe).

The Au content within the quenched products that represent $Te_{0.9}Pb_{0.1}$ melts was investigated by LA-ICP-MS techniques at the University of Tasmania (see Cook et al., this volume for details of analytical method). Several spot analyses were made of the supercooled melt (Fig. 3g), as well as of the typical dendritic areas (e.g. Fig. 3c). The results indicate Au contents in the range between 26 and 64 ppm, and Ag contents in the range 1,437-2,080 ppm. We note the presence of several other elements, including Fe (2,134 to 12,654 ppm), Bi (1,102 to 1,213 ppm), Sb (25 to 291 ppm), Se (142 to 270 ppm) and Cu (494 to 899 ppm). The signals for most of these elements are relatively parallel and steady throughout the ablation, with the exception of Fe that shows a particularly irregular trend (Fig. 5).

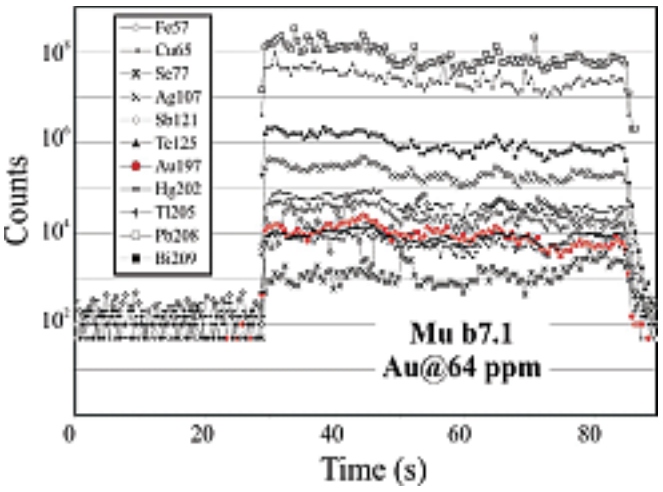

Figure 5. LA-ICP-MS depth profile of two-component quenched bleb with fine-grained dendritic texture. Hole diameter: 40 µm. Calculated using Te as internal standard.

5. DISCUSSION

The results of this experiment show that the initial assemblages, mineralogically very diverse, can be easily and rapidly homogenised as melts at 420ºC. Incorporation of other minor elements (Fe, Bi, Sb, Se, etc.), or higher amounts of Ag, will lower this temperature by at least 10-15ºC, due to melting (freezing) point depression (e.g., Anderson, 2005). The textures observed in the quenched material, in corroboration with the compositional plot in the Au-Pb-Te solvus diagram (Prince et al., 1990), can be used to interpret the cooling paths obtained during this experiment. This is, however, a simplified interpretation of the results for the Au-Ag-bearing sample, since the presence of Ag in significant amounts will require a 4-component system (Te-Pb-Au-Ag). Secondly, in this case, the heterogeneity produced during cooling in the natural system, which is slower - by several orders of magnitude - than the quenching method used here, will produce local segregation in the molten precipitate (observed in the distribution of Au-Ag-tellurides in the host minerals). The annealing would thus reproduce the initial Au-Ag-Te-Pb precipitate(s) only if the sample represents the bulk of that precipitate. Bearing in mind all these considerations, we can nonetheless make some useful petrogenetic comments for the Musariu occurrence.

The textures in the quenched products, with exception of areas next to unmelted Alt, indicate hypoeutectic textures with respect to Alt (Reed-Hill and Abbaschian, 1994). The dendrites of native Te (e.g., Fig. 3d) represent one of the common textures obtained in alloy systems resulting from dendritic freezing, a phenomenon that can be associated either with thermal or constitutional supercooling (Reed-Hill and Abbaschian, 1994). The former occurs when the liquid-solid interface moves into a supercooled liquid whose temperature falls in advance of the interface. The second is the result of a solid freezing with a composition that is different from the liquid from which it forms, a scenario we consider for the studied material. When the supercooled layer is too thin to support

development of dendrites, the liquid-solid interface becomes unstable and will attract formation of a cellular texture throughout the melted material, in which the cell 'walls' are regions of high-solute concentration (bright areas in Fig. 3e), as is the case for the smaller patches in the studied material.

We can interpret the cooling paths for the melts obtained during annealing by considering an oblique view of T-X (composition) sections for the ternary eutectic in the system Au-Pb-Te at 388ºC (Fig. 6a). We have plotted the average mean compositions of the main types of quenched products. The plots representing the Au-Ag-bearing sample are shown shifted to lower temperatures, assuming an estimated reduction by 10-15ºC due to incorporation of Ag. Melting started in each sample from the lowermost temperature of one or the other eutectics recorded in the quenched materials, i.e., 410ºC (native Te+Alt) for the Pb-Te melts and 388ºC (native Te+Alt+$AuTe_2$) for the Au(Ag)-Te-Pb melts. The melts attained saturation at the compositions measured in the quenched products (Fig. 6a). Crystallisation started from each compositional point projected on the melt interface along a straight line (from native Te to each composition).

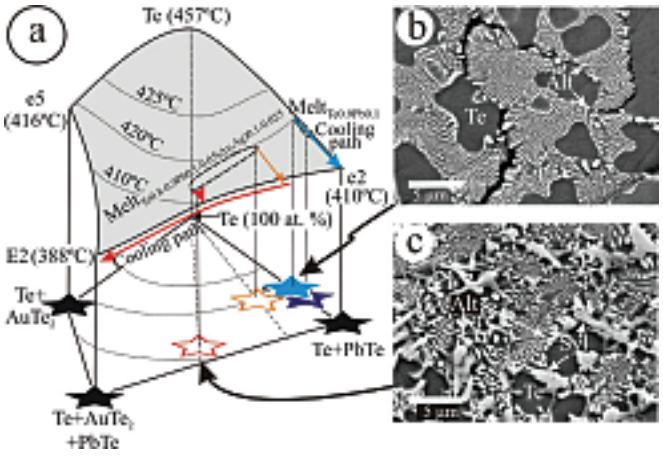

Figure 6. Oblique view of the T-composition section for the ternary eutectic at 388ºC in the system Au-Pb-Te. The shaded area at the top represents the melt section between native tellurium and the eutectics e2, E2 and e5. The triangle underneath represents the compositional section for this area that includes the mean compositions of quench products (see also Fig. 4). Light blue represents two-component melt (representative textures are shown in b), dark blue is the supercooled melt (Fig. 3g), orange and red arrow for three-component melts (native tellurium + altaite + sylvanite), where orange is the cellular texture and red the dendritic (textures shown in c) and mottled textures. Isotherms are shown on both surfaces by thin lines. Dashed lines are tie-lines connecting native tellurium and individual compositions. Cooling paths for the two- and three-component melts are shown by blue and red arrows, respectively.

There are two cooling paths representing the melts in each of the two samples. In the Pb-Te sample, the native Te crystallised until it reached the eutectic at 410ºC when symplectites of native Te and Alt are formed (Fig. 6b). The micro-segregation observed within symplectite domains (Fig. 3h) can also be attributed to formation of cellular textures due to supercooling effects as described above. Preservation of a homogenous melt in the small blebs, with a composition close to the bulk composition of the native Te and the symplectites, is further evidence for supercooling effects. In the melts obtained in the Au-Ag-bearing sample, the crystallisation of native Te continued until it reached the cotectic line between the eutectics at 410ºC and 388ºC (native Te-PbTe-$AuTe_2$), at which point crystallisation of symplectites of native Te and Alt occurred, with melt composition moving along this line until Syl starts to crystallise (Fig. 6c) when the ternary eutectic is attained (note that this should have been Cal in a Ag-free system). The Ag content in the quenched products obtained from melts adjacent to unmelted Alt is too high to allow this type of interpretation using the Au-Pb-Te diagram. Further investigations are required to characterise those products.

The homogenisation obtained via melts in the studied material supports formation of the telluride assemblage at Musariu from Te-rich precipitates. The amounts of Bi, Sb, Fe, Au, Ag measured in the quenched Pb-Te sample by LA-ICP-MS show that these elements can be incorporated within such melts and will act as centres for telluride nucleation during a slower cooling path than the one used in the experiment. Following crystallisation of Bi-tellurides and altaite at temperatures around 400ºC, the other tellurides observed in the samples were formed as the precipitates cooled further, Au and Ag being preferentially incorporated within altaite, whereas

Fe remained within native tellurium. The association of native tellurium and stützite indicates an upper formation temperature of 330ºC (Cabri, 1965), whereas frohbergite and pyrite become stable below 230ºC, within a narrow fTe_2-fS_2 field (Afifi et al., 1988).

The entire assemblage has been overprinted after complete crystallisation of the Te-rich precipitates. This is seen in the crosscutting relationships between swarms of pyrite and all other crystallised components. This superposed event is also assisted by local brecciation and dissolution-reprecipitation reactions, resulting in readjustment of pre-existing mutual grain boundaries (e.g., scalloped morphologies).

The amounts of precious metals measured in the quenched melts that do not contain Au-Ag-bearing minerals (Au@47 ppm; Ag@1,700 ppm), even though lower than in the melts that contain Syl by several orders of magnitude (Au@2-6 wt. %; Ag@1-3 wt. %), suggest nonetheless that all the initial precipitates are exsolved from Au-bearing fluids. In turn, if we take the lowermost values as a rough approximation of Au concentration in the fluid that exsolved such melts, the higher values measured in the quenched materials represent an evaluation of the capacity that Pb-Te melts have to scavenge Au (and Ag) from that fluid if the opportunity for melt formation occurs. This investigation will be complemented by additional experiments that will constrain the lower temperature for melt formation and the upper temperature for complete homogenisation.

ACKNOWLEDGEMENTS

CLC acknowledges receipt of an Australian Research Council Discovery grant. The staff at Adelaide Microscopy are thanked for their kind assistance with the electron microprobe work.

REFERENCES

Afifi, A.M., Kelly, W.C., Essene, E.J., 1988. Phase relations among tellurides, sulfides, and oxides: II. Application to telluride-bearing ore deposits. Econ Geol 83, 395-404.

Anderson, G., 2005. Thermodynamics of Natural Systems, 2nd edition. Cambridge Univ. Press, 648 pp.

Berbeleac, I., 1980. Native tellurium and tellurides mineralization from Musariu, Brad Region (Metalliferi Mts.), Romania. An. Inst. Geol. Geofiz. 56, 153-168.

Berbeleac, I., David, M., 1982. Native tellurium from Musariu, Brad Region, Metaliferi Mts., Romania. In: Ore Genesis; The State of the Art (G.C. Amstutz et al., Eds.). Springer, Berlin, p. 283-295.

Borcoş, M., 1968. Observaţii in legătură cu determinarea condiţilor termodinamice de formare a unor filoane şi zăcăminte hidrotermale din regiunea Munţilor Metaliferi. II. Sectorul Brad-Bulza-Baia de Arieş. St. cerc. Geol. Geofiz. Gegr., ser. Geol. 13, 363-376.

Cabri, L.J., 1965. Phase relations in the Au-Ag-Te system and their mineralogical significance. Econ. Geol. 60, 1569-1606.

Ciobanu, C.L., Gabudeanu, B., Cook, N.J. 2004. Neogene ore deposits and metallogeny of the Golden Quadrilateral, South Apuseni Mts., Romania. IAGOD Guidebook Series 12, 23-88.

Ciobanu, C.L., Cook, N.J., Pring, A., 2005. Bismuth tellurides as gold scavengers. Mineral Deposit Research: Meeting the Global Challenge (J.W. Mao and F.P. Bierlein, eds.), Springer, Berlin-Heidelberg-New York, p 1383-1386.

Cook, N.J., Ciobanu, C.L., 2004. Bismuth tellurides and sulphosalts from the Larga hydrothermal system, Metaliferi Mts., Romania. Mineral. Mag. 68, 301-321.

Cook, N.J., Ciobanu, C.L., Damian, G., 2004. Tellurides and sulphosalts from deposits in the Golden Quadrilateral. IAGOD Guidebook Series 12, 111-144.

Cook, N.J., Ciobanu, C.L., Danushevskiy, L., 2007, this volume. LA-ICP-MS determination of gold in Bi-minerals from deposits in the Fennoscandian Shield.

Cooke, D.R., Simmons, S.F., 2000. Characteristics and genesis of epithermal gold deposits. Rev. Econ. Geol. 13, 221-244.

Gather, B., Blachnik, R., 1974. The gold-bismuth-tellurium system. Z. Metallkunde 65: 653-656.

Legendre, B., Souleau, C., 1972. Etude du systeme ternaire Au-Pb-Te. Bull. Chim. de France 2, 473-479.

Lin, J.C., Lin, K.C., Hsieh, K.C., Sharma, R.C., Chang, Y.A., 1986. Binary Alloy Phase Diagrams (T.B. Massalski, Ed., ASM Intern., p. 1850-1851.

Prince, A., Raynor, G.V., Evans, D.S., 1990. Phase diagrams of ternary gold alloys. Inst. of Metals, London, 505 pp.

Reed-Hill, R.E., Abbaschian, R., 1994. Physical Metallurgy Principles, 3rd edition. PWS Publ. Co., Boston, 926 pp.

Tomkins, A.G., Mavrogenes, J.A., 2002. Mobilization of gold as a polymetallic melt during pelite anatexis at the Challenger deposit, South Australia: a metamorphosed Archean gold deposit. Econ. Geol. 97, 1249-1271.

Udubaşa, G., Istrate, G., Dafin, E., Braun, A., 1976. Mineralizaţiile polimetalice de la Bocşa (N de Săcărîmb, Munţii Metaliferi). D.S. ale Şedinţelor 62, 97-124.

Au-Bi-Te melts: Annealing-quenching experiments on material from the Oya gold deposit (Japan)

Cristiana L. CIOBANU, Mineralogy Group, South Australian Museum, North Terrace, Adelaide, S.A., 5000 Australia, and Department of Earth and Environmental Sciences, University of Adelaide, S.A., 5005, Australia (Cristiana.Ciobanu@adelaide.edu.au)

John MAVROGENES, Department of Geology and Research School of Earth Sciences, Australian National University, Canberra, ACT 0200 Australia

Nigel J. COOK, Natural History Museum, University of Oslo, Boks 1172 Blindern, NO-0318 Oslo, Norway

Masaaki SHIMIZU, Department of Earth Sciences, University of Toyama, Japan

Abstract: A sample from the Oya gold deposit was investigated by LA-ICP-MS microanalysis and annealing-quenching experiments. The material consists of a simple assemblage native gold + tellurobismuthite in quartz. The association corresponds to the highest temperature eutectic (475ºC) in the system Au-Bi-Te at dry experimental conditions. Our experiments were carried out at temperatures 15ºC higher than this to observe the extent of homogenisation and compositional fields in the quenched material. The extended homogenisation observed, and textures produced are consistent with a limited range of Au-Bi-Te melts exsolved from fluids via immiscibility. The content of minor components in the minerals, in particular Ag and Pb, would lower the eutectic temperature. The presence of other components, such as Cl, I, Br and H_2O, at the time of melt exsolution may have similar effects. Further investigation on this material will attempt to establish lowermost limits on melt temperature. The temperatures given in published fluid inclusion studies (270-350ºC) are more than 100ºC lower than those required for the melt hypothesis, leaving the genetic interpretation for this deposit open to debate. Such a hypothesis may, however, have application to deeper intrusion-related, orogenic gold and skarn deposits if oxidised fluids are involved, where temperatures in excess of 400ºC are commonplace.

Key Words: gold ores, tellurobismuthite, gold, bismuth, tellurium, melts, annealing, quenching, experimental studies, Oya, Japan.

1. INTRODUCTION

Bismuth tellurides are commonly present in paragenetic association with gold and/or Au-minerals in deposits that span across metamorphic and magmatic environments (Cook and Ciobanu, 2005). Ciobanu et al. (2005) discussed how melts from the Au-Bi-Te system can act as Au scavengers from hydrothermal fluids, if melt separation from those fluids occurs. This mechanism was indicated as best suited for orogenic Au and skarn systems. Similar scenarios can also be considered for intrusion-related Au deposits, which commonly carry a conspicuous Bi geochemical signature (Baker et al., 2005). The concept of polymetallic melts assisting formation of gold deposits during high-grade metamorphism was tested for the Challenger deposit, Australia by a series of annealing-quenching experiments on samples that contained blebs of native gold in association with sulphides, maldonite and native bismuth (Tomkins and Mavrogenes, 2002). The conditions of annealing (p, T) were estimated from peak metamorphic parameters and the quenched textures indicated homogenisation of Au-bearing blebs via melting.

We undertook the same type of experiments to test if the Bi-Te melt scavenger may have operated during formation of the Oya gold deposit, Japan. This deposit comprises Au-Ag-Te veins associated with an intrusion, and has been classified as hypo/mesothermal type (Shikazono and Shimizu, 1988). The sample investigated consists of native Au (Au) and tellurobismuthite (Bi_2Te_3; Tbs), an association that represents the equivalent of the

highest temperature eutectic in the Au-Bi-Te system (474ºC; Gather and Blachnik, 1974). The solubility of Au in synthetic Bi_2Te_3 strongly varies with temperature, i.e, within the range 0.002 atom.% at 200ºC to 0.02 atom.% at 400ºC (Keys and Dutton, 1963 in Prince et al., 1990). Could such Au contents be measured in Tbs from natural specimens? If the Tbs in Oya was formed from Bi-Te-Au melts exsolved from a magmatically derived fluid, what is the residual Au incorporated within it? We used the LA-ICP-MS technique to answer these questions and to discuss the genetic implication this may have.

2. THE OYA DEPOSIT

Oya (Ohya; Miyagi Prefecture) is one of 17 Au Japanese vein deposits that are considered of hypo-mesothermal type (Shikazono and Shimizu, 1988; Fig. 1). Published fluid inclusion studies on these deposits indicate formation temperature in the ranges 270-320ºC (Enjoji and Takenouchi, 1976), and 270-350ºC (Shikazono and Shimizu, 1988). The later authors classified Japanese Au-Ag deposits using a combination of criteria, including regional setting, deposit morphology, commodities produced and physicochemical conditions of ore formation.

Oya, situated in the NE of Honshu, is part of a district that includes several other deposits of the same type. The mine was active between 1915 and 1971 when 2.5 Mt of ore was exploited with an average grade of 6.3 g/t Au and 2.3 g/t Ag. The veins are hosted by Triassic sandstone and slate as well as by Cretaceous diorite (outcropping at the northern end of the orefield).

The veins have a N-S strike and are found in an area of 3 by 1.5 km. There are 5 main groups with vein lengths varying from 200 to 1000 m, depths of maximum 250 m, and with widths between 0.1 to 0.6 m. Apart from native gold and Tbs, the ore also includes sulphides such as pyrrhotite and pyrite. Considering the above setting, as well as the lack of any substantial alteration in the country rocks, we contend that Oya may be considered an intrusion-related type of deposit, as those discussed by Baker et al. (2005). Such deposits would have temperature ranges higher than those obtained in the fluid inclusion studies above.

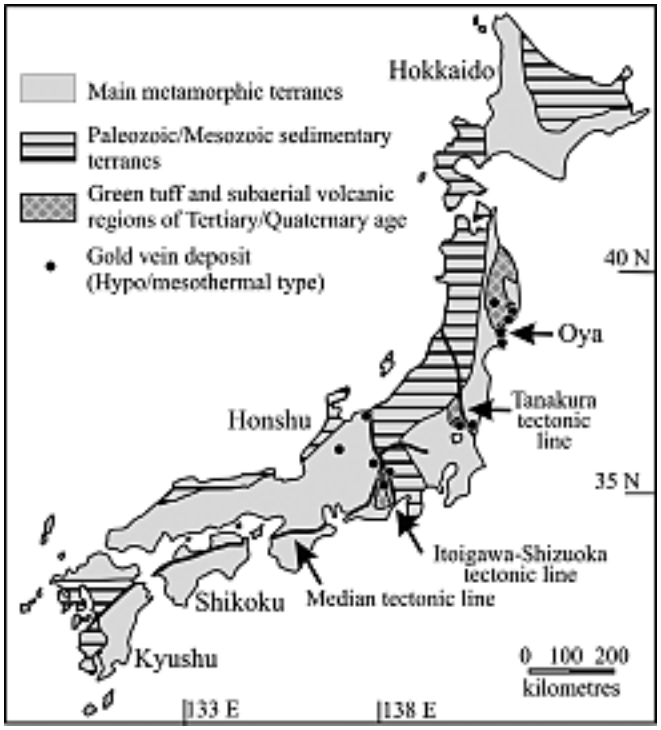

Figure 1. Geological sketch map of Japan showing the location of the Oya deposit (simplified from Shikazono and Shimizu, 1988).

3. EXPERIMENTAL

A representative sample of the high-grade ore in Oya was selected for LA-ICPMS investigation prior to annealing quenching experiments. This consists of mm-size patches of native gold and tellurobismuthite (Tbs) (Table 1) in a quartz matrix; minor carbonate is also present. Equilibrium crystallization between Tbs and native gold can be inferred from the observed textures; i.e., straight and/or curvilinear contacts; crystallization from a molten precipitate can be suggested from the latter type (Fig. 2a). Native gold contains 15 wt.% Ag, corresponding to a $Au_{0.8}Ag_{0.2}$ (Table 1).

4. LA-ICP-MS STUDY

Experimental

LA-ICP-MS analysis was carried out using the Agilent HP4500 Quadripole ICP-MS instrument at

CODES, University of Tasmania, equipped with a high-performance New Wave UP-213 Nd:YAG Q-switched laser ablation system and MEOLaser 213 software. We performed spot analyses (8-40 µm in diameter, depending on size of the target mineral). Total analysis time was 90s (30s pre-ablation and 60s ablation time). Calibration was performed on a doped pyrite standard; Te served as the internal standard for the telluride minerals.

Table 1. Electron microprobe data for tellurobismuthite and native gold before and after annealing-quenching, and 'bulk' analyses of quenched products. Performed at Adelaide Microscopy; Cameca SX-51 microprobe, 20 kV, 20 na, standards: Au (Au), Ag_2Te (Ag, Te), PbS (Pb, S), Bi_2Se_3 (Bi, Se), As (CoAsS), Sb (Sb_2S_3). Na=not analyzed.

wt. %	Before experiment		After experiment		Melts (beam size 10 microns)						
	Tbs	Au	gr4.Tbs	gr3 Au	gr1	gr2	gr3	gr4	gr5	bleb1	e1
No pts.	17	3	1	1	2	3	3	3	1	7	Tbs+Au
Au	na	88.18	0.03	98.65	32.00	35.79	34.16	27.28	30.33	30.31	
Ag	0.06	12.82	0.40	3.61	4.75	6.18	3.55	4.04	4.26	4.45	
Pb	0.69	0.07	1.02	0.00	0.80	0.81	0.00	4.39	0.86	0.81	
Bi	49.46	0.33	49.80	0.48	28.55	21.36	27.50	22.30	32.27	32.17	
Sb	0.82	0.00	0.36	0.00	0.21	0.25	0.27	0.29	0.33	0.19	
As	na	0.02	0.03	na	0.00	0.00	0.00	0.05	0.00	0.03	
Te	47.61	0.04	47.65	0.14	37.00	38.36	37.61	42.76	34.95	35.28	
Se	0.05	0.01	0.05	0.03	0.02	0.02	0.03	0.02	0.09	0.02	
S	0.02	0.04	0.00	na	0.01	0.00	0.01	0.00	0.00	0.03	
Total	98.3	101.5	99.3	102.9	103.3	102.8	103.1	101.1	103.1	103.3	
Formulae	to 5	to 1	to 5	to 1							
Au		0.78	0.001	0.93	0.25	0.28	0.27	0.22	0.24	0.24	0.30
Ag	0.005	0.21	0.030	0.06	0.07	0.09	0.05	0.06	0.06	0.07	0.00
Au+Ag	0.01	0.99	0.03	0.99	0.32	0.37	0.32	0.27	0.31	0.31	0.30
Pb	0.03	0.001	0.040	0.000	0.006	0.006	0.000	0.033	0.007	0.006	0.00
Sb	0.05	0.000	0.020	0.000	0.003	0.003	0.004	0.004	0.004	0.002	0.00
Bi	1.90	0.003	1.91	0.004	0.21	0.16	0.21	0.17	0.25	0.24	0.28
Te(+Se+S)	3.01	0.003	3.00	0.003	0.45	0.46	0.46	0.52	0.44	0.44	0.42
Bi*/(Bi+Te)*	0.40		0.40		0.33	0.26	0.31	0.28	0.37	0.36	0.40
Te*/(Bi+Te)*	0.60		0.60		0.67	0.74	0.69	0.72	0.63	0.64	0.60

Results

Gold concentration was measured in tellurobismuthite from six patches in which this mineral was present either alone or in variable proportions with Au. The Au content is in the range 0.13-12.2 ppm (n = 17, mean 2.57 ppm, detection limit 0.002-0.01 ppm), stretching across two orders of magnitude (Fig. 3) and with a random variation from one patch to another. All the analyses except one show a relative steady Au signal, either maintained throughout the ablation (Fig. 3b), as in two thirds of the spots, or for the interval before crossing into another mineral. From the latter spectra we interpret that grains of native gold occur underneath Tbs that alone appears on the surface of the polished block.

Characteristic for Tbs in Oya is the inhomogeneity of Pb content (in the range 0-2.9 wt. %) within individual grains. This correlates positively with Ag, although the latter has values that are two orders of magnitude lower (0-0.3 wt. %). In contrast, Sb values are relatively constant (0.7-0.9 wt. %). Some fluctuation is also observed in the Se and S values (0-0.07 wt. % and 0-0.05 wt. %, respectively). Even though a set of 8 other minor elements were analyzed, only 5 (Sb, Se, Pb, Ag, Cu) have analytical precision <50% and were considered as valid measurements.

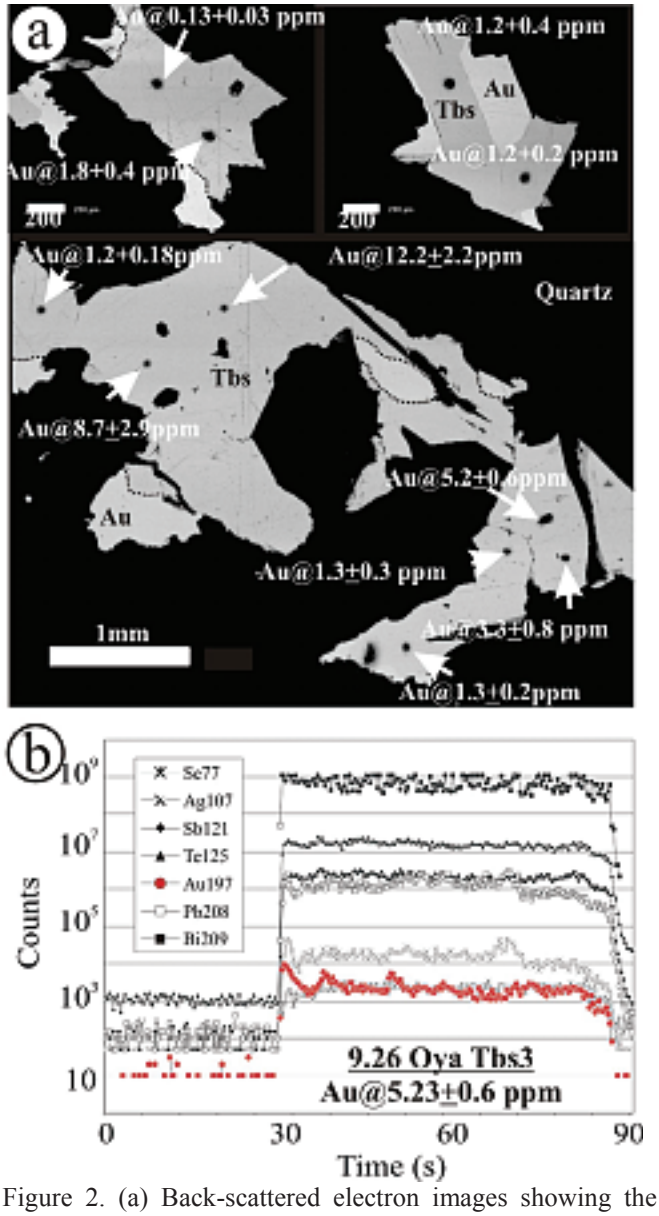

Figure 2. (a) Back-scattered electron images showing the analysed assemblage of native gold and Tbs and gold concentrations determined in some of the individual ablated points. (b) Representative LA-ICP-MS depth profile for Tbs. Note the steady gold signal during the ablation.

Plotted values show comparable trends as those reported above from microprobe measurements. The Cu trend (not plotted) roughly reproduces the Pb and Ag patterns, although without the excellent correlation seen between these elements. The plot indicates inhomogeneity of Pb and Ag from one analytical spot to another and this does not correlate with the Au variation. The same lack of correlation is seen between Sb and Se, showing steady trends across the dataset, *vs*. Au content.

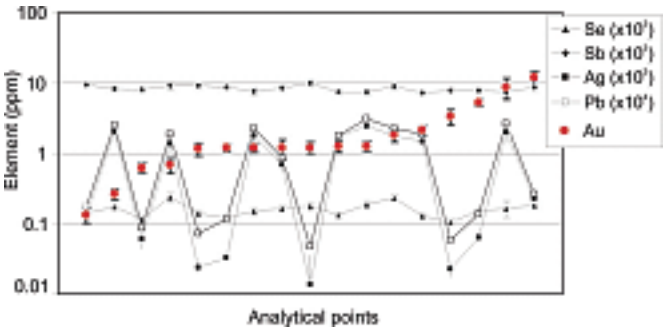

Figure 3. Concentrations of Au (together with Se, Sb, Ag and Pb) in all the ablated points in Tbs, arranged in order of increasing Au abundance. Note lack of correlation between Au and any other element, excellent correlation between Pb and Ag, as well as relatively constant values for Sb and Se.

5. ANNEALING-QUENCHING EXPERIMENTS

A thin slice was cut from the above sample and placed in a graphite crucible for heating in a furnace. Considering the temperature for the eutectic assemblage present in the sample described above, the experiment was set at 490ºC, i.e., 15ºC above the eutectic temperature. The experiments were run at 1 bar given the minor effect of pressure on telluride melts. The aim was to attain homogenisation of the Tbs-Au patches via melting and to observe the resulting quenching textures. The sample was taken out and quenched in water after 2 hours. The sample, as well as several melt droplets formed on the surface, were separately mounted in resin and polished for investigation by SEM and electron microprobe.

All the patches (up to 1 mm) found in the mounted block show quenching textures indicating homogenisation *via* melting. Non-melted domains of native Au or Tbs were found separately in some of these (Fig. 4a, b). In all the patches, as well as

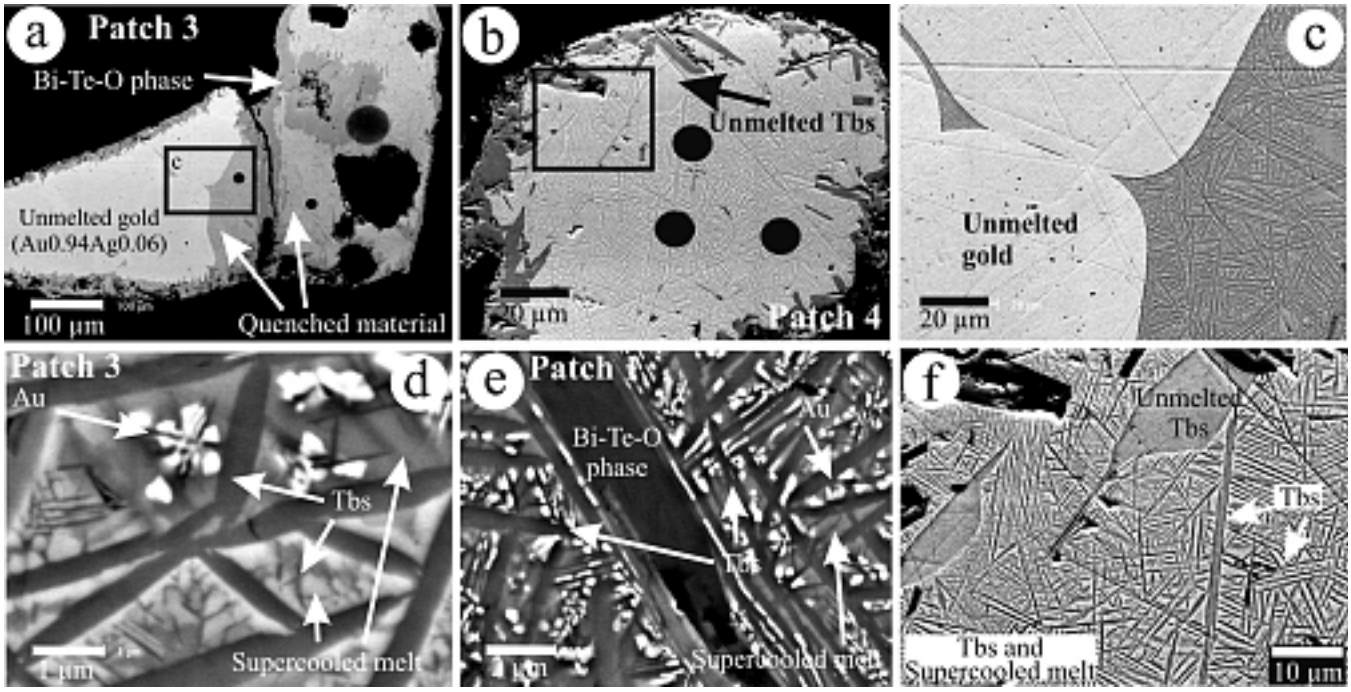

Figure 4. Back-scattered electron images of quenched materials obtained by annealing of Oya sample. (a) and (b) Patches that contain portions of unmelted native gold (in a) and Tbs (in b) adjacent to quench products. Both contain a Bi-Te-O phase armouring and intruding the patches and, in b, crosscutting relict Tbs. (c) Detail of quenched product in a, showing Tbs network as the primary product of crystallisation and corrosion of native gold by melt. (d) and (e) Details of three component quenching products, Tbs, native gold and supercooled melt. Note, in e, the same Bi-Te-O phase replacing Tbs which formed as a primary product from the melt (compare with b). (f) Detail of two-component quench material (in b). Note relationship of quench material with relict Tbs. Black spots represent points of electron probe microanalysis.

in the separately-mounted blebs, the quenching textures comprise the same regular network of Tbs laths (1-2 µm in width) as the first product of crystallisation (Fig. 4c-f). The domains between these lamellae show variation in the texture, size and number of components, from one patch to another. In such domains, skeletal native gold is present in all cases (Fig. 4d, e) except the one in which Tbs relicts are preserved (Fig. 4f). A second component, always present in these domains, is thinner lamellae of Tbs. In the quenched textures of those blebs mounted separately, in which the textures are the finest of all, Tbs and Au form symplectite domains rimmed by coarser gold grains. In the same domains between the Tbs laths, there is always a third component (supercooled melt?); this has a brighter colour than Tbs on back-scattered electron images (Fig. 4d, e). The patch that contains relict Tbs and no gold is composed of this phase occurring interstitial to Tbs lamellae (Fig. 4f). The patches are armoured by a Bi-Te-O-phase (Fig. 4a) that crosscuts the relict Tbs domains (Fig. 4b), and also forms along the Tbs laths within the coarser network (Fig. 4e). This indicates that some degree of oxidation of the melts, or a portion thereof, occurred during the experiment. The crosscutting relationships are indicative of the relict character of Tbs in Fig. 4b.

We measured the averaged 'bulk' compositions of the quenched products (resulting from melts) in 5 patches and one bleb using a defocused electron microprobe beam (size 10 µm) (Table 1). Even though the differences between individual patches are relatively small, i.e., a few wt. % for the major components, the patch that contains no gold in the quenched material is distinct because it has the lowest Au and highest Te contents in the dataset. All the analysed patches include Ag (3.61-6.19 wt.%). The Ag content in the unmelted native gold and the adjacent quenched melt are the same (3.6 wt.%). We note that this is a much lower value than the Ag measured in native gold before the experiment, suggesting that Ag migrated into the melt during annealing. The Pb content varies in individual patches (up to 4.39 wt.%), as found in the starting material. The melts have variable Bi/Bi+Te ratios, indicating that the compositions are higher in Te relative to Bi and are offset from the expected ratio of 0.4 that characterises Tbs (the only Bi-telluride in the starting material). This can be partly attributed to analytical error due to the inherent inhomogeneity of the intergrowths in the quenched material. However, a second and more plausible factor is the oxidation reaction that occurred during the experiment and which consumed Bi at a faster rate than Te.

A plot of the mean compositions of the patches (ignoring Pb and Ag) on the Au-Bi-Te diagram (Prince et al., 1990; Fig. 5) shows that they are offset from the eutectic line Tbs-Au where they should ideally have been considering a two-component starting material. We can, however, approximate their position on this line by taking their Au ratios into consideration (grey field on Fig. 5). The melts that include gold in the quenched material form a cluster parallel to the cotectic line between the Tbs+Au and Tbs+Au+calaverite (Cal) eutectics, except the patch without gold.

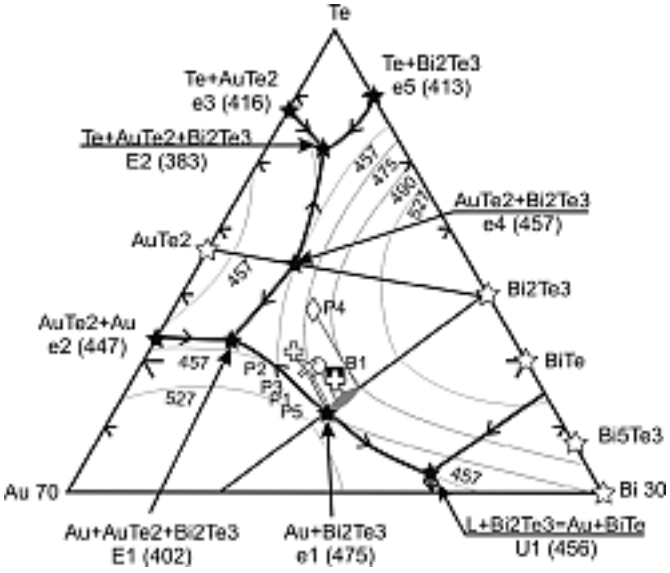

Figure 5. Mean compositions of patches and blebs of quenched melts (P1-P5, B1, see Table 1), plotted on the Te-rich segment of the ternary Au-Bi-Te solvus diagram (after Prince et al., 1990). This shows their position relative to eutectics (E, e) and phase fields. The points are offset from the Bi_2Te_3-e1 line, but Au content in each is used to bring them onto the line. Grey oval represents the compositional field of the melts obtained by annealing. Temperatures in ºC; see text for aditional explanation.

6. DISCUSSION

Tellurobismuthite, one of the simplest structures in the tetradymite group (Cook et al., in press) consists only of 5-atom Te-Bi-Te-Bi-Te layers and can incorporate elements such as Pb, Sb, substituting for Bi, and Se, and S for Te. In the present data, Sb and Se show constant contents throughout the LA-ICP-MS analytical dataset for Tbs (Fig. 3). In contrast, Pb is highly variable and correlates with Ag, an element that, although reported in rucklidgeite, $(Bi,Pb)_3Te_4$, is not generally considered to be incorporated into the Tbs structure. A coupled Pb+Ag ↔ Bi substitution is ruled out by the fact that the values for the two elements differ by an order of magnitude. The lack of correlation between Au and Ag on most of the LA profiles for Tbs indicates that the two elements are not incorporated in the same site in the structure. Instead, sub-μm inclusions of galena may be present within Tbs. The high number of Tbs LA-ICP-MS analyses with a relatively steady Au signal indicates that this element is in solid solution rather than present as tiny particles, as for example in the Orivesi deposit, Finland (Cook et al., this volume). However, the Au contents are much lower than those in Orivesi (1-313 and 0.13-12.2 ppm in Orivesi and Oya, respectively), for which a comparable temperature range is considered. The values obtained for Oya are below the saturation limit for Au in Bi_2Te_3 at 400ºC (Keys and Dutton, 1963 in Prince et al., 1990) by at least 1 order of magnitude. This may indicate that the solubility of Au in Tbs is lower when co-crystallising with Au, especially in a melt scenario as that postulated for Oya. Variation in Au values within the same patch (Fig. 2a) may be attributed to specific rates of nucleation of Tbs in individual aggregates that result from molten precipitates, especially if inhomogeneity of the Au distribution occurs during slow cooling of the precipitate. The melt compositions obtained after quenching support the idea of variability in some minor elements (e.g., Pb) within individual patches.

Annealing-quenching experiments, although hampered by an oxidation that influenced the results, can nonetheless provide useful insights into understanding the role played by melts from the Au-Bi-Te system in assisting formation of Au deposits. The Oya material was chosen because of the simple association representing the highest temperature eutectic in that system.

The fact that all the quenched products show crystallisation of Tbs as an early component indicates that, in our experiment, all the melts were formed from the eutectic point (475ºC), following the Tbs solvus branch up-temperature (giving the observed hypoeutectic textures relative to gold; Reed-Hill and Abbaschian, 1994). This is despite the fact that at this temperature, Au-rich melts (gold solvus branch) can also form in the Au-Bi_2Te_3 system (Gather and Blachnik, 1974). The latter scenario would have resulted in formation of gold instead of Tbs as a first product interstitial to the Au-Tbs symplectites. Melting continued up-temperature from the eutectic incorporating variable amounts of Tbs and Au, depending upon the different proportions of the two components and their relative geometries in individual patches. The geometry affecting the melt compositions is not necessary the same as during deposition of molten precipitates in the veins. The fact that melts obtained by equilibration either with Au or Tbs (Fig. 4a, b) have comparable compositions with the other melts indicates, however, that the initial precipitates in the analysed sample had a limited compositional range at this temperature. Although equivocal, this may be considered an argument favouring exsolution of melts from fluids, since the alternative precipitation-upon-saturation process would be more likely to produce an uneven distribution of Tbs and Au at the same location.

The lower the amount of Au incorporated, the higher the temperature at which crystallisation starts for the melts obtained during annealing. The temperatures of the melts and the respective eutectics shown in Fig. 5 need however to be amended to take the minor components (e.g., Ag and Pb) into consideration. These temperatures would be lowered by at least 10-15ºC due to the effect of the melting (freezing) point depression (e.g., Anderson, 2005). We can interpret the cooling paths during annealing by considering an

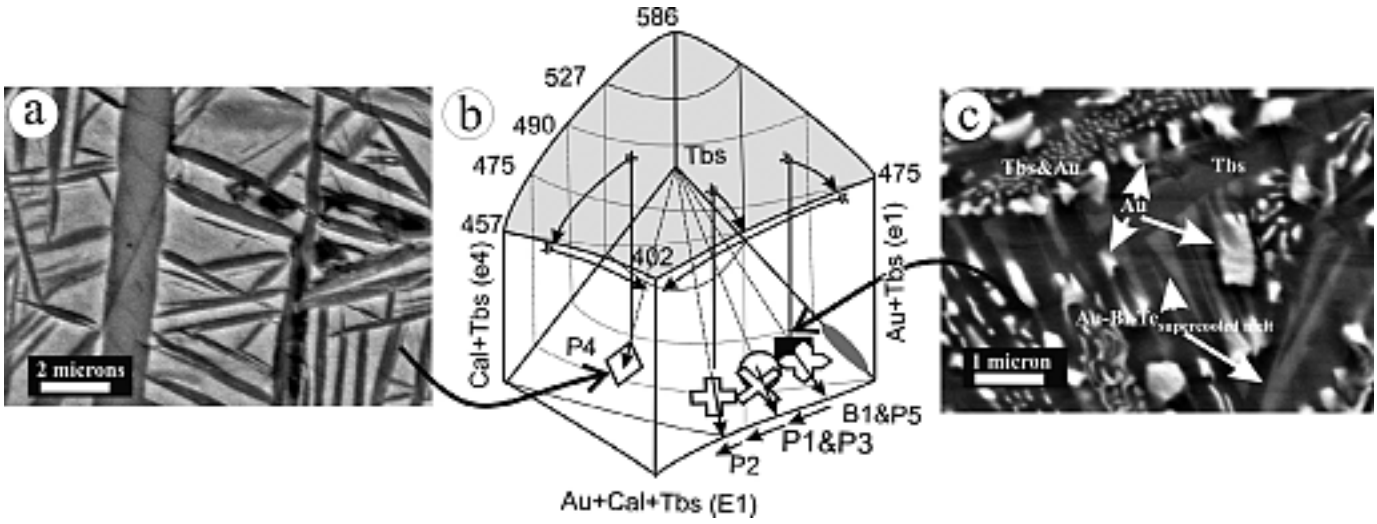

Figure 6. Interpretation of the two types of quench textures: (i) two-component, Tbs (dark) and supercooled melt (light) in a; (ii) three-component, Tbs, native gold and supercooled melt in c, using (in b) an oblique view of the T-composition section for the ternary eutectic at 402ºC in the Au-Bi-Te system. The shaded area at the top represents the melt section between Tbs and the eutectics e4, E1 and e1. The triangle underneath represents the compositional section for this area that includes the mean compositions of quench projects (see also Fig. 5). Isotherms are shown on both surfaces by thin lines. Dashed lines are tie-lines connecting Tbs and individual compositions. Ideal cooling paths are shown by double-tailed arrows; true cooling paths, as recorded in the textures, are shown by simple arrows.

oblique view of T-X (composition) sections for the ternary eutectic in the Au-Bi-Te system at 402ºC (Fig. 6b). Crystallisation of all melts started when the liquid surface was met at each respective composition, and this continued along a straight line (from Tbs to the respective composition) until it reached one of the cotectic lines that joins at 402ºC to form the ternary Tbs-Au-calaverite (Cal) eutectic. The melt products that include gold then began to crystallise the Tbs+Au association (Fig. 6c) when they reached the line (Tbs-Au)-(Tbs-Au-Cal) (Fig. 6b). In contrast, the melt without gold (Fig. 6a) froze before reaching the (Au-Cal)-(Au-Cal-Tbs) line.

Although freezing of metallic alloys normally requires cooling rates in excess of 105 K/s (Reed-Hill and Abbaschian, 1994), the small size of this patch can be considered to impact upon the critical rate at which cooling is faster than crystallisation and transforms the melt into a supercooled liquid (Fig. 6a). The composition of product that is interstitial to Tbs in this figure cannot be determined precisely because it is intergrown with Tbs, but is clearly not Cal (which should appear darker than Tbs on BSE images). For the same reasons, we consider that the third phase occurring in the other quenching materials (Figs. 4c, d and 6c) also represents a supercooled melt formed before reaching the ternary eutectic at 402ºC. Apart from the already mentioned minor elements in the melts, other components such as Cl may also lower the temperature at which melts form, although these temperatures will probably remain at values around or just above 450ºC.

7. CONCLUDING REMARKS

The Japanese hypo/mesothermal gold veins were classified as such by comparison with numerous younger Tertiary-Quaternary deposits that show clear epithermal affiliation and temperatures in the range 200-270ºC. Gold-bismuth-telluride assemblages, like that in the Oya deposit, are to be expected in the kind of intrusion-related Au-Bi deposits described by Baker et al. (2005) if the fluids would be oxidised (pyrite field). Such deposits, many of which are associated with Sn-W provinces, are characterised by either (i) high-temperature (>350ºC), immiscible brine (>30 wt.% NaCl equiv.) and low-salinity (<5 wt.% NaCl equiv.) vapour that commonly contains CO_2, in a shallow environment, or (ii) abundant low-salinity, CO_2-

rich aqueous fluids (<10% NaCl equiv.), in deeper environments (>5 km).

The presently available fluid inclusion data for Oya do not allow us to suggest that this deposit conforms to either of these environments or to make any inferences about whether Oya is a member of the broad 'intrusion-related' deposit type at all. A deeper environment would allow calculation of higher temperatures because of pressure correction of the fluid inclusion measurements.

The results of this study show that the temperature estimation for the Au-Bi-Te melt model (~450ºC) is appreciably higher than the temperature range given in the published fluid inclusion studies (270-350ºC). Further experiments are required to constrain the lowermost melt temperature of such an assemblage. The content of other metals, in particular Ag and Pb, as well as the role played by Cl, I, Br and H_2O at the time of melt exsolution from fluids (Mavrogenes and collaborators, unpubl. data) would lower the melt-forming temperature based on the Au-Bi-Te system under dry experimental conditions.

Even though the melt scenario may not be valid at Oya, this approach can be applied to deposits that have temperatures of formation in the range of 400-450ºC, including deeper intrusion-related gold, orogenic gold and skarn systems. The association discussed here is co-stable with pyrite-hematite and would not apply to mineralising systems in which reduced fluids are considered.

REFERENCES

Anderson, G., 2005. Thermodynamics of Natural Systems, 2nd edition. Cambridge Univ. Press, 648 pp.

Baker, T., Pollard, P.J., Mustard, R., Mark, G., Graham, J.L., 2005. A comparison of granite-related tin, tungsten, and gold-bismuth deposits: implications for exploration. SEG Newsletter no 61, 5, 10-17.

Ciobanu, C.L., Cook, N.J., Pring, A., 2005. Bismuth tellurides as gold scavengers. Mineral Deposit Research: Meeting the Global Challenge (J.W. Mao & F.P. Bierlein, eds.), Springer, Berlin, p 1383-1386.

Cook, N.J., Ciobanu, C.L., 2005. Tellurides in Au deposits: implications for modelling. In: Mineral Deposit Research: Meeting the Global Challenge (J.W. Mao & F.P. Bierlein, eds.), Springer, Berlin, p. 1387-1390.

Cook, N.J., Ciobanu, C.L., Wagner, T. and Stanley, C.J., 2007, in press, Minerals of the system Bi-Te-Se-S related to the tetradymite archetype: review of classification and compositional variation. Can. Mineral.

Cook, N.J., Ciobanu, C.L., Danushevskiy, L., 2007, this volume. LA-ICP-MS determination of gold in Bi-minerals from deposits in the Fennoscandian Shield.

Enjoji, M., Takenouchi, S., 1976. Present and future researches of fluid inclusions from vein-type deposits. Mining Geol. Spec. Issue 7, 85-100.

Gather, B., Blachnik, R., 1974. The gold-bismuth-tellurium system. Z. Metallkunde 65: 653-656.

Prince, A., Raynor, G.V., Evans, D.S., 1990. Phase diagrams of ternary gold alloys. Inst. of Metals, London, 505 pp.

Reed-Hill, R.E., Abbaschian, R., 1994. Physical Metallurgy Principles, 3rd edition. PWS Publ. Co., Boston, 926 pp.

Shikazono, N., Shimizu, M., 1988. Electrum: Chemical composition, mode of occurrence, and depositional environment. Univ. Tokyo Press, 81 pp.

Tomkins, A.G., Mavrogenes, J.A., 2002. Mobilization of gold as a polymetallic melt during pelite anatexis at the Challenger deposit, South Australia: a metamorphosed Archean gold deposit. Econ. Geol. 97, 1249-1271.

LA-ICP-MS determination of gold in Bi-chalcogenides from four deposits in the Fennoscandian Shield

Nigel J. COOK, Natural History Museum, University of Oslo, Boks 1172 Blindern, NO-0318 Oslo, Norway

Cristiana L. CIOBANU, Mineralogy Group, South Australian Museum, North Terrace, Adelaide, S.A., 5000 Australia, and Department of Earth and Environmental Sciences, University of Adelaide, S.A., 5005 Australia

Leonid DANUSHEVSKIY, CODES, University of Tasmania, Hobart, Tasmania, Australia

Summary. Gold concentrations in Bi-chalcogenides (tellurobismuthite and laitakarite) from four deposits in the Fennoscandian Shield have been determined by LA-ICP-MS. Both minerals contain gold above background levels, with tellurobismuthite from Orivesi (Kutamejärvi), Finland, with concentrations between 1 and more than 300 ppm. The concentrations of gold vary over two orders of magnitude within individual analysed patches. The gold signal in the majority of individual LA-ICP-MS profiles is irregular. Laitakarite from Orijärvi (Finland) contains lesser concentrations (up to 10 ppm). Tellurobismuthite in two Sveconorwegian orogenic gold occurrences differ markedly; 798 and 2,472 ppm in Glava (Sweden) and <1 ppm at Moberg (Norway). The present dataset shows that Bi-chalcogenides may, in some cases, be considered as gold carriers, and can contain gold at similar levels as pyrite. Measured concentrations in tellurobismuthite are, with the exception of Glava, lower than those obtained in published experimental work on that mineral. This is interpreted as due to the formation of discrete sub-μm sized inclusions of gold within the Bi-minerals during post-depositional overprinting. The influence of metamorphism is clearly an important factor in determining the distribution of gold within Bi-chalcogenides.

Key Words: gold ores, tellurobismuthite, laitakarite, gold, laser ablation, ICP mass spectra, Orivesi, Orijärvi, Finland, Glava, Sweden, Moberg, Norway

1. INTRODUCTION

Tellurides, selenides and sulphosalts of bismuth are a group of minerals that are not uncommon as accessories in Au-deposits and Au-enriched base metal deposits from across the Fennoscandian Shield (Fig. 1), as in other parts of the world. In some cases, they are persistent trace minerals throughout entire orebodies (e.g., Orivesi, Finland). In other cases, they occur together with higher-than-average gold concentrations within relatively limited parts of the ore. Bismuth tellurides are reported from about 40 of the 100 or so gold deposits in the shield, whereas Bi-selenides are known from only few deposits (e.g., Orijärvi, SW Finland, Falun, Bergslagen, Sweden and in parts of the Skellefte District, Northern Sweden).

A number of recent publications by the present two senior authors (Ciobanu et al., 2005, 2006a, b) have drawn attention to the role which Bi-minerals, and minerals of the tetradymite group (Cook et al., 2007), in particular, may play in concentrating gold in a given deposit. Available data (Gather and Blachnik, 1974) suggests that the solubility of Au in Bi-Te intermetallic compounds is ca. 1 mol. %; similar values are given for the solubility of Au_2Bi in Bi_5Te_3 and Bi_7Te_3, and of $AuTe_2$ in Bi_2Te_3. The solubility of Au in synthetic Bi_2Te_3 strongly varies with temperature, i.e., within the range 0.002 atom.% at 200ºC to 0.02 atom.% at 400ºC (Keys and Dutton, 1963 in Prince et al., 1990). The discrepancy between these values underlines that there is uncertainty about the levels that Au may reach in these phases. What Au contents could be found in Bi-tellurides from natural specimens? Are the values high enough for them to be considered as gold carriers? To answer these questions, we used the LA-ICPMS technique to measure Au contents in some key deposits.

We have chosen three deposits from different parts of the shield, which share tellurobismuthite

(Bi_2Te_3) as the dominant Bi-telluride. A further deposit contains laitakarite (Bi_4Se_3) as the main Bi-phase reported. Are the differences in gold contents among these of any genetic significance?

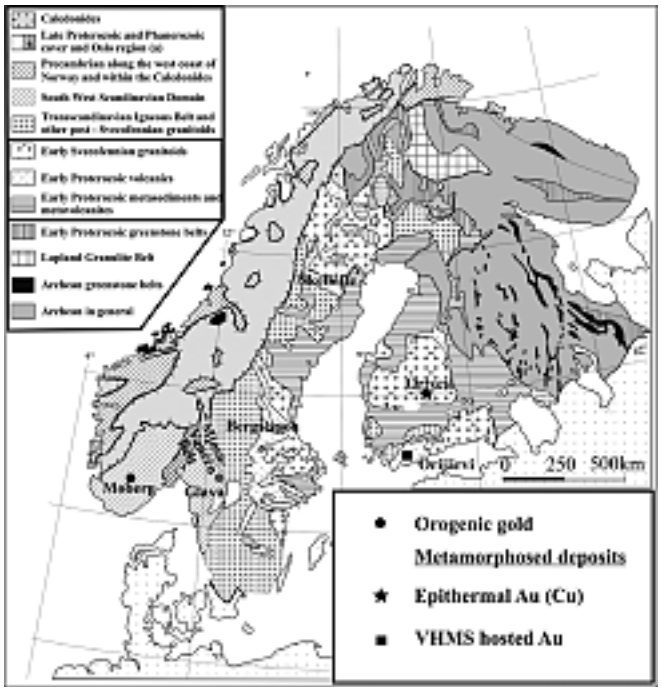

Figure 1. Geological sketch map of the Fennoscandian Shield showing the location of the studied deposits. Geology and main divisions after Sundblad (2003).

2. DEPOSITS & MINERAL ASSEMBLAGES

Orivesi (Kutemajärvi), Finland

The Orivesi deposit is presently one of the largest operating gold mines in Finland. The deposit was discovered in 1981 and mining commenced in 1994. Kojonen (2006) gives an average grade of 9.7 g/t Au and remaining known ore reserves as 0.658 Mt at an average grade of 9.8 g Au/t.

The deposit is hosted within sericite-quartz schists belonging to the 1.9 Ga Svecofennian volcano-sedimentary Tampere schist belt. Kojonen et al. (1999) and others have described the deposit, considering it to represent a metamorphosed epithermal deposit. Metamorphic conditions are estimated at ca. 470-570ºC and 3-4 kbar. The genesis of the deposit is, however, debated.

Although the telluride assemblages include numerous other species (including tetradymite, tsumoite, rucklidgeite, joséite-B, kawazulite, hessite, petzite, krennerite, sylvanite, coloradoite, frohbergite, melonite and altaite), tellurobismuthite (Tbs) is the most widespread. Gold is chiefly present as native gold in pyrite, arsenopyrite and quartz, intergrown with telluride minerals or as free grains in the silicate matrix. We studied a mica-bearing schist in which Tbs forms mm- to cm-sized patches in quartz (Fig. 2).

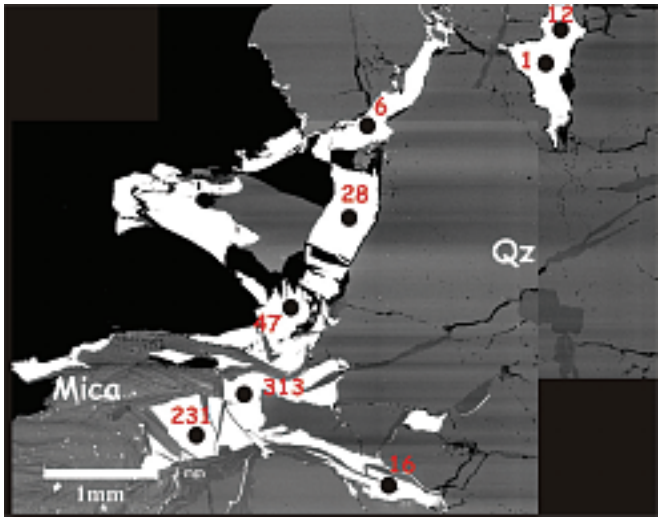

Figure 2. Back-scattered SEM image showing grains of tellurobismuthite (bright white) in a matrix of quartz and white mica. Black spots mark ablation spots. Measured gold contents are indicated in red (ppm).

Glava (Sweden)

The small Glava Au-Ag-Cu vein deposit, Värmland, Sweden (e.g., Scherbina, 1941; Oen and Kieft, 1984), is an example of an orogenic deposit in the Southwest Scandinavian domain of Sveconorwegian (ca. 0.9 Ga) age (Sundblad, 2003). The deposit is one among many located in a belt between the lakes Vänern (Sweden) and Mjøsa (Norway), (e.g., Alm and Sundblad, 1994). The deposits are hosted within a suite of 1.6-1.1 Ga granitoids, gneisses and metasediments.

Glava stands out as one of the most mineralogically diverse in the Fennoscandian Shield with repect to tellurides and selenides (hessite, tetradymite, tellurobismuthite, volynskite, altaite, native tellurium, petzite, sylvanite, stützite, clausthalite, Co-bearing melonite, calaverite,

empressite, naumannite, weissite, rucklidgeite (Scherbina, 1941; Oen & Kieft, 1984). The assemblage also contains kawazulite and Se-bearing tellurobismuthite (Cook et al., 2007) and the rare Au-Cu telluride kostovite, $AuCuTe_4$ (Bonev et al., 2005).

At Glava, bornite is the main sulphide, although others (chalcopyrite, pyrite, sphalerite, galena, arsenopyrite, molybdenite, chalcocite, digenite, wittichenite, cobaltite, linnaeite, pyrargyrite, greenockite, cobaltite, and mckinstryite) may be present throughout the deposit.

In the sample studied, bornite veinlets occur in a pink granitic gneiss. Chalcocite replaces bornite; magnetite and hematite are also present. The granite is altered by epidote-bearing veinlets, which also carry coarse titanite; they clearly postdate bornite deposition. Tellurides and selenides occur as small inclusions, a few µm to 100µm in size, within the bornite and along the alteration veinlets (Fig. 3). The selenides, in particular, are characterised by a droplet-like morphology when enclosed within bornite. In the altered area, tellurides are associated with patchy bornite.

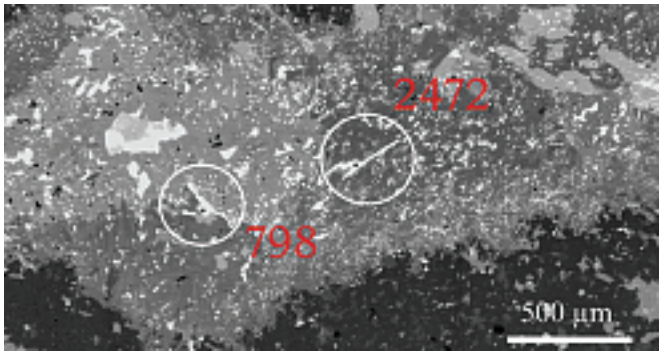

Figure 3. Back-scattered SEM image showing inclusions of telluride minerals (white) along an epidote veinlet; Ablated tellurobismuthite grains are circled. Gold concentrations (ppm) in individual spot analyses are given in red.

Native gold and electrum forms small inclusions which are always associated with the Bi-tellurides (-selenides) or as skeletal filaments in kawazulite, tellurobismuthite or hessite. The assemblage contains the association native tellurium + tellurobismuthite, which is indicative of precipitation from oxidised fluids. In these samples, tellurobismuthite is by far the dominant telluride. This may occur alone, or in association with any of the other telluride/selenide species.

Moberg (Norway)

Moberg is among several probable orogenic gold deposits within Late Proterozoic Sveconorwegian terranes in Norway. These localities include numerous hydrothermal quartz veins and minor sulphide occurrences in Telemark County (Mosnap and Grusen are others). Moberg was one of the small mines that flourished in southern Norway during the reign of King Christian III, 1536-1559, producing Cu (+ Ag and Au?) until abandoned around the middle of the 16th Century. The deposits are base metal-bearing quartz veins but also contain gold and bismuth minerals (Vogt, 1886). The veins are associated with dykes and Precambrian granites that intrude the supercrustal sequence (Telemark Suite). Vogt shows one vein at the contact between granite and quartz-rich mica schist. The specimen we investigated consists of mm-sized patches of Tbs within quartz (Fig. 4).

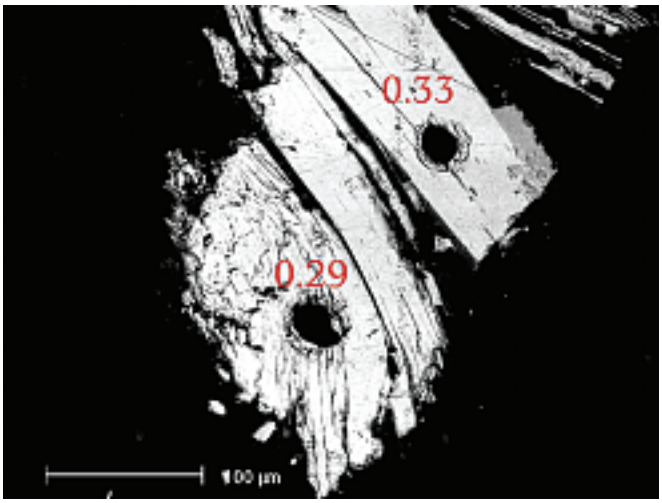

Figure 4. Back-scattered SEM image showing blades of tetradymite (white) in a quartz matrix, with ablation holes. Gold concentrations (ppm) in individual spot analyses are given in red.

Orijärvi (Finland)

Southwestern Finland is part of a metallogenetic belt that extends from Bergslagen in south-central Sweden to northern Estonia (Sundblad, 2003). Orijärvi is the most significant sulphide ore in SW Finland. The deposit is hosted by 1.9 Ga old supracrustal rocks, which were deformed and metamorphosed during the Sveco-karelian orogeny (Väisänen et al., 2002 and references therein). The Orijärvi deposit is situated in the middle part of the Uusimaa belt, on the northern side of Orijärvi pluton. The deposit is hosted by altered volcanic rocks that form a 700 m wide Al-Mg-(Fe) alteration halo, with cordierite and anthophyllite as key minerals (Latvalahti, 1979). Orijärvi is an area typical of a high-grade metamorphic terrain (600±50°C, 3-5 kbar; Schreurs and Westra, 1985), in which the association of massive sulphide ores with cordierite-anthophyllite rocks was at the heart of the debate as to whether the association is due to intrusion-related metasomatism (e.g., Eskola, 1914) or to regional metamorphism of fossil VHMS systems (e.g., Berge, 1978).

The ores are dominated by sphalerite and galena, with subordinate pyrite and chalcopyrite, Orijärvi is the type locality for laitakarite, $Bi_4(Se,S)_3$ (Vorma, 1960). Although Orijärvi was exploited principally for base metals, sub-ppm levels of gold (0.4 ppm) have been reported (www.gsf.fi).

Laitakarite at Orijärvi is described from veinlets, in which minor chalcopyrite, pyrrhotite and molybdenite are also present, located at the contact between amphibolite and cordierite-anthophyllite rocks, a few metres from the main sulphide body (Vorma, 1960). Associated phases include native bismuth, bohdanowiczite ($AgBiSe_2$), clausthalite, native silver and Se-bearing galena (Ciobanu et al., 2002).

In the studied sample (Fig. 5), laitakarite forms mm-scale veinlets in cordierite-anthophyllite schist overprinted by a chlorite-bearing retrograde assemblage. Deformation of laitakarite is accompanied by replacement, seen in marginal haloes of Ag_2S and inclusions of native bismuth that dissipate, as trails of droplets, into the host rock away from the veinlets.

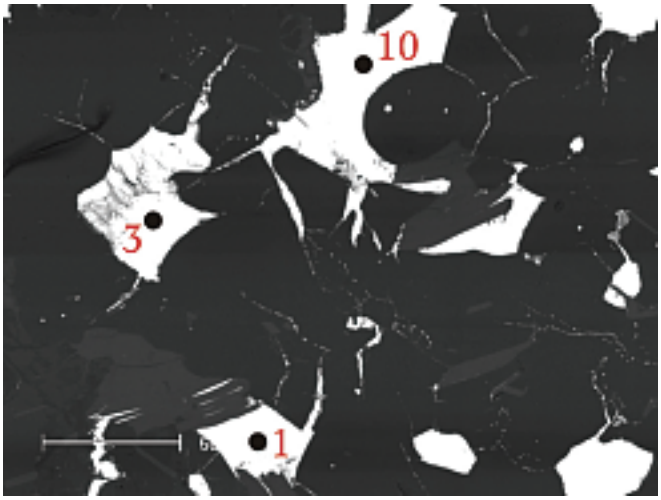

Figure 5. Back-scattered SEM image showing ablated grains of laitakarite (white) in cordierite-anthophyllite schist. Scale bar: 50 µm. Gold concentrations (ppm) in individual spot analyses are given in red.

3. LA-ICPMS ANALYSIS

Experimental

LA-ICP-MS analysis was carried out using the Agilent HP4500 Quadripole ICP-MS instrument at CODES, University of Tasmania, equipped with a high-performance New Wave UP-213 Nd:YAG Q-switched laser ablation system and MEOLaser 213 software. We performed spot analyses (12-80 µm in diameter, depending on size of the target mineral), monitoring the following isotopic abundances: ^{197}Au, ^{130}Te, ^{209}Bi, ^{208}Pb, ^{107}Ag, ^{77}Se, ^{121}Sb and ^{75}As. Total analysis time was 90s (30s pre-ablation and 60s ablation time). Calibration was performed on a doped pyrite standard; Te served as the internal standard for the tellurides and Se for laitakarite.

Results

Representative LA-ICP-MS depth profiles for each of the investigated deposits are shown in Figures 6, 8, 9 and 10.

Tellurobismuthite from *Orivesi* is characterised by varying concentrations of gold, ranging from 1 to 313 ppm (8 analyses). We note generally

smooth ablation profiles, indicating relatively homogeneous distribution of gold within the Bi-telluride, although occasional 'bumps' (as seen on Fig. 6) suggest that sub-microscopic inclusions of gold minerals may also be present.

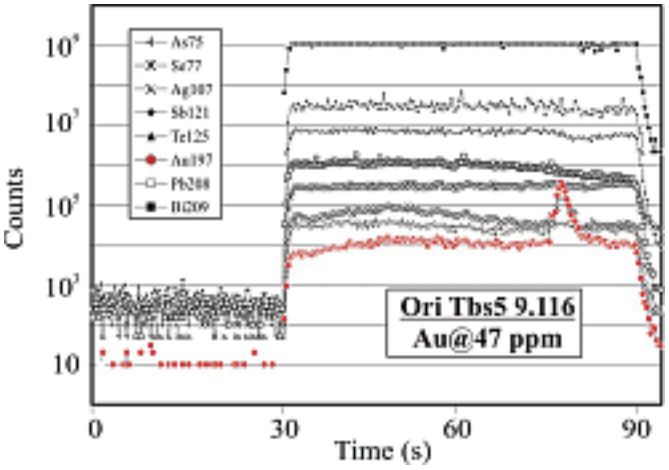

Figure 6. Laser ablation profile of a representative grain of tellurobismuthite from Orivesi. Hole diameter 80 µm, ablation frequency 5 Hz.

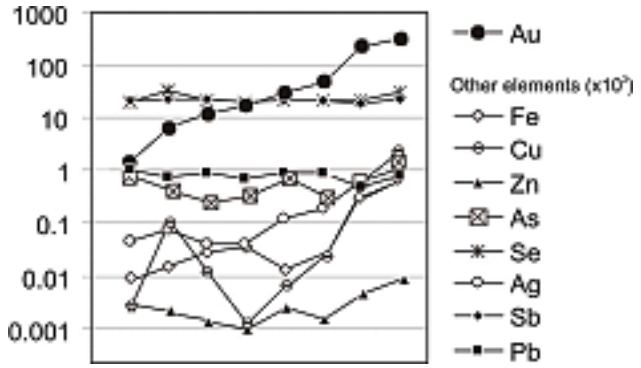

Figure 7. Concentrations of gold in tellurobismuthite from Orivesi (individual spot analyses, ppm, arranged in order of increasing concentration) compared with the concentrations of other elements to assess inter-element covariance.

A feature of the Orivesi data set is that gold concentrations are not covariant with those of other elements that commonly substitutes within the structures of Bi-tellurides (Sb, Pb, Se). Au does, however, show covariance with Ag and Fe, and to a lesser extent with Zn, As and Cu.

Although the small size of individual grains in the *Glava* sample hampered analysis, two LA-ICP-MS spot analyses of Tbs showed the mineral to be a significant host for gold, with concentrations of 798 and 2,472 ppm. However, the ablation profile showed wt.% levels of Cu, indicating some ablated material was from adjacent bornite.

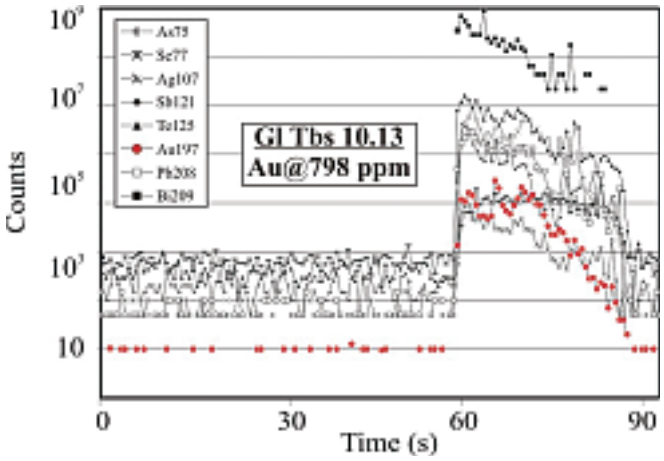

Figure 8. Laser ablation profile of a representative grain of tellurobismuthite from Glava. Hole diameter 12 µm, ablation frequency 5 Hz.

Two LA-ICP-MS spot analyses of Tbs from *Moberg* gave gold concentrations of 0.3 ppm.

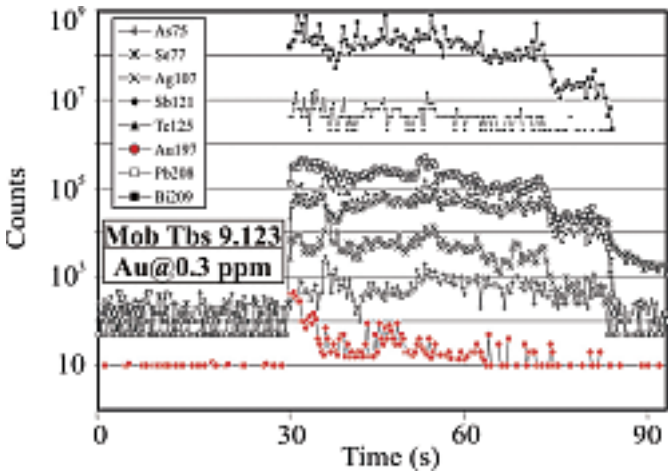

Figure 9. Laser ablation profile of a representative grain of tellurobismuthite from Moberg. Hole diameter 25 µm, ablation frequency 5 Hz.

Laitakarite from *Orijärvi* is characterised by smooth ablation profiles, indicating an inhomogeneous distribution of gold at concentrations ranging between less than the minimum detection limit (0.02 ppm) to 10.3 ppm (5 analyses).

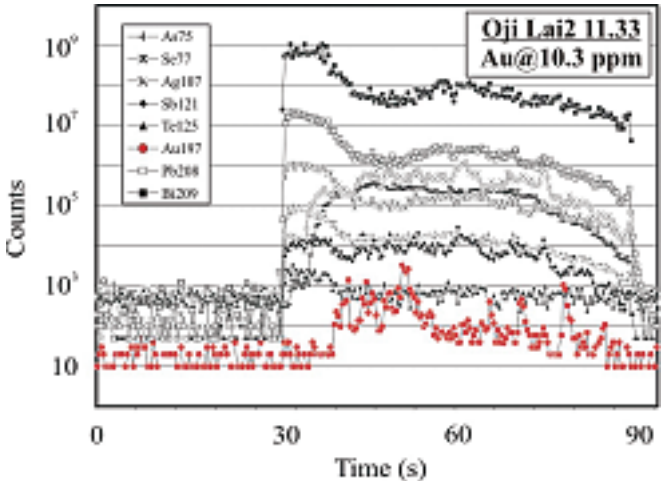

Figure 10. Laser ablation profile of a representative grain of laitakarite from Orijärvi. Hole diameter 30 µm, ablation frequency 5 Hz.

4. DISCUSSION AND CONCLUSIONS

The dataset shows that all the analysed Bi-minerals contain measurable amounts of gold. However, the concentrations of gold vary from one deposit to another, as well as within individual analysed patches. For example, at Orivesi, the measured Au content within a 1 mm patch of Tbs ranges across two orders of magnitude. Although the gold signals can be steady across the ablated depth profile, this tends to be the exception rather than the rule. The highest amount of Au was recorded in the orogenic gold occurrence at Glava, at values above those given by Keys and Dutton, 1963 in Prince et al., 1990). However, these values should be regarded as only preliminary. Investigation of a larger population of coarser Tbs grains will be required to give a definitive assessment of the average concentration for this occurrence. In contrast, the same type of occurrence at Moberg shows minimal gold values.

Gold concentrations in Tbs from Orivesi (1-313 ppm) are the closest to published values on synthetic analogues. We note, however, that only two of the eight analyses are >100 ppm and therefore correspond to the upper limit for Au incorporation in Tbs at 400ºC. Three of the values are between 10 and 100 ppm, the remaining three are <10 ppm (Figs. 2 and 7). This correlates with the fact that the gold trends on the profiles are paralleled by those of a number of other elements, notably As and Fe, which normally do not substitute into Tbs. This supports the conclusion that inclusions of gold and sub-µm sulphide inclusions occur within the Tbs patches. The amount of gold actually in solid solution within Tbs is no more than 50 ppm (e.g., Fig. 6). Similar conclusions can be drawn for the Moberg and Orijärvi occurrences, where inclusions of gold are present within the Bi-minerals.

All analysed minerals belong to the tetradymite group of Bi-chalcogenides, Bi_xX_y (X=Te, Se,S; Cook et al., 2007). Their structures consist of two types of layers: (i) Bi-Bi two-atom layer; and (ii) X-Bi-X-Bi-X five-atom layer. The individual members of the group are characterised by different stacking sequences between the two layer types, in which Tbs has only 5-atom layers and laitakarite features a simple repetition of 2- and 5-atom layers. Weak Van der Waals bonds connect the layers, whereas covalent and metallic bonds are found in the 5- and 2-atom layers, respectively. Even if Au is incorporated in solid solution within the structure, this will be readily released to form discrete sub-µm inclusions between the layers. Thus, although the values obtained in the synthetic experiments show values higher than we found in natural specimens, the latter would be more likely to form discrete gold inclusions during any geological event (metamorphism, deformation) that affects the ores after initial deposition. This is very well illustrated by the presence of µm-scale gold filaments within Tbs from Orivesi in other samples from the deposit. Such exsolution of gold is clearly associated with metamorphic overprinting. The same applies to the inhomogeneities observed in laitakarite from Orijärvi. In contrast, the two orogenic gold occurrences studies show that although these minerals can form from the same fluids that deposited gold, the concentration of gold can be as much as hundreds of ppm (Glava) or as low as fractions of ppm (Moberg), depending on as-yet unknown factors.

Gold enrichment via partial melting during metamorphism can occur if a diverse telluride association is present in the primary assemblage

Tomkins et al., 2007), especially if that assemblage is Bi-rich (Ciobanu et al., 2006a). Orivesi could represent an epithermal telluride deposit that underwent regional metamorphism at 470-570ºC and 3-4 kbar. However, Tbs alone (as in the investigated material) would not have melted below 586ºC. The Au values obtained in Tbs are not inconsistent with the levels of incorporation to be expected under primary epithermal conditions at ca. 300ºC. Laitakarite from Orijärvi probably belongs to a Bi-mineral association of the type considered a pathfinder in stringer zones in a VMS environment (Marcoux et al., 1996). If prograde metamorphism (600±50°C, 3-5 kbar) could have produced partial melting of assemblages containing laitakarite (with native elements and other selenides), the greenschist-facies retrograde metamorphism noted throughout the studied material, would have been below the upper stability of laitakarite alone (stable up to 460°C). On the other hand, the telluride-rich assemblages, their associations and droplet-like shape at Glava is consistent with formation as melts at around 400°C exsolved from orogenic fluids during regional metamorphism at amphibolite facies. For example, the association native tellurium + Tbs represents one of the binary eutectic assemblages at 412°C in the system Au-Bi-Te (Gather and Blachnik, 1974). If so, the Bi-tellurides would have acted as efficient gold scavengers (Ciobanu et al., 2005), in turn explaining the high Au contents of Tbs at Glava. At Moberg, the low values obtained for Au in Tbs may be interpreted as indicating lower formation temperatures (<200°C?). However, considering the fact that the distribution of gold in a given grain aggregate can be inhomogeneous additional material deserves to be investigated.

The present dataset shows that Bi-chalcogenides may, in some cases, be considered as gold carriers, and can contain gold at similar levels as pyrite. However, unlike pyrite, where Au content generally correlates with As, there is no apparent correlation with other elements in Bi-chalcogenides, except with Ag in some cases. Supporting the above, preliminary HR-TEM studies of the same grains reported here (except Glava) has shown no correlation between stacking disorder at the lattice scale and gold concentration (e.g., extensive disordering in Tbs from Moberg; Ciobanu et al., 2006c).

Even if gold is released during post-depositional events to form visible native gold (e.g., at Orivesi), the association with the Bi-minerals is retained, often as daughter inclusions, suggesting that the Bi-minerals should be considered in any mineral recovery strategies.

ACKNOWLEDGEMENTS

We are grateful to Krister Sundblad for material from Orijärvi and for various fieldtrips throughout the region and to Kari Kojonen for guidance during a 1999 field excursion to Orivesi. CLC acknowledges receipt of an Australian Research Council Discovery grant.

REFERENCES

Alm, E., Sundblad, K., 1994. Sveconorwegian polymetallic quartz veins in Sweden. N. Jb. Mineral. Mh. 1, 1-22.

Berge, J.W., 1978. A re-examination of the association of magnesium and massive sulfide ores. Geol. Fören. Stockholm Förh. 100, 155-170.

Bonev, I.K., Petrunov, R., Cook, N.J. Ciobanu, C.L., 2005. Kostovite and its argentian varieties: Deposits and mineral associations. Geochem., Mineral. Petrol. 42, 1-22.

Ciobanu, C.L., Cook, N.J., Sundblad, K., 2002. Genetic insights from exotic trace mineral associations at Orijärvi and Iilijärvi, S.W. Finland. Metallogeny of Precambrian Shields, Ky'iv, Ukraine, 13–26 Sept. 2002. Abstract volume: pp 41-45.

Ciobanu, C.L., Cook, N.J., Pring, A., 2005. Bismuth tellurides as gold scavengers. In: Mao, J.W., Bierlein, F.P. (eds.) Mineral deposit research: meeting the global challenge, Springer, pp 1383-1386.

Ciobanu, C.L., Cook, N.J., Damian, F., Damian, G., 2006a. Gold scavenged by bismuth melts: An example from Alpine shear-remobilisates in Highis Massif, Romania. Mineral Petrol. 87, 351-384.

Ciobanu, C.L., Cook, N.J., Pring, A., Brugger, J., Netting, A., Danushevskiy, L., 2006b, LA-ICP-MS evidence for the role of Bi-minerals in controlling gold distribution in ores. 12th Quadrennial IAGOD Symposium, Moscow, Russia, 21-24 Aug. 2006.

Ciobanu, C.L., Pring, A., Cook, N.J., Self, P., 2006c. High-resolution transmission electron microscopy study of natural Bi-chalcogenides of the tetradymite group. 19th IMA General Meeting, Kobe, Japan. Program and Abstracts, 193.

Cook, N.J., Ciobanu, C.L., Wagner, T. and Stanley, C.J., 2007, Minerals of the system Bi-Te-Se-S related to the

tetradymite archetype: review of classification and compositional variation. Can. Mineral.

Eskola, P., 1914, On the petrology on the Orijarvi region in southwestern Finland. Geol. Surv. Finland Bull. 40, 1-277.

Gather, B., Blachnik, R., 1974. The gold-bismuth-tellurium system. Z. Metallkunde 65, 653-656.

Kojonen, K., 2006. Au-Ag telluride-selenide deposits in Finland. In: Proceedings of the 2006 Field Workshop of IGCP-486 `Au-Ag-Te-Se deposits´, Izmir, Turkey, 24-29 Sept. 2006 (Cook, N.J., Özgenc, İ., Oyman, T., eds.). Geochemistry and Ore Deposits Division, Department of Geology, Dokuz Eylul University, Izmir, Turkey.

Kojonen, K., Sorjonen-Ward, P., Saarnio, H., Himmi, M. 1999. The early Proterozoic Kutema gold deposit, Southern Finland. In: C.J Stanley et al. (eds) Mineral Deposits: Processes to Processing. A.A. Balkema, Rotterdam, pp 177-180.

Latvalahti, U., 1979. Cu-Zn-Pb ores in the Aijala-Orijärvi area, Southwest Finland. Econ. Geol. 74, 1035-1059.

Marcoux, E., Moëlo, Y., Leistel, J.M., 1996. Bismuth and cobalt minerals: indicators of stringer zones to massive-sulfide deposits, South Iberian Pyrite Belt. Mineral Deposita 31, 1-26.

Oen, I.S., C. Kieft. 1984. Paragenetic relations of Bi-, Ag-, Au-, and other tellurides in bornire veins at Glava, Värmland, Sweden. N. Jb. Mineral. Abh., 149, 245-266.

Prince, A., Raynor, G.V., Evans, D.S., 1990. Phase diagrams of ternary gold alloys. Inst. of Metals, London, 505 pp.

Scherbina, A.S. 1941. Die goldreiche Kupferglanz-Bornit-Lagerstätte von Glava im Vermland, Schweden, und ihre geologische Stellung. N. Jb. Mineral. Geol. Paläontol. B, 76A, 337-458.

Schreurs, J., Westra, L., 1985. Cordierite-orthopyroxene rocks: the granulite facies equivalents of the Orijärvi cordierite-anthophyllite rocks in West Uusimaa, southwest Finland. Lithos 18, 215-228.

Sundblad, K., 2003. Metallogeny of gold in the Precambrian of Northern Europe. Econ. Geol. 98, 1271-1290.

Tomkins, A.G., Pattison, D.R.M., Frost, B.R., 2007. On the initiation of metamorphic sulfide anatexis J. Petrol., 48, 511-535

Väisänen, M., Mänttäri, I, Hölttä, P., 2002. Svecofennian magmatic and metamorphic evolution in southwestern Finland as revealed by U-Pb zircon SIMS geochronology. Precambr. Res. 116, 111-127.

Vogt, J.H.L., 1886. Norske ertsforekomster. III. Om den Thelemark-Sætersdal'ske ertsformation. Archiv for Mathematik og Naturvidenskab 10, 16-59.

Vorma, A., 1960. Laitakarite a new Bi-Se-mineral. Bull. Comm. Geol. Finlande 188, 1-10.

Bi-tellurides in gold veins, BiTel Knoll (CLY prospect), southeastern British Columbia, Canada

Nigel J. COOK, Natural History Museum, University of Oslo, Boks 1172 Blindern, NO-0318 Oslo, Norway

Cristiana L. CIOBANU, Mineralogy Group, South Australian Museum, North Terrace, Adelaide, S.A. 5000 Australia and Department of Earth and Environmental Sciences, University of Adelaide, S.A., 5005, Australia

William R. HOWARD, 215 Silver Mead Cres. NW Calgary AB T3B 3W4, Canada

Abstract. Gold ores from BiTel Knoll (CLY Group), Nelson District, B.C., Canada, contain a number of Bi minerals, notably tellurides and tellurosulphides of Bi. The Bi-mineral assemblage is varied from sample to sample. Typical minerals are joséite-B (Bi_4Te_2S), joséite-A (Bi_4S_2Te), unnamed Bi_2Te, hedleyite (Bi_7Te_3), ingodite (Bi(Te,S)), native bismuth (Bi), bismuthinite (Bi_2S_3) and ikunolite (Bi_4S_3). The Bi-assemblages in the two veins are of reduced type (species with $Bi/(Te+S)\geq1$). They differ in the presence of native bismuth only in the Blue Quartz vein and ingodite only in the Eloise vein. Native gold is present as inclusions in Bi-mineral patches in both veins. Gold concentrations measured in Bi-minerals from the Eloise vein are in the range between 0.02 and 57 ppm. Concentrations vary by orders of magnitude between samples in different locations. Phase relationships and the distribution of Au in Bi-minerals support a hypothesis in which the mineralization, although formed from Au-Bi-Te-S melts exsolved from fluids, has been overprinted by a subsequent (orogenic?) event.

Key Words: gold ores, veins, tellurides, bismuthinite, electron probe data, laser ablation, ICP mass spectra, British Columbia, Canada

1. INTRODUCTION

The CLY Group of claims comprises a set of veins and skarns located near the contact to the mid-Cretaceous Bunker Hill sill, an outlier of the Wallack Creek granite, which in turn belongs to the Bayonne magmatic belt. This marks the boundary between Lower Jurassic rocks of the Quesnel Terrane to the NW and Paleozoic sedimentary rocks of the Kootenay Terrane. The geological setting of the region, structural geology of the claim area, and sulphide mineralogy have been described by Howard (this volume).

Some of the veins are sulphide-poor (at BiTel Knoll in the NE part of the claims area), others are sulphide (pyrite-pyrrhotite) rich (Bunker Hill) or are veins overprinting earlier skarn (Lefevre). All the veins contain variable amounts of gold. Geochemistry shows a strong correlation between Au and Bi in all veins in the claims area (Howard, this volume). This is most pronounced in the veins from the BiTel Knoll area, where higher gold assays are expressed as visible gold and, in some cases, are accompanied by bismuth minerals, including tellurides and tellurosulphides (collectively called 'tellurides' here). Other veins, in Bunker Hill, are characterised by micron-sized inclusions of gold within pyrite (pseudomorphosed after pyrrhotite). Rare Bi-minerals were, however, identified, but appear restricted to sulphosalts such as cosalite.

This study focuses on two veins from BiTel Knoll (Eloise vein and Blue Quartz vein) in which both native gold and bismuth minerals are present. Hand specimens from the veins show a pronounced fracturing. The blue colour is considered to be due to incorporation of bismuth minerals within the quartz. Polished blocks prepared from other veins (e.g., Ella and Clarissa veins) contained μm-sized inclusions of native gold within quartz but did not contain Bi-minerals.

The aim is to present the mineral associations in these veins. We also carried out LA-ICP-MS analysis on the Bi-minerals in the Eloise vein sample to determine their gold contents. Such

measurements are useful, together with paragenetic observations, to discuss the distribution and partitioning of gold in different species and comment on their genesis.

2. SAMPLE DESCRIPTION

Blue quartz vein

The only sulphide in the samples is scarce molybdenite, both in host rock and vein. Iron- and Ti-oxides are abundant in the host rock (biotite schist/amphibolite?), whereas rare-earth minerals are present only in the vein. Both bismuth minerals and gold (~$Au_{75}Ag_{25}$) occur as μm-sized blebs along the fractures in quartz (Fig. 1). The Bi-mineral assemblage is dominated by joséite-A (Bi_4S_2Te), bismuthinite and native bismuth. Other species are joséite-B (Bi_4Te_2S), hedleyite (Bi_7Te_3) and ikunolite (Bi_4S_3). The blebs can be mono-component, but are typically multi-component, in which native gold is also part of the assemblage (e.g., Fig. 1a). Joséite-B is found especially in blebs that contain native bismuth (Fig. 1b) and also Bi_2Te and/or hedleyite (Fig. 1a, c). Sulphur-rich blebs dominated by joséite-A may occasionally also contain ikunolite (Fig. 1d). These Bi-rich associations are similar to those typically reported from gold skarns. Although the samples are affected by weathering, native bismuth is part of the primary association, based on mutual relationships with the Bi-tellurides (e.g., Fig. 1b, c). Most abundant are blebs containing an association of native Bi + bismuthinite.

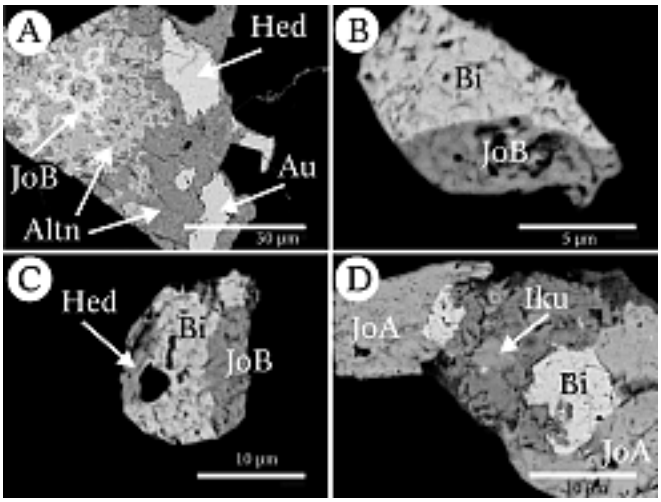

Figure 1. Back-scattered electron images showing assemblage of gold and Bi-minerals (Blue Quartz vein). Altn: alteration, Au: gold, Bi: native bismuth, Hed: hedleyite, Iku: ikunolite, JoA: joséite-A, JoB: joséite-B.

Eloise vein

Polished blocks from samples at two locations along the vein were studied. In both locations, native gold and Bi-minerals are present, although they differ in association.

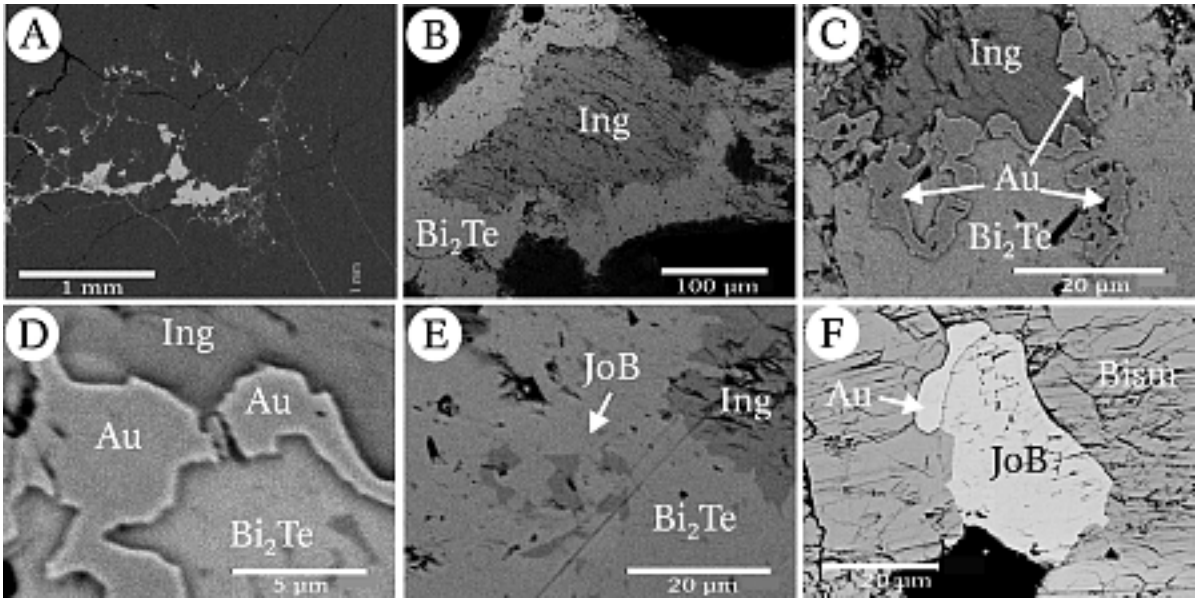

Figure 2. Back-scattered electron images showing Bi-minerals in sample 'Eloise' (a-e) and 0412a (second location, f). Bi_2Te: unnamed Bi_2Te, Bism: bismuthinite, Ing: ingodite, JoB: joséite-B, Au: gold.

In one of the two, several relatively coarse (50-100 μm) patches of Bi-minerals (<50% remain non-weathered) occur in the vein as larger masses interconnected by a fine network of filled fractures (Fig. 2a, bright). The patches consist mainly of (i) ingodite, Bi(Te,S), and unnamed Bi_2Te (Fig. 2b, c) and (ii) ingodite and coarse symplectites of joséite-A and joséite-B. Bismuthinite may be part of the assemblages. Native gold is present in (i) as a rim at the contact between the two Bi-minerals (Fig. 2c, d). It also forms separate grains, tens of μm in size, at the margins of assemblage (i), connected by veinlets to the Bi-mineral mass. Ingodite is enveloped by unnamed Bi_2Te. The latter contains irregular μm-sized inclusions of joséite-B (Fig. 2e).

Samples from the second location, on the northern side of the vein, contain mm-sized patches of bismuthinite (<50% remain non-weathered). Tellurides, such as ingodite, joséite-A and joséite-B occur either as 10-20 μm-sized inclusions, or as larger (100-500 μm) masses at the margin of bismuthinite. The inclusions can be euhedral or are slightly deformed. A comparable deformation is observed along the cleavage planes of host bismuthinite. Scarce native gold is present as <10 μm-sized inclusions in bismuthinite, sometimes combined with tellurides (Fig. 2f). The same coarse symplectites between joséite-A and –B as in samples from the other location described above are observed in the larger patches at the margins of bismuthinite.

3. ELECTRON MICROPROBE DATA

A CAMECA SX-51 instrument at Adelaide Microscopy, Adelaide, South Australia was used, at an operating voltage of 20 kV and beam current of 20 a.

Microprobe data for identified species are presented in Tables 1-3. Data for unnamed Bi_2Te and hedleyite in the Blue Quartz Vein were obtained by EDAX and are not included in the table. We point to the variable contents of Pb in joséite-A and -B and that Pb is preferentially enriched in joséite-A in the Eloise vein. In the Blue Quartz vein, neither joséite-A nor -B contain Pb, which is actually higher in the coexisting ikunolite.

Table 1. Mean analyses of Bi-minerals in the sample'0414'.

	Jo-A	Jo-B	Iku	Bism
	n=13	n=2	n=2	n=3
Cu	0.00	0.00	0.00	0.06
Pb	0.17	0.06	4.15	0.10
Cd	0.22	0.17	0.26	0.17
Bi	80.00	74.15	83.66	80.16
Sb	0.11	0.13	0.02	0.15
Te	11.97	21.84	0.97	0.04
Se	0.12	0.06	0.15	0.02
S	6.36	2.98	10.33	18.52
Total	99.09	99.37	99.56	99.53

Empirical formulae:
Joséite-A: $(Bi_{3.95}Pb_{0.02}Sb_{0.01})_{3.98}Te_{0.97}S_{2.05}Se_{0.02}$
Joséite-B: $(Bi_{4.00}Sb_{0.01})_{4.01}Te_{1.93}S_{1.05}Se_{0.01}$
Ikunolite: $(Bi_{3.72}Pb_{0.19})_{3.91}S_{3.09}$
Bismuthinite: $(Pb_{0.01}Cu_{0.01}Bi_{1.97})_{1.99}S_{3.01}$

Table 2. Mean analyses of Bi-minerals in the 'Eloise' sample.

	Jo-A	Jo-B	Ing	Bi_2Te	Bism
	n=8	n=6	n=10	n=12	representative
Cu	0.00	0.00	0.00	0.00	0.23
Pb	3.03	0.68	1.74	0.79	1.03
Cd	0.32	0.27	0.18	0.25	0.04
Bi	75.34	74.99	68.54	76.78	78.73
Sb	0.11	0.17	0.15	0.32	0.46
Te	14.39	21.49	23.54	22.09	0.02
Se	0.10	0.11	0.15	0.21	0.17
S	6.29	2.88	5.57	0.34	18.31
Total	100.59	99.58	99.87	100.77	98.99

Empirical formulae:
Joséite-A: $(Bi_{3.68}Pb_{0.15}Sb_{0.01})_{3.84}Te_{1.15}S_{2.00}Se_{0.01}$
Joséite-B: $(Bi_{4.03}Pb_{0.04}Sb_{0.02})_{4.08}Te_{1.89}S_{1.01}Se_{0.02}$
Ingodite: $(Bi_{0.94}Pb_{0.02})_{0.97}Te_{0.53}S_{0.50}Se_{0.01}$
Unnamed Bi_2Te: $(Bi_{1.97}Pb_{0.02}Sb_{0.01})_{2.00}(Te_{0.93}S_{0.06}Se_{0.01})_{1.00}$
Bismuthinite: $Cu_{0.03}Cu_{0.02}Bi_{1.96}S_{2.98}Se_{0.01}$

Table 3. Mean analyses of Bi-minerals in the sample'0412'.

	Jo-A	Jo-B	Ing	Bism
	n=9	n=7	n=16	representative
Cu	0.00	0.00	0.00	0.34
Pb	2.89	0.42	3.29	0.73
Cd	0.20	0.27	0.30	0.00
Bi	75.57	74.13	66.96	79.04
Sb	0.11	0.14	0.16	0.41
Te	13.99	21.09	21.65	0.11
Se	0.10	0.07	0.06	0.03
S	6.31	3.24	5.81	18.83
Total	99.17	99.37	98.24	99.53

Empirical formulae:
Joséite-A: $(Bi_{3.70}Pb_{0.14}Sb_{0.01})_{3.85}Te_{1.12}S_{2.01}Se_{0.01}$
Joséite-B: $(Bi_{3.97}Pb_{0.02}Sb_{0.01})_{4.01}Te_{1.85}S_{1.13}Se_{0.01}$
Ingodite: $(Bi_{0.93}Pb_{0.05})_{0.98}Te_{0.49}S_{0.53}$
Bismuthinite: $(Pb_{0.02}Cu_{0.03}Bi_{1.95}Sb_{0.02})_{2.02}S_{2.98}$

4. LA-ICP-MS ANALYSIS

Analysis was carried out on the material from Eloise only. The small size of the phases in the Blue Quartz vein precluded satisfactory analysis.

Experimental

LA-ICP-MS analysis was carried out using the Agilent HP4500 Quadripole ICP-MS instrument at CODES, University of Tasmania, equipped with a high-performance New Wave UP-213 Nd:YAG Q-switched laser ablation system and MEOLaser 213 software operating at 5 Hz. We performed spot analyses (12-80 μm in diameter, depending on size of the target mineral), monitoring the following isotopic abundances: ^{197}Au, ^{130}Te, ^{209}Bi, ^{208}Pb, ^{107}Ag, ^{77}Se, ^{121}Sb, ^{57}Fe, ^{65}Cu, 66Zn and ^{75}As. Total analysis time was 90s (30s pre-ablation and 60s ablation time). Calibration was performed on a doped pyrite standard; Bi served as the internal standard for the tellurides and bismuthinite. Detection limits for gold were 0.01 to 0.05 ppm.

Results

In the 'Eloise' sample, we analysed (1) Symplectites of joséite-A and –B, (2) ingodite and (3) unnamed Bi_2Te (Figs. 3 and 4, with Au concentrations given in ppm). Au concentrations in the Bi-tellurides ranged from <1 ppm to 57 ppm. Representative LA-ICP-MS depth profiles are shown in Figs. 5 and 6. In the first patch (Fig. 3), three LA-ICP-MS spot analyses of Bi_2Te give Au contents stretching across an order of magnitude (3.6 to 57 ppm). We note the excellent correlation between the Au signal and the Ag and As signals on Fig. 5. Antimony, Pb and Se show trends parallel to Bi and Te, at values in agreement with microprobe data. Although steady for the first third of the ablation, the Au signal jumps over one order of magnitude and is then steady again for the remainder of the spot.

In the second patch (Fig. 4), the maximum gold value was obtained from a symplectite of joséite-A and –B (26 ppm). Two LA-ICP-MS spot analyses of coexisting ingodite give 3 and 10 ppm. These values are two orders of magnitude higher than in the first patch (0.05 ppm). The profile (Fig. 6) was integrated for Au over the second half of the ablation where Sb increases and Pb decreases. Gold is below detection limits in the first half of the profile. As in the previous case, the Au signal is paralleled by the As and Fe signals.

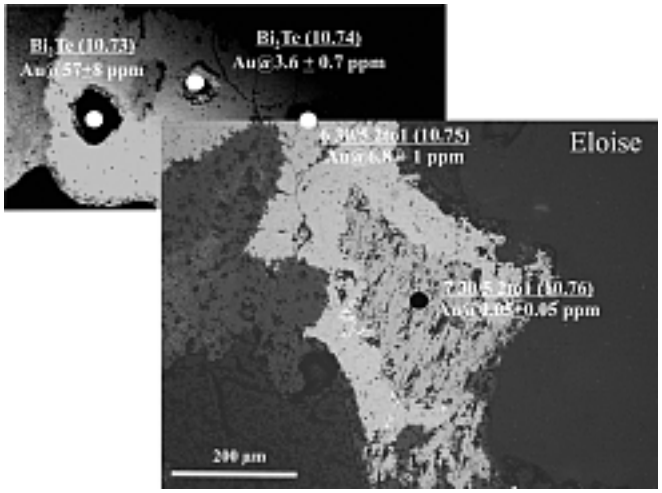

Figure 3. Back-scattered electron images showing ablated grains of Bi-tellurides in sample 'Eloise'. Gold concentrations are given in ppm.

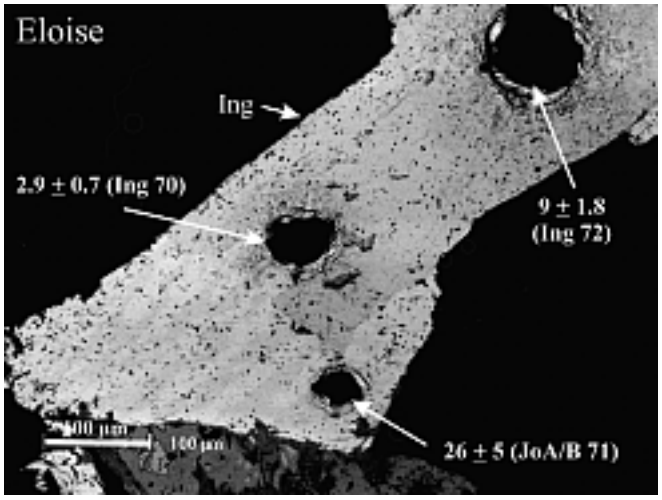

Figure 4. Back-scattered electron images showing ablated grains in sample 'Eloise'. Gold concentrations are given in ppm.

In samples from the second location, two analyses were made of the joséite-A and -B symplectites in the same area (Figs. 7 and 8), with values of 0.13 and 0.65 ppm. Ingodite was analysed by four spots of which two gave Au values below the detection limit (ca. 0.005 ppm);

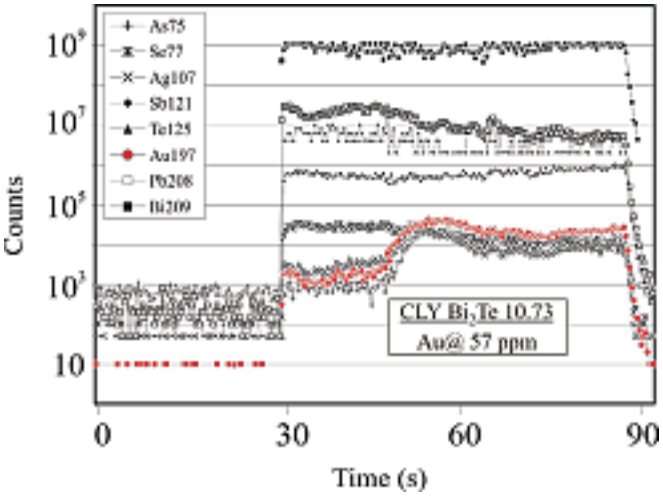

Figure 5. Laser ablation profile of a representative grain of Bi_2Te (point 73, see figure 3). Note that Au concentrations are strongly correlated with Ag and As.

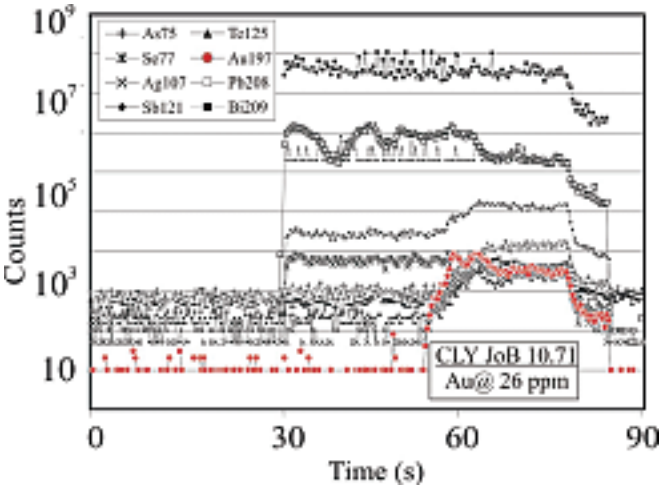

Figure 6. Laser ablation profile of a symplectite between joséite-A and - B (point 71, see figure 4). Note that the first half of the spectra after activation of the laser (30-55s) shows no Au (or Ag) present. Following transition into an included mineral at ca. 55s, Au, Ag and Sb increase markedly.

patch as the tellurides (Fig. 7) and an additional five spots were taken from another patch in which tellurides form small inclusions (attempts to determine Au in one of these inclusions failed because the laser intersected a gold inclusion below the surface). Gold values stretch over two orders of magnitude: 0.02 to 2 ppm in the first case, and from 0.07 to 0.42 ppm in the second.

Figure 9 shows the 11 individual spot analyses of bismuthinite, arranged in order of increasing Au content. Gold contents correlate well with those of Ag, as well as both As and Fe. The other minor components in bismuthinite (Pb, Cu, Sb and Se) show generally flat, parallel trends across the dataset. The same correlation between Au and some trace elements (Ag, As, Fe) was noted in individual spot analyses of tellurides above.

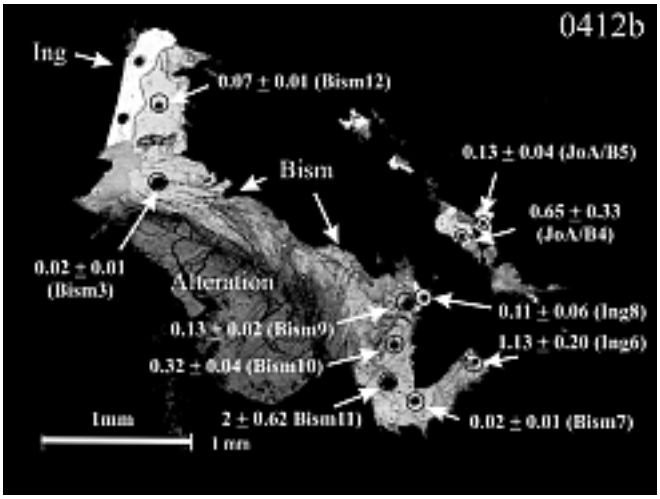

Figure 7. Back-scattered electron images showing ablated grains in sample '0412b'. Au concentrations are in ppm.

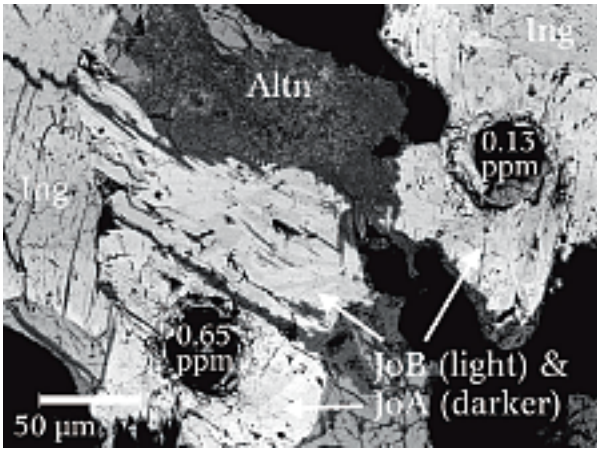

Figure 8. Coarse intergrowths of joséite-A and -B (brighter areas) in bismuthinite matrix (middle grey). LA-ICP-MS laser spots are clearly visible. Scale bar: 50 µm.

The full dataset for tellurides and sulphosalts is summarised in Fig. 10, arranged in order of increasing Au concentration. The figure also shows error bars for each individual analysis. From this, we see that Au contents from the first location are higher by at least one order of magnitude. The gold content in bismuthinite is comparable to that in the coexisting tellurides. The highest Au concentrations do not appear to be restricted to one telluride species in particular. For example, ingodite can be the most and least Au-enriched within individual patches.

ingodite can be the most and least Au-enriched within individual patches.

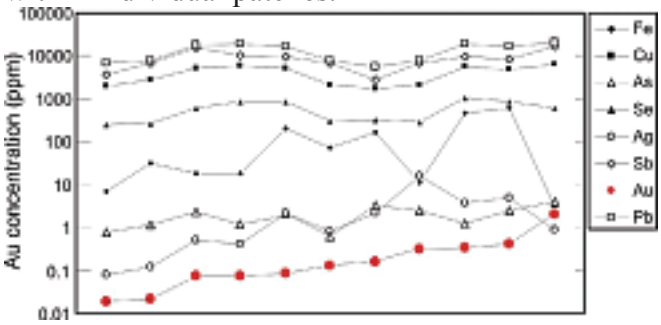

Figure 9. Laser ablation data for individual bismuthinite analyses arranged in order of increasing Au content from left to right. Note that both Ag and Fe correlate with Au. Lead, Cu, Se and Sb (common minor or trace components of bismuthinite) show relatively flat profiles.

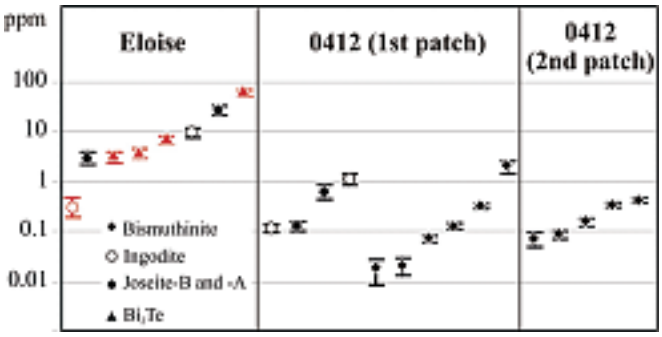

Figure 10. Laser ablation data for individual Bi-telluride analyses arranged in order of increasing Au content, sub-divided by sample. For Eloise, values from patch in Fig. 3 are in red and from Fig. 4 in black.

5. DISCUSSION AND CONCLUSIONS

In both veins, native gold is included within Bi-mineral associations that are characteristic for the Bi-rich side of the system Bi-Te-(S). They represent reduced associations (pyrrhotite, magnetite stability) since all species can be at equilibrium with native bismuth given their Bi/(Te+S)≥1 ratio. Native bismuth is however present only in the Blue Quartz vein, forming associations resembling those known from the gold skarn at Hedley. Native bismuth + Bi_2Te/ Bi_7Te_3 and Bi+Bi_2S_3 correspond to eutectics at 266ºC and 270ºC in the Bi-Te and Bi-S systems, respectively. This, together with the droplet-like shape, may be taken to presume their precipitation from fluids in a molten state, as considered for gold skarns (Meinert, 2000) and intrusion-related veins at Pogo, Fort Knox and elsewhere in the Tintina belt, Alaska (McCoy, 2000). However, the Blue Quartz associations differ from these examples in the fact that they lack maldonite or its breakdown products (symplectites of native gold = bismuth). Maldonite is the Au-bearing phase included in the two eutectic associations from the Bi-rich side of the Au-Bi-Te system (Bi + Au_2Bi, 241ºC and Bi_7Te_3+ Bi + Au_2Bi, 235ºC. Crystallization from melts will always conclude in forming eutectic associations following partial crystallization along the solvus curve (Ciobanu et al., 2005, 2006a, b). This implies that even though the droplets may have initially been precipitated in a molten state, they have suffered internal redistribution of Au (if this was indeed at all included in the melts). Relationships between phases with Bi_4X_3 (X=Te,S), i.e., joséite-B replaced by joséite-A and/or ikunolite, also suggest that the Bi-mineral assemblages are overprinted during a subsequent event. This is characterised by fluids with an increased content of S relative to Te (higher S/Te ratios in the replacing phases). Potentially, the same event could have redistributed and/or introduced gold.

The Bi-mineral associations in the Eloise vein differ from the above in that they do not contain primary native bismuth, and also include ingodite, a tellurosulphide with Bi/(Te+S) = 1, which is not observed in the Blue Quartz vein. Here, the relationships between (i) phases with the same Bi/X=4:3 ratio (symplectites of joséite-B and –A) and (ii) skeletal inclusions of joséite-B in Bi_2Te indicate immiscibility via exsolution rather than an overprint. The mantling of ingodite by Bi_2Te, however, and the rim of native gold formed at the boundary between the two (Fig. 2c, d) can be interpreted as replacement of ingodite that also may have released Au. This would explain the low values of Au in ingodite from this patch (0.05 ppm) relative to another in which no native gold is observed (9 ppm). The replacement can be paralleled with the transitory reaction liquid + BiTe = Bi_5Te_3 + Au at 374ºC in the system Au-Bi-Te. The jump over an order of magnitude in the Au signal obtained during ablation of Bi_2Te (Fig. 5) is indicative of formation of sub-µm-scale

Cook et al., this volume) during any overprinting event that would assist solid-state diffusion and/or fluid infiltration. The good correlation with other elements, such as Fe and As, which do not commonly replace the main components in the structure, also supports such an hypothesis. Although the Au signal across the joséite-B/-A symplectites (Fig. 6) shows a similar jump during the ablation interval, this can be interpreted as preferential concentration of Au in the component with lower Pb and higher Sb (joséite-B), rather than nucleation of Au inclusions. This is concurrent with the lack of evidence for overprinting in this particular patch.

Measured gold concentrations in the same bismuth tellurides within patches from samples in the second location from the Eloise vein are two orders of magnitude lower than those from the first location. There is no preferential concentration of Au in any specific telluride species or in bismuthinite (Fig. 10). Moreover, the ranges of Au values are the same in bismuthinite whether it contains inclusions of native gold or not. The good correlation across the dataset between Au and the same elements observed for the tellurides, i.e., Fe, As, Ag, indicates partitioning of Au at comparable values between the tellurides and the sulphosalt.

The residual Au content in Bi-minerals, the exsolution relationships, and also the fact that all Bi-minerals contain residual amounts of Au support the hypothesis that at Eloise, as in the Blue Quartz vein, they may have formed by crystallization of molten Bi-Te-S-(Au) precipitates. In the Eloise vein, however, no eutectic associations are preserved, given the fact that the overprint has modified the Bi/X ratios in the species. The highly variable gold contents in the Bi-tellurides from one location to another along the vein, as well as between patches in the same sample, indicates the impact of the overprinting event that assisted Au redistribution and is beneficial for nucleation of native Au.

The data presented here, however, needs to be supplemented in order to obtain a better, quantitative assessment of the role played by the overprinting in the BiTel Knoll veins. This study shows nonetheless the ability of Bi-minerals to incorporate Au and also to track overlapping events by subtle changes in their chemistry. An overprint is shown also by the replacement relationships between Fe-Ti-oxides in the same Bi-mineral samples. The presence of molybdenite (also abundant in other deposits from the same region, e.g., Hedley), as well as REE-phosphates, shows the affiliation of the mineralising fluid to a magmatic source, e.g., Bunker Hill Sill. The subsequent event, with an important role in remobilising and concentrating Au from the pre-existing Bi-Te-(S) assemblages in the veins, may be attributed to one or the other tectonic events (Late Cretaceous?) postdating intrusion emplacement in the area.

REFERENCES

Ciobanu, C.L., Cook, N.J., Pring, A., 2005. Bismuth tellurides as gold scavengers. In: Mao, J.W., Bierlein, F.P. (eds.) Mineral Deposit Research: Meeting the Global Challenge, Springer, p. 1383-1386.

Ciobanu, C.L., Cook, N.J., Damian, F., Damian, G., 2006a. Gold scavenged by bismuth melts: An example from Alpine shear-remobilisates in Highis Massif, Romania. Mineral. Petrol. 87, 351-384.

Ciobanu, C.L., Cook, N.J., Pring, A., Brugger, J., Netting, A., Danushevskiy, L., 2006b, LA-ICP-MS evidence for the role of Bi-minerals in controlling gold distribution in ores. 12th Quadrennial IAGOD Symposium, Moscow, Russia, 21st -24th Aug. 2006. CD-ROM abstract volume.

Cook, N.J., Ciobanu, C.L., Danushevskiy, L., 2007, this volume. LA-ICP-MS determination of gold in Bi-minerals from deposits in the Fennoscandian Shield.

Howard, W.R., this volume. Structural setting and geochemical correlations in bismuth (sulfo)telluride-native gold–bearing veins, CLY Group, B.C., Canada: A reduced intrusion-related gold system.

McCoy, D.T., 2000, Mid-Cretaceous plutonic-related gold deposits of interior Alaska: metallogenesis, characteristics, gold associative mineralogy and geochronology. Ph.D. thesis, University of Alaska at Fairbanks AK. 245 pp.

Meinert, L.D., 2000, Gold in skarns related to epizonal intrusions. In: 'Gold in 2000', Reviews in Economic Geology 13, 347-375.

Compositional variations in the tetrahedrite-tennantite fahlores and polybasite-pearceite series from the Chiprovtsi Ag-Pb deposit, northwestern Bulgaria

Dimitrina DIMITROVA
Thomas KERESTEDJIAN
Maria PETROVA
Tsvetoslav ILIEEV

Geological Institute, Bulgarian Academy of Sciences, 24 Acad. Georgi Bonchev Str., 1113 Sofia, didi@geology.bas.bg; thomas@geology.bas.bg

Summary: Tetrahedrite-tennantite fahlores and minerals of the polybasite-pearceite series from the Chiprovtsi Ag-Pb deposit (NW Bulgaria) have been studied by reflected light microscopy and electron microprobe analysis. The microprobe analyses revealed a wide variety of compositions within the fahlore solid solution series, regarding Ag, Zn, Fe and Cd content. Fahlores from the Chiprovtsi deposit tend to exhibit intermediate to high Sb/As ratio, as well as higher Zn content. All varieties of fahlores in respect to Ag content are recorded, as well as the highest Ag contents in tetrahedrite reported in the literature (up to 3.56 apfu). The Ag content of fahlores in the deposit has lateral and vertical dependence. Polybasite-pearceites also have elevated Ag content (up to 14.69 apfu Ag). According to their Sb/As ratio they could be classified as polybasites to antimonpearceites.

Key Words: silver ores, lead ores, tetrahedrite, tennantite, polybasite, pearcite, fluid inclusions, Chiprovtsi, Bulgaria

1. INTRODUCTION

Chiprovtsi was one of the largest lead-silver deposits in Bulgaria and the main silver source of the country. The mine was closed in 1999 after producing 4.79 Mt of ore at 1.84% Pb and 110 g/t Ag since 1951 (Milev *et al*. 1996). Silver has been extracted mainly from tetrahedrite-tennantite fahlores and less from other Ag sulphides and sulphosalts (argentite, pyrargyrite, polybasite, stephanite), as well as Ag-Pb sulphosalts (diaphorite, owyheeite) within galena.

2. GEOLOGICAL SETTING

The Chiprovtsi lead-silver deposit is hosted in low-grade metamorphic rocks (marbles and schists) of the Diabase-Phyllitoid Complex (Precambrian - Early Ordovician age) (Kalvacheva, 1986; Carrigan *et al*., 2003) (Fig. 1). The formation of the main Pb-Ag metasomatic replacement mineralization is considered to be of Carboniferous age (Amov *et al*., 1981) and it is of stratabound type within the thick siderite and calcite marble layers of the metamorphic series. The genesis of the deposit remains uncertain and it has been classified as both granite intrusion-related and stratabound telethermal (Atanassov and Pavlov, 1983; Dragov *et al*., 1991). According to Dragov *et al*. (1991), Amov *et al*. (1981) and Zidarova and Zidarov (2000) the main lead-silver mineralization has been overprinted by late geological events: 1) the Sveti Nikola granite intrusion (Late Carboniferous age, Carrigan *et al*. 2005), causing the formation of the iron skarn mineralization of the Martinovo deposit (westernmost part of the ore district); and 2) hydrothermal fluid introduction of currently uncertain age (suggested Late Cretaceous or Palaeogene), causing the fluorite replacement mineralization in the marbles of the Lukina Padina mine section (easternmost part of the ore district). Nd-Sr isotope study of fluorites (Zidarova *et al*., 2005) suggests mixed, but crustal dominated origin of the fluids, as mantle degassing is considered for the possible source of fluorine.

3. SAMPLING AND ANALYTICAL TECHNIQUES

Polished sections were prepared from representative samples, collected from metasomatic replacement bodies and veins in the siderite marbles on: 520, 590, 620, 650 levels of Yavorov Dol; 420 level of Sinya Voda; 700 level of Rupski Dol; 445, 495 and 550 levels of Lukina Padina mine sections of the Chiprovtsi mine. The mineral relationships in 149 polished sections

were examined by reflected light microscopy. 111 microprobe analyses of tetrahedrite-tennantite fahlores and polybasites were performed by a JEOL Superprobe 733 electron microscope equipped with an ORTEC energy-dispersive system at the Geological Institute, BAS and by a JEOL JSM 35 CF electron microprobe equipped with a Tracor Northern TN-2000 analyzing system at the laboratory of Eurotest Control AD, Sofia. The accelerating voltage of the probe was 25 kV. The following standards were used: Ag, Sb_2S_3 (for Sb), FeS_2 and $CuFeS_2$ (for Fe), Cu_3AsS_4 (for Cu, As and S), ZnS (for Zn), CdS (for Cd), PbTe (for Pb) and HgS (for Hg).

Fluid inclusion microthermometric measurements were made in single crystal quartz, barite and calcite plates, using a Chaixmeca freezing-heating stage.

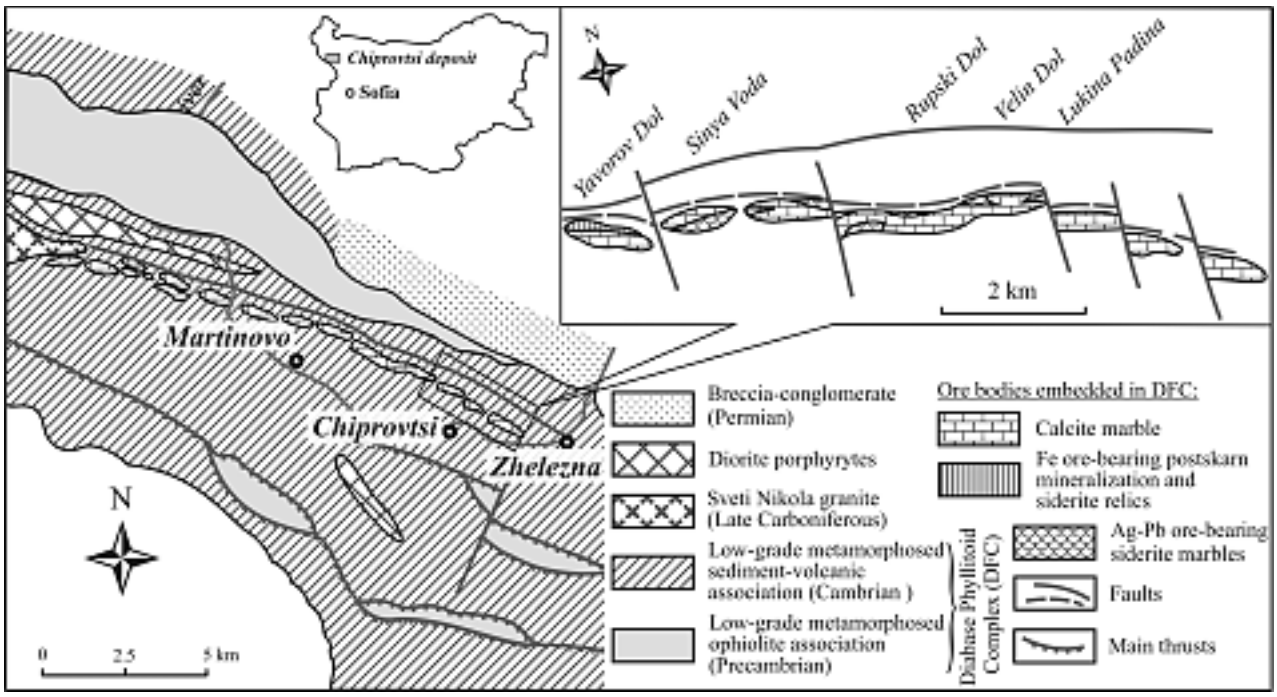

Figure 1. Simplified geological map of the Chiprovtsi deposit, modified after Haydoutov (1991), and sketch of the ore bodies, modified after Obretenov (1988).

4. RESULTS

The term "fahlore" is used with the modifiers "tetrahedrite", "tennantite" and "freibergite" to describe minerals with $I\bar{4}3m$ structure, approximating the structural formula $^{III}(Ag,Cu)_6{}^{IV}[(Ag,Cu)_{2/3}(Fe,Zn)_{1/3}]_6[^{III}(Sb,As)^{IV}S_3]_4{}^{VI}S$, as it has been accepted by several authors (Ramdohr, 1980; Mozgova and Tsepin, 1983; Ebel and Sack, 1989; Sack *et al*., 2005). Using the more simplified formula $(Cu, Ag, Fe, Zn)_{12}(Sb, As)_4S_{13}$, our samples show some Cd, Hg and Pb, most probably substituting for Zn or Fe. As it has been reported (Sack, 2000, 2005; Sack *et al*., 2005) fahlores form a complete solid solution above 270ºC.

Polybasite-pearceites also form a solid solution series, approximating the formula $(Ag_{1-x},Cu_x)_{16}(Sb,As)_2S_{11}$, with x between approximate limits of 0.04 to 0.57 (Harlov and Sack, 1994).

These mineral series often occur together, accompanied by other Ag sulphides and sulphosalts as argentite, pyrargyrite and stephanite in different types of Ag-rich mineral deposits.

Mineral chemistry and ore petrology

The tetrahedrite-tennantite fahlores occur always with galena and/or sphalerite and chalcopyrite, which are the main ore minerals of the mineralization. The ore mineralization is stratified within calcite-siderite marbles as large metasomatic replacement bodies, nests and veinlets. The ore-forming succession is hardly

distinguished, because of the late overprinting processes, but according to our and previous (Dragov, 1997) studies, sphalerite is formed earlier than galena, fahlores and chalcopyrite. Polybasite-pearceites are observed in lesser amounts and always accompanying fahlores. In some cases they form exsolution-like textures with freibergite, chalcopyrite and argentite (Fig 2a,b) in samples from Yavorov Dol, while in samples from Lukina Padina, they form thin rim at the Zn-rich tetrahedrite-tennantite periphery.

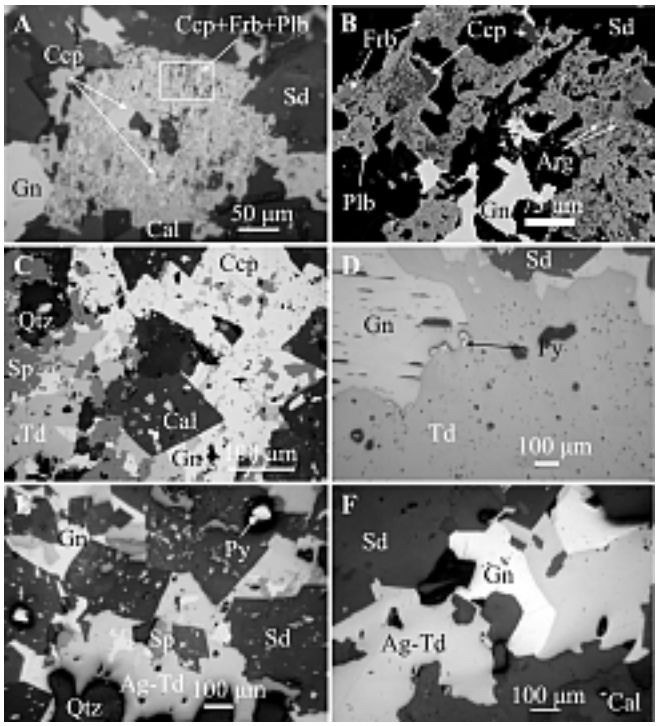

Figure 2. Photomicrographs: a) chalcopyrite-freibergite-polybasite exsolution-like textures with galena, in veinlet within siderite-calcite matrix, YD; b) same as previous, BSE image, YD; c) chalcopyrite-sphalerite-galena-tetrahedrite nest within calcite-quartz matrix, YD; d) galena-tetrahedrite-pyrite nest within siderite marbles, LP; e) and f) high-Ag tetrahedrite with sphalerite and/or galena as nest or veinlet within siderite marbles, YD and LP. Abbreviations: Gn - galena; Ccp - chalcopyrite; Sp - sphalerite; Frb - freibergite; Plb - polybasite; Td - tetrahedrite; Ag-Td - argentian tetrahedrite; Arg - argentite; Py - pyrite; Sd - siderite; Cal - calcite; Qtz - quartz. Location abbreviations as in fig. 3.

As it was noticed earlier by Dragov (1997) the tetrahedrite-tennantite fahlores in Chiprovtsi tend to exhibit intermediate to high Sb/As ratio, i.e. from intermediate to Sb end-members of the fahlore series. This trend is clearly proved by this study and the results are plotted on Fig. 3a. The Ag, Zn and Fe contents in the fahlores range in wide limits, but a Zn domination trend is clearly observed on Fig. 3b for all the analyses, except few freibergites. A full range of Ag contents are recorded - from 1.43 wt.% (0.13 apfu) to 35.21 wt.% (6.38 apfu) in freibergites.

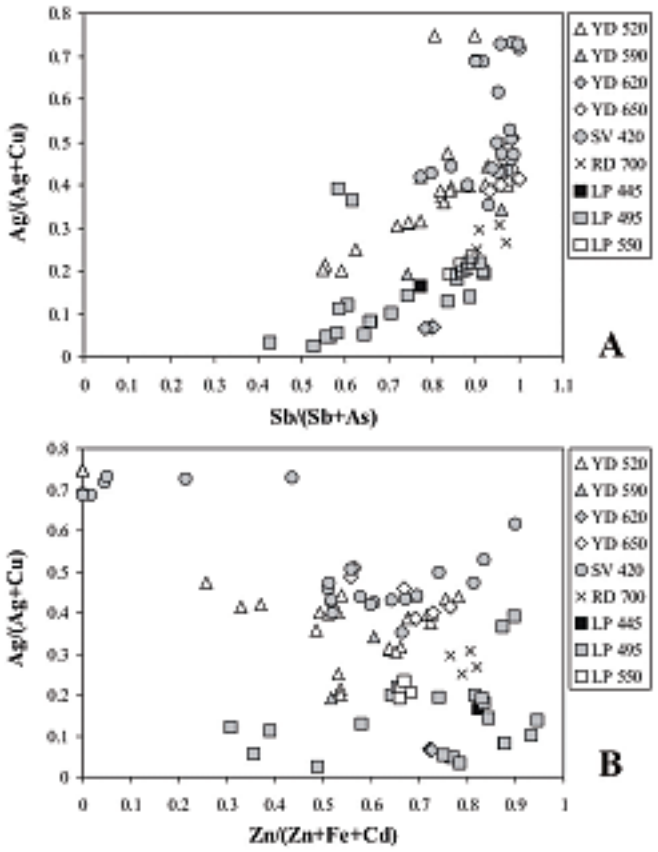

Figure 3. Element distribution trends in the Chiprovtsi fahlores in two modes: Ag/(Ag+Cu) vs. Sb/(Sb+As) (A); and Ag/(Ag+Cu) vs. Zn/(Zn+Fe) (B). Abbreviations in the legend: YD – Yavorov Dol, SV – Sinya Voda, RD – Rupski Dol, LP – Lukina Padina, 520 – level.

Excluding freibergites, high-Ag fahlores, showing Ag content between 15 and 19 wt.% (2.40-3.20 apfu) are also observed. According to Samussikov and Gamyanin (1994), tetrahedrites may have Ag content up to 3.7 apfu, while between 3.7 and 10 apfu Ag, the members should be regarded as freibergites. If we stick to this rule, then the high-Ag fahlores from the Chiprovtsi deposit almost reach the upper limit – 21.05-21.13 wt.% Ag (3.51-3.56 apfu), which is higher than the the values reported by Sack *et al*. (2005) for high-Ag fahlores in Galena mine Idaho, USA. Fahlores from the Chiprovtsi deposit, in general,

exhibit apparent non-stoichiometry, especially for their S content, which partly depends on Ag and Sb content, as at higher Ag and Sb contents (freibergites) S content is lower than 13 apfu, approaching 12.4 apfu.

The distribution of Ag in fahlores also has a spatial (lateral and vertical) dependence. Highest contents, i.e. freibergites are found in the lower levels of the western mine sections Yavorov Dol and Sinya Voda, while Ag-poor species exist in the eastern part (Lukina Padina mine section).

Polybasite-pearceites also exhibit elevated Ag content up to 69.89 wt.% approximating the formula $Ag_{14.69}Cu_{1.71}Fe_{0.16})_{16.56}(Sb_{1.78}As_{0.12})_{1.90}S_{10.54}$.

In most cases, they contain small amounts of As (0.13-3.66 wt.%), which classify them as antimonpearceites. One case of As-rich member of the series – 6.36 wt.% As (from Lukina Padina), can be classified as arsenpolybasite.

Like in fahlores, some S deficiency is detected for the Ag-rich polybasites, which is probably due to the structure distortion caused by elevated Ag content.

High-Ag-Sb sulphosalts – stephanite and pyrargyrite are found either together with freibergite, argentite, galena and sphalerite or filling together with galena veinlets, crosscutting the siderite matrix (Fig. 4).

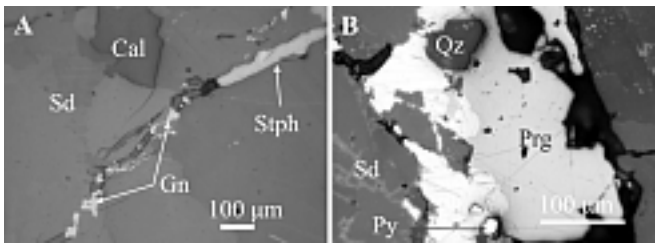

Figure 4. Photomicrographs: a) galena-stephanite veinlet crosscutting siderite and calcite, YD; b) galena-pyrargyrite-pyrite veinlet within siderite, SV. Abbreviations: Stph -, stephanite; Prg - pyrargyrite. Location abbreviations as in fig. 3.

5. FLUID INCLUSION STUDY

A microthermometric fluid inclusion study was performed on small, euhedral, transparent quartz, barite and calcite plates, collected from cavities in samples from 520 level of Yavorov Dol (quartz), 620 level of Sinya Voda (quartz, barite and calcite) and Rupski dol (quartz), 495 and 606 levels of Lukina Padina (quartz and calcite) sections of the mine. The fluid inclusions observed in quartz, barite and calcite from all locations are mainly secondary and primary inclusions are found rarely.

The quartz crystals are 1-2 mm wide to 2-5 mm long. Primary inclusions in samples from Yavorov Dol, Sinya Voda and Rupski Dol mine sections are very rare, up to 10 µm in size, showing measured homogenization temperatures (*Th*) of about 250-260°C, unlike the *Th* measured in quartz from Lukina Padina section, which exhibit a maximum at 140-150°C (Fig. 5).

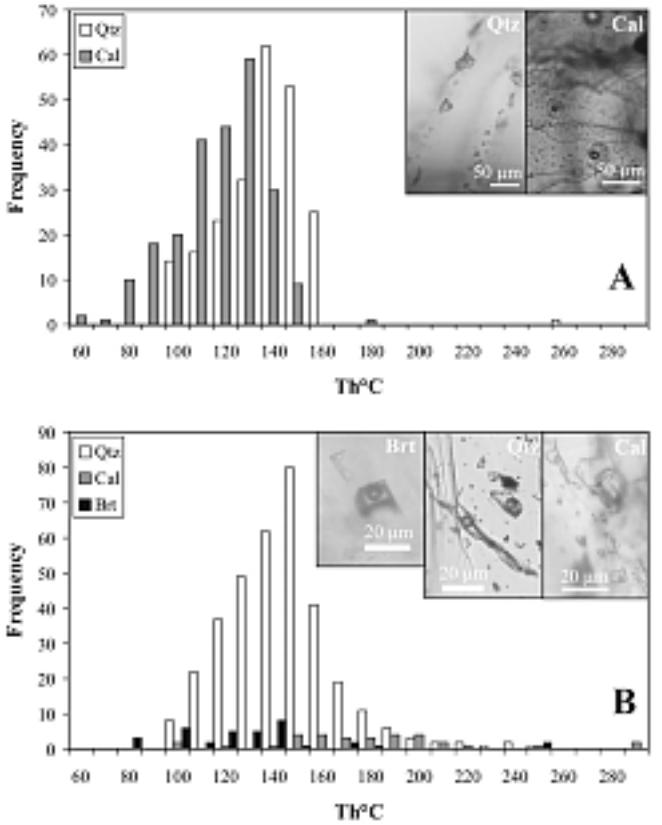

Figure 5. Homogenization temperatures (*Th* °C) of fluid inclusions measured in calcite, barite and quartz crystals from: A) Lukina Padina; and B) Yavorov Dol, Sinya Voda and Rupski Dol mine sections.

The secondary fluid inclusions are up to 10 µm in size, usually distributed in groups along microfractures parallel to faces of m $\{10\bar{1}0\}$ and respectively show lower temperatures.

Barite plates are 2-3 mm wide to 2-5 mm long. The primary and secondary fluid inclusions are 2-15 µm in size. The measured *Th* of primary

inclusions exhibit maximum at 250°C, unlike the secondary ones, which show a maximum at 140°C (Fig. 5b).

Calcite is predominantly small to medium-grained, rarely found as transparent to translucent euhedral crystals up to 1-2 mm in size. Fluid inclusions in it are observed everywhere, from small (1-5 μm) to relatively large ones – up to 20-50 μm. Unlike the other studied minerals, calcite contains not only fluid inclusions of H_2O-CO_2 system, but also H_2O-H_2O, showing much higher *Th*, reaching 290°C (Sinya Voda). The average *Th* in the samples from Yavorov Dol, Sinya Voda and Rupski Dol is about 160-200°C, unlike those measured for Lukina Padina 130-140°C.

6. DISCUSSION AND CONCLUSIONS

The formation of high Ag-Sb sulphosalts like polybasite, pyrargyrite and stephanite, as well as freibergite suggests a high Ag and Sb fugasity in the ore-forming fluids. This may be a result of the late geological events in the western part of the area, connected to the granite intrusion and related skarn and postskarn hydrothermal deposition. These fluids are also characterized by high S and Fe fugacities, manifested in the formation of the Fe ore mineralization (magnetite-löllingite-arsenopyrite-pyrite) of the Martinovo deposit. During this process the primary high-Ag tetrahedrites and galena interact with the Fe- and S-rich fluids, forming other Ag-Pb, Pb sulphosalts (diaphorite, owyheeite, bournonite) and high-Ag minerals as freibergite and polybasite, as well as stephanite and pyrargyrite. This process takes place in relatively high temperatures.

Applying the temperature dependent Ag solubility diagram of Sack (2005), several conclusions about the fahlores from the Chiprovtsi deposit could be drawn out. First of all, most of the Ag-poor fahlores are detected in the Lukina Padina section and fall below the 170ºC curve, i.e. are formed in relatively low temperatures. This fact is also supported by the fluid inclusion studies of quartz and calcite from Lukina Padina, which show *Th* of primary inclusions between 140 and 160ºC. This is probably a result of the overprinting reactions with the late fluorite forming fluids, which bring in Hg, Fe and F. Hg is rarely recorded in the fahlores in our samples, although Ag-Hg fahlore variety is reported there by Atanassov (1975).

On the contrary, most fahlores from the western part of the deposit fall in the field above 200-250ºC. Few analyses fall in the field above 400ºC and belong to the samples from the deepest level 420 of Sinya Voda mine section. Highest Ag contents (freibergites) are formed at higher temperatures, allowing a complete solid solution series and various elements are also scavenged in it. On cooling they form own mineral species and exsolution-like textures as seen in samples from Yavorov Dol (Fig. 2a, b). This fact also complies with the fluid inclusion results (*Th* measured in barites and quartz from Yavorov Dol and Sinya Voda sections are below 250ºC). This is consistent with the conditions of the postskarn hydrothermal events related to the granite intrusion or the much later hydrothermal fluids that formed the fluorite bodies and barite-calcite veins.

Very likely, the original fahlores, not influenced by the late overprinting processes are formed in the temperature field between 200ºC and 250ºC, where intermediate and high-Ag fahlores occur. The influence of the late processes results in redistribution mainly of Ag and to a lesser extent of Sb content in the minerals. However, these processes form various compositions within the fahlore solid solution series with respect to Ag content, as well as several high-Ag sulphosalts (pyrargyrite, stephanite and polybasite-pearceites), argentite, and even native silver. The Ag contents (up to 3.56 apfu) in tetrahedrites, are the highest reported in Bulgaria, but also in the world, as far as it is known in the literature.

ACKNOWLEDGEMENTS

This study is supported financially by the National Science Foundation grant NZ-MU-1507/05.

REFERENCES

Amov, B., Arnaudov, V., Pavlova, M., Dragov, P., Baldjieva, Ts., Evstatieva, S., 1981, Lead isotope data on

the Paleozoic granitoids and ore mineralizations from the Western Balkan Mountains and the Tran district (West Bulgaria). I. Isotopic ratios and geochronology. Geologica Balc, 11, 2, 3-26.

Atanassov, V., 1975, Argentian mercurian tetrahedrite, a new variety, from the Chiprovtsi ore deposit, Western Stara Planina Mountains, Bulgaria. Mineral. Mag, 40, 11, 233-237.

Atanassov, V., Pavlov, I., 1983, Notes about mineralogy and paragenetic zoning of minerals deposits in Chiprovtsi ore region. Ann Ecol Sup Min Geol, 28, 2, 159-178 (in Bulgarian).

Carrigan, C.W., Mukasa, S.B., Haydoutov, I., Kolcheva, K., 2003, Ion microprobe U-Pb zircon ages of pre-Alpine rocks in the Balkan, Sredna Gora and Rhodope Terranes of Bulgaria: Constraints on Neoproterozoic and Variscan tectonic evolution. J Czech Geol Soc, 48, 32-33.

Carrigan, C.W., Mukasa, S.B., Haydoutov, I., Kolcheva, K., 2005, Age of Variscan magmatism from the Balkan sector of the orogen, Central Bulgaria. *Lithos*, 82, 125-147.

Dragov, P., 1997, Fahlores in the Chiprovtsi Ag-Pb deposit (NW Balkan). Rev. Bulg. Geol. Soc, 58, 1, 3-14 (in Bulgarian).

Dragov, P., Galiy, S.A., Zhukov, F.I., 1991, Carbon, oxygen and sulphur isotopes in minerals from the Chiprovtsi ore zone. Rev Bulg Geol Soc, 52, 3, 50-61 (in Bulgarian).

Ebel, D.S., Sack, R.O., 1989, Ag-Cu and As-Sb exchange energies in tetrahedrite-tennantite fahlores. Geochim. Cosmochim. Acta, 53, 2301-2309.

Harlov, D. E., Sack, R.O., 1994, Thermochemistry of polybasite-pearceite solution. Geochim. Cosmochim. Acta, 58, 4363-4375.

Haydoutov, I., 1991 Origin and Evolution of the Precambrian Balkan-Carpathian Ophiolite Segment. Sofia, BAS Press, 179p. (in Bulgarian).

Kalvacheva, R., 1986 Acritarch stratigraphy of the Ordovician System in Bulgaria. In: Proceedings of IGCP project 5 “Correlation of Prevariskan and Variskan events in the Alpine Mediterranean Mountain belts”, Sardinia, 38-43.

Milev, V., Stanev, V., Ivanov, V., 1996 The Extracted Ores in Bulgaria during 1878-1995 - Statistical Reference Book. Sofia, Zemya 93, 196p.(in Bulgarian).

Mozgova, N.N., Tsepin, A.I., 1983, Gray Ores: Aspects of Chemical Composition and Properties. Nauka, Moscow, 279p.

Obretenov, N., 1988, Chiprovtsi ore field – Chiprovtsi deposit. In: Dimitrov, R. (Ed.). Lead-zinc deposits in Bulgaria. Sofia, Technika, 193-206 (in Bulgarian).

Ramdohr, P., 1980, *The Ore Minerals and Their Intergrowths*. Oxford, Pergamon, 1174p.

Sack, R.O., 2000, Internally consistent database for sulphides and sulphosalts in the system Ag_2S-Cu_2S-ZnS-Sb_2S_3-As_2S_3. Geochim. Cosmochim. Acta, 64, 3803-3812.

Sack, R.O., 2005, Internally consistent database for sulphides and sulphosalts in the system Ag_2S-Cu_2S-ZnS-FeS-Sb_2S_3-As_2S_3: Update. Geochim. Cosmochim. Acta, 69, 1157-1164.

Sack, R.O., Fredericks, R., Hardy, L.S., Ebel, D.S., 2005, Origin of high-Ag fahlores from the Galena Mine, Wallace, Idaho, USA. Am. Mineral., 90, 1000-1007.

Samussikov, V.P., Gamyanin, G.N., 1994, Nomenclature of mineral species of Cu-Ag isomorphous tetrahedrite. In: 16th General Meeting of IMA, Pisa, Italy, 363-364.

Zidarova, B., Zidarov, N., 2000, Main elements of the local geogenetic model for fluorite formation: III. Chiprovtsi East deposit. Comp Rend Acad Bulg Sci, 53, 5, 63-66.

Zidarova, B., Peytcheva, I., von Quadt, A., Zidarov, N., 2005, Geochemical and Nd-Sr characteristics of fluorite from "Chiprovtsi-East". – In: Zidarov et al. (eds.) Ten years Central Laboratory of Mineralogy and Crystallography Acad. I. Kostov, BAS, BAS press, Sofia, 103-106 (in Bulgarian).

Structural setting and geochemical correlations in bismuth (sulfo) telluride-native gold–bearing veins, CLY Group, British Columbia, Canada: A reduced intrusion-related gold system

William (Bill) R. HOWARD 215 Silver Mead Cres. NW Calgary AB T3B 3W4 Canada
(wm.howard@shaw.ca)

Abstract: New found native gold + native bismuth + bismuthinite + bismuth (sulfo)tellurides occur in fracture-controlled clots in m-plus wide outcropping quartz veins on the CLY Group claims in the historic Nelson Mining Division, southernmost British Colombia. Mineralization has all criteria of the 'Reduced Intrusion-related Gold' model. Veins in three different sets occur over a 1.5 km N-S extent. Some are sheeted (i.e., near parallel and repeated); sulphide content is very low. The Eloise Vein on BiTel Knoll is like the Pogo deposit Liese Zone (3.51 M. oz) in structural-metamorphic setting and Au–Bi–Te mineralogy. The Clarissa Transverse Sheeted Veins and five auriferous Clease quartz veins and shears are analogous to mineralization in the Fort Knox deposit, Alaska (~5.4 M. oz). These are operating mines in the Tintina Gold Province, Alaska and Yukon, northern cordillera. In the Fairbanks district, reduced proximal arsenopyrite-pyrrhotite bearing tungsten + gold skarns occur about Fort Knox. On CLY Group Au(Ag)–Bi–Te–W–Mo ± As bearing quartz veins overprint the proximal Lefevre W + Au skarn. A numerical exploration model objectively ranks the potential of CLY for an economic deposit as high. This impartial analysis is irrespective of the favourable tectonic setting, rare mineralogy and outcrop features of the more than 19 known gold showings.

Key words: gold ores, quartz veins, gold, bismuth, tellurium, bismuthinite, tellurides, British Columbia, Canada

1. REGIONAL TECTONIC SETTING

CLY Group is the name of a Au–Bi–Te prospect situated at the ancestral North American accretionary margin at the maximum point of curvature of the Kootenay Arc, along a since-folded crustal suture zone (Fig. 1). Inboard Kootenay terrane rocks of ancestral North America (blue) include Cambro-Ordovician Index Formation metasediments and –volcanics of the Lardeau Group (Logan and Colpron 2006). Outboard younger Slide Mountain terrane rocks are ophiolitic (grey). The Quesnel Terrane is represented by Lower Jurassic shoshonitic andesites of the Rossland Group (greens and orange). All are intruded by the Salmo and Wallack Creek Stocks. These are part of the Mid-Cretaceous Bayonne magmatic belt granitoids (light red; Logan, 2002a, b) that 'stitch' two major crustal scale structures, the Waneta and Tillicum Creek Faults (Einarsen, 1995; Höy and Dunne, 1999). Concomitant Mid-Cretaceous compression oriented SSW-NNE (arrows on Fig. 1) reactivated all earlier structures. An outlying felsic granitoid of Wallack Creek Stock, named the Bunker Hill Sill [BH Sill] is spatially and genetically related to the Au-Bi-Te mineralization in CLY (Caron, 2006). BH Sill granitoids are I-type felsic biotite ± muscovite ± hornblende granites. They have a reduced petrochemistry with near zero magnetic susceptibility and very low magnetite content (R.G. Anderson, pers. comm., 2006). Abundant sheeted tourmaline veinlets, tourmalinite breccia, quartz crystal-lined fractures and generally coarse grain size is evidence the BH Sill is exposed near its roof (Howard, 2005, 2006b). In form it may be cupola or dyke-like.

2. DISTRICT-SCALE STRUCTURAL SETTING

On the CLY Group property, recently found native gold + bismuth (sulpho)telluride showings are spatially and genetically related to the km-scale BH Sill (Fig. 1). This felsic granitoid intrudes uncertainly correlated Lower Paleozoic to Triassic (?) metasedimentary and –volcanic rocks of the Harcourt Ck Assemblage [HCA] (Einarsen, 1995), a division of the enigmatic CS Unit (Little 1985). Howard (2000, 2005) further subdivides the HCA into three structural units. The structurally upper (and youngest) unit includes metabasalts with MORB petrochemistry (Einarsen, 1995). These correlate with Permian

Kaslo Group metabasalts in the central Kootenay Arc (Roback et al., 1994). Together with fault-bounded slivers of serpentinite and pyroxenite (also Permian?) the HCA is considered an ophiolite, a structural slice or sliver of Slide Mountain terrane. The large age range is mostly Middle to Upper Paleozoic, (?) Devonian to Permian and likely also includes Triassic rocks. At the west intrusive contact of the BH Sill on BiTel Knoll, the HCA argillaceous quartzite is silicic, hornfelsed and well veined (Fig. 2).

Elements and minerals in the showings fit the zonal arrangement of Hart (2005) from Au–Bi–Te in the central granitic pluton to Pb–Zn–Ag distal to the intrusion (Caron et al., 2006). CLY veins are *intrusion-hosted* in the granitoid and *proximal, intermediate and distal-placed* with respect to the BH Sill. CLY meets all exploration criteria for an economic Reduced Intrusion-Related Gold [RIRG] system (McCoy et al., 1997, 2002; McCoy, 2000; Hart et al., 2002; Baker, 2003; Hart 2005; Hart and Goldfarb, 2005; Lefevre and Hart 2005). Comparing bismuth–gold linkages CLY is exemplary (Fig. 3).

3. VEIN MINERALOGY

Base metals and sulphide minerals are generally scarce in auriferous qtz veins and shears; the sulphur content is only tens of ppm. Mineral assemblages include native gold, native bismuth, bismuthinite, ingodite, joséite-A, joséite-B, ikunolite, hedleyite, unnamed Bi_2Te and unidentified secondary bismuth minerals (Cook and Ciobanu, 2006; Part II in Howard 2006a). This is the first report of ingodite Bi(Te,S) in Canada, and the first report of ikunolite $Bi_4(S,Se)_3$ and unnamed Bi_2Te in the Western Hemisphere. In the only two polished sections prepared, Eloise Vein has six of the twelve Bi–Te–S minerals identified in gold ore of the Pogo (3.51 M. oz) deposit, i.e., native bismuth, bismuthinite, ingodite, joséite-A, joséite-B and hedleyite (Rombach et al., 2002).

CLY quartz veins, veinlets, shears and tungsten + gold skarn have high Bi contents to > 2,000 ppm (Fig. 3) and abundant Te to >100 ppm. Both strongly correlate with Au (Ray, 2003; Howard, 2006a). Bi and Te are key pathfinder elements for RIRG deposits in primary (Flanigan et al., 2000) and secondary (Baker, 2003) geochemical media.

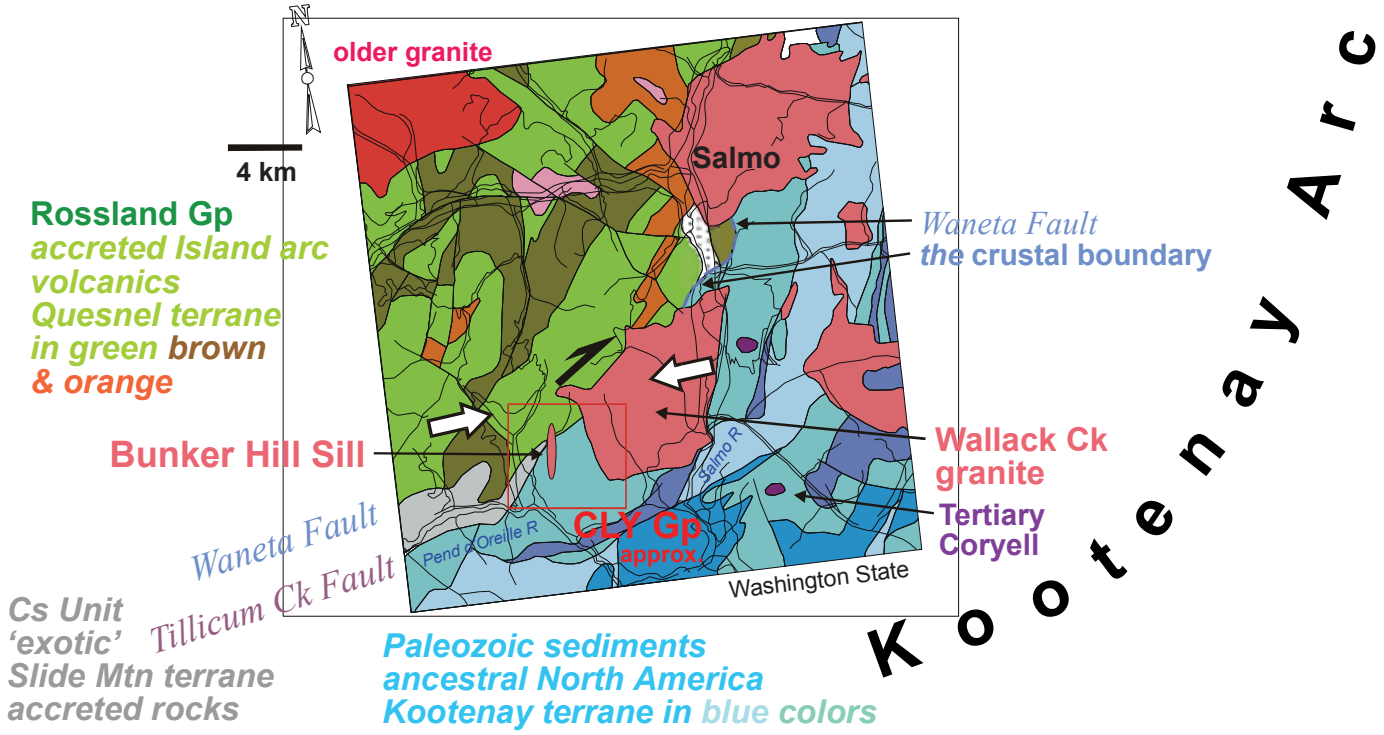

Figure 1. District scale tectonic setting of CLY prospect at the North American accretionary margin. The Kootenay Arc regional structure bends at the Canada-US border. Serpentinite and pyroxenite demarcate the Tillicum Ck Fault.

Figure 2. BiTel Knoll showings, CLY property centre. (Left) Clarissa Transverse Sheeted veins at the BH Sill intrusive contact. Card has cm (top) and inch scales. (Right) Eloise Vein South outcrop. A particular granular silica phase and fractures internal to the vein host clots of gold-associated Bi–Te minerals including ingodite. Vein extends to beyond the left tree.

4. HISTORIC UNDERGROUND MINING AND GOLD CONCENTRATIONS IN VEINS

Small-scale underground mining in the 1930's recovered 3.33 Kg gold (107 oz) and 9,364 Kg silver from three adits of the Bunker Hill Mine, 220 m SW of the central BiTel Knoll showings. For the average 4 foot vein width mined in Adit 2 the gold accumulation value was 13.1 g/t*m at a minimum grade 10.7 g/t. The linear direction of the mined ore shoot is known. Mined veins have low fineness (e.g., 588 for the *intermediate placed* Adit 2 Underhand Stope Vein) compared with the new found BiTel Knoll veins (834 for the *very proximal* Eloise Vein, mean of 10 samples).

Measured gold accumulation values as grade times m width intervals from surface sampling include 9.74 g/t*m for the *intrusion-hosted* Clease 0446-BHCK-13 Shear and 5.1 g/t*m, the mean of six measured samples of the *intermediate placed* Adit 1 Gallery Quartz Vein (Howard 2000, 2006b). This outcrops discontinuously for 46 m.

5. NUMERICAL EXPLORATION MODEL FOR HIGH GOLD POTENTIAL

The numerical exploration model of Flanigan et al. (2000) shows high potential for an *intrusion-hosted to very proximal* subtype of RIRG deposit on CLY Gp (Fig. 3). The model of Flanigan et al. considers three numerical linkages of Bi with Au in mineralized rock in many developed deposits and presently producing mines in the Tintina Gold Belt in the Northern North American Cordillera: the Pearson correlation coefficient $r_{Bi–Au}$, the slope of the best-fit regression line (both using log-transformed data) and the Bi to Au ratio (raw or untransformed data). These linkages measure closeness to the mineralizing intrusive source.

Flanigan et al.'s model is objective as it is arithmetical and irrespective of [1] the favourable outcrop features of the showings, all well drift covered [2] their prospective structural setting near a crustal suture zone [3] crossing vein sets [4] vein density (Lang et. al 2001) sufficient for a RIRG deposit (fig. 2) and [5] the uncommon to very rare gold-associative minerals present (Cook and Ciobanu in Howard, 2006a, b, also 2005).

6. GENETIC CONSIDERATIONS

The Bi-mineral occurrences discussed here support the strong geochemical correlation between Bi and Au, which is typical for intrusion-related Au deposits (Baker et al., 2005). Noting morphologies such as 'droplet' shaped inclusions

and phase assemblages that represent equivalents of eutectic associations in the Au-Te-Bi system, Ciobanu et al. (2004) discussed the formation of Au deposits via Bi-Te-Au melts exsolved from fluids. The Bi-mineral associations found in Clarissa, Eloise and Blue Quartz veins include abundant droplets and patches of Bi-(sulfo) tellurides that are suggestive of deposition in a molten state. All the encountered species have Bi:(Te+Se+S) ratios ≥1 (stable at reducing conditions, i.e., pyrrhotite and magnetite fields). However, the eutectics on the Bi-rich side of the Au-Bi-Te system include maldonite instead of native gold as is observed in the CLY assemblages. Cook et al. (2007, this volume) discuss the textural relationships, Au contents and trends within the Bi-species in more detail. The conclusion is that, even if originally deposited as melts exsolved from a magmatically-derived fluid, the associations record extensive reworking and recrystallization during a subsequent (orogenic?) event that overprint and modify them.

7. EXPLORATION TARGET

CLY Gp targets a near surface, open pittable, M. oz Intrusion-related quartz vein gold deposit with extreme enrichment in both bismuth and tellurium. These elements triply co-associate with gold in over 19 showings on the property.

This large Au–Bi–Te system is little-explored. Sulphide content is low with little potential for acid rock drainage. Mineralization is non-refractory 10-100 µm-sized particulate gold that could be recovered by low-cost gravity separation (McCoy et al., 2002). Local infrastructure is

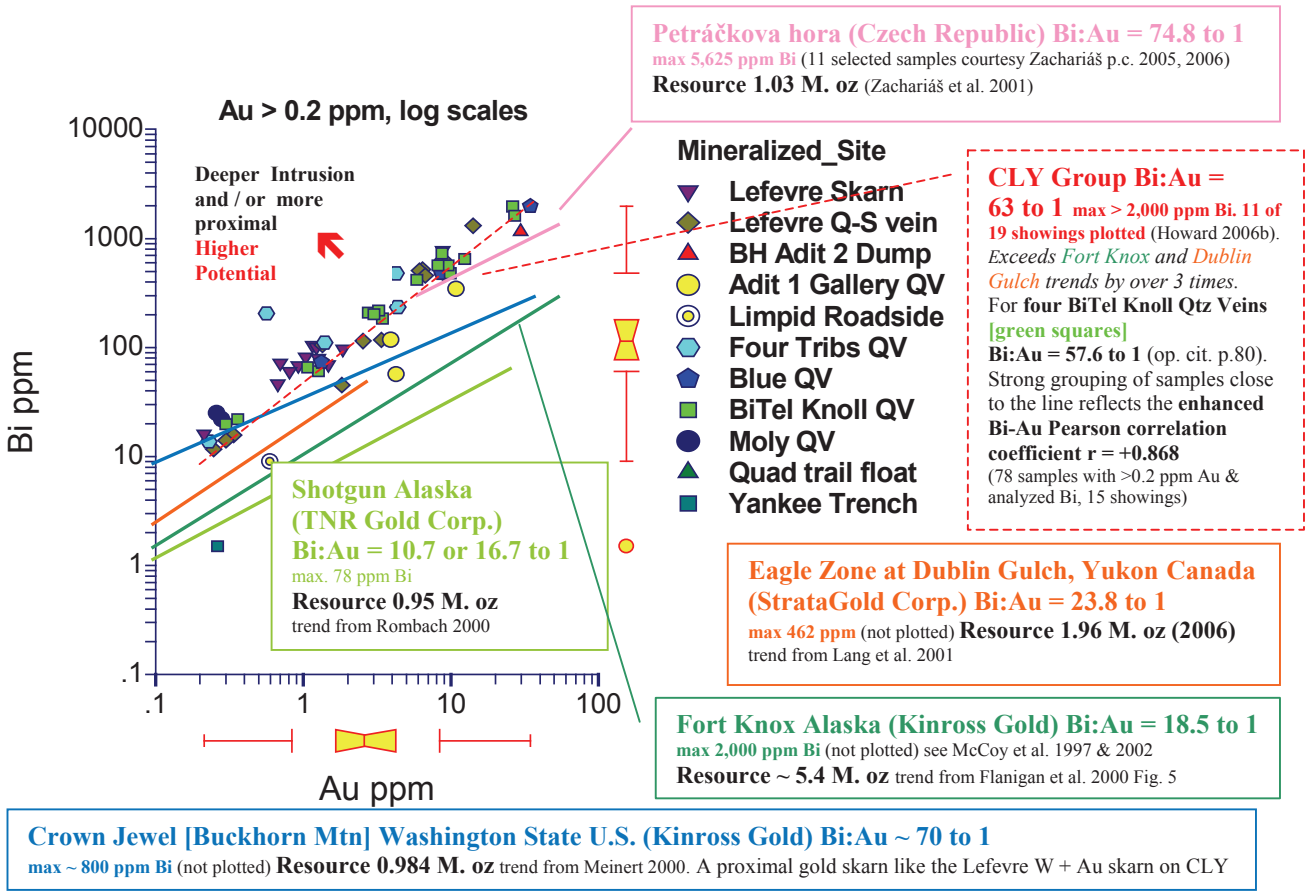

Figure 3. Graph displaying three Bi-Au linkages of CLY Gp rocks. Axes are log scale. Significant explored deposits with mean Bi:Au ratio, max. ppm Bi and gold resource are noted for comparison. The slope of CLY regression line (dashed) is steepest known. Petráčkova hora (Czech Republic; Zachariáš et al., 2001, p.c. 2006 selected samples) is most similar in ratio and Dublin Gulch (Yukon) in slope. Graph axes are logarithmic; thus a slight increase in the slope is a large numerical increase. The mean CLY Bi:Au ratio of 63 to 1 is stable on successively trimming the data by 5, 10 or 15% from each side of the distribution. The last case considers only the central 70% of the ratios (Howard, 2006b, p. 81). The untrimmed ratio is 66.7.

excellent with new logging roads. L. Caron, P. Eng. writes "in my opinion, the property has good potential to host an economic bulk-tonnage intrusion-related gold deposit (April 2007)." She recommends a $600,000 first year exploration programme, half for 1,700 m of large-diameter core drilling and half for further ground surveys. A private company is currently seeking financing for this. Howard (2007) selects six targets for exploratory drilling.

REFERENCES

Baker, T., 2003, Intrusion-hosted gold deposits: Explorable characteristics. Short Course at Cordilleran Exploration Roundup, Vancouver B.C., Jan. 26 2003.

Baker, T., Pollard, P.J., Mustard, R., Mark, G., Graham, J.L., 2005. A comparison of granite-related tin, tungsten, and gold-bismuth deposits: implications for exploration. SEG Newsletter no. 61, p. 5, 10-17.

Caron, L., April 13 2007, Memo 'Proposed Work Program and Budget – CLY Property' 3 p. private report for Wm. R. Howard.

Caron, L., P.Eng, Oct. 3 2006, CLY Property, NTS 82F/02, Salmo Area, SE British Columbia. 9 pp. + 2 p. tables + map. Private Evaluation Report for Kinross Gold Corp.

Ciobanu, C., Cook, N., Pring, A., 2005, Bismuth tellurides as gold scavengers. In: Mineral Deposit Research: Meeting the Global Challenge (J.W. Mao and F.P. Bierlein, eds.), Springer, Berlin-Heidelberg-New York, p. 1383 - 1386.

Cook, N., Ciobanu, C., Howard, W.R., 2007, Bi-tellurides in gold veins, BiTeKnoll (CLY prospect), southeastern British Columbia, Canada. This volume.

Einarsen, J.M., 1995, Structural Geology of the Pend d'Oreille area and tectonic evolution of the southern Kootenay Arc. Unpubl. Ph.D. Thesis, University of Calgary, Calgary AB, 172 pp.

Flanigan, B., Freeman, C., Newberry, R., McCoy, D., Hart, C., 2000, Exploration models for mid and Late Cretaceous intrusion-related gold deposits in Alaska and the Yukon Territory, Canada. In: Cluer, J.K. et al. (Eds.), Geology and Ore Deposits 2000: The Great Basin and Beyond. Geological Society of Nevada Symposium Proceedings May 15-18 2000, p. 591-614. http://www.avalonalaska.com/pub/TGTpap4web.pdf

Hart, C.J., et al., 2002, Geology, Exploration and Discovery in the Tintina Gold Province, Alaska and Yukon. Society of Economic Geologists Special Publication 9: Integrated Methods for Discovery: Global Exploration in the 21st Century, p. 241–274.

Hart, C.J.R., Goldfarb, R., Oct. 25 2005, Short Course 'Intrusion-Related Gold Systems – with emphasis on Yukon and Alaska'. Minerals South Conference, Cranbrook B.C.

Hart, C.J.R., 2005, Classifying, Distinguishing and Exploring for Intrusion-Related Gold Systems. The Gangue, Newsletter of the Geological Association of Canada Mineral Deposits Group, issue 87, p. 1 & 4-9. http://www.gac.ca/SECTIONS/GANGUE/Gang87.pdf

Lefevre, D.V. and Hart, C.J.R., 2005, Plutonic-Related Au Quartz Veins & Veinlets L02 B.C. Mineral Deposit Profile http://www.geology.gov.yk.ca/metallogeny/mineral_deposit_profiles/of2005_5/l02_plutonic_related_au_quartz_veins_and_veinlets.pdf

Howard, W.R., 2000, CLY Group Total Field VLF-EM Geophysical, Soil / Rock Geochemical, and detailed Geologic Surveys, Bunker Hill Mine area, NTS 082F03 W ½ Nelson Mining Division, B.C. Assessment Report 26, 159. www.em.gov.bc.ca/DL/ArisReports/26159.PDF

Howard, W.R., 2005, BiTel Knoll Mineralized Rock Geochemical Survey on CLY Group, Bunker Hill Mine area, B.C. Assessment Report 27,893. 70 pp., 2 maps, 20 tables, 5 appendices, 18 figs. www.em.gov.bc.ca/DL/ArisReports/27893.PDF

Howard, W.R., 2006a, unreleased Assessment Report Part I: 'Rare to exceptionally rare Gold-associated Bi–Te–S–(Se) ore minerals new to Canada: ingodite ikunolite unnamed Bi_2Te associated with hedleyite joséite-A joséite-B native gold…' 93+ pp. 2 tables, 8 figs., 1 map. Part II: 'Mineralogical investigation of polished sections from CLY Group, Southeastern B.C., Canada – Preliminary Report' by N. Cook and C. Ciobanu, 11 pp., Aug. 10 2006.

Howard, W.R., 2006b, unreleased Assessment Report 'Geochemistry and Structural Geology of Reduced Intrusion Related gold [RIRG] showings on CLY Group claim # 516584, notably the Pogo-like Eloise Vein and the Fort Knox-like Clarissa Sheeted Veins on BiTel Knoll and the five Clease Quartz Veins and Shears. Auriferous bismuth telluride-bearing mineralization including especially rare ingodite ikunolite unnamed Bi_2Te hedleyite joséite-B and joséite-A, with native gold grains native bismuth and bismuthinite defining deposit type L-02 'Plutonic-Related Au Quartz Veins & Veinlets' in Salmo Sheet NTS 082F03 W 1/2, Nelson Mining Division B.C.' 129+ pp., 11 tables, 24 figs., 3 maps.

Howard, W.R., Mar. 26 2007, Letter Report to L. Caron discussing Six Exploratory Drill Targets on CLY Group. 14 pp. + 2 pp. refs.

Howard, W.R., Apr. 17 2007, Executive Technical Summary "Rock geochemistry of CLY Group surpasses Dublin Gulch, Fort Knox and other Intrusion-related gold deposits: new found showings of native gold with rare bismuth (sulfo)telluride minerals have numerical linkages exceeding Million oz. deposits. High potential, objectively illustrated." 6 pp.

Höy, T., Dunne, K.P.E., 1999, Geological compilation of the Trail map-area, southeastern British Columbia (082F/3,4,5,6). British Columbia Ministry of EMPR Geoscience Map 1998-1 a colour compilation map at 1:100,000 scale

Lang, J.R., ed., 2001, Regional and System-Scale controls on the Formation of Copper and/or Gold Magmatic-Hydrothermal Mineralization. The Mineral Deposit

Research Unit, University of British Colombia Special Publication 2, Vancouver B.C.

Little, H.W., 1985, Geological Notes Nelson West Half (82F, W1/2) Map Area. GSC Open File 1195, 47 pp.

Logan, J.M., 2002a, Intrusion-related Gold Mineral Occurrences of the Bayonne Magmatic Belt. Geological Fieldwork 2001, BC MEMPR, Paper 2002-1, p. 237-246. http://www.em.gov.bc.ca/DL/GSBPubs/GeoFldWk/2001/17-JL-p237-246.pdf

Logan, J.M., 2002b, Intrusion - Related Mineral Occurrences of the Cretaceous Bayonne Magmatic Belt, Southeast British Columbia (NTS 82/E,F,G,J,K,L,M,N). BC MEMPR Geoscience Map 2002-1 scale 1:500 000 at http://www.em.gov.bc.ca/mining/Geolsurv/bedrock/mapsonline/dwfs/GM2002-1.htm

Logan, J.M., Colpron, M., 2006, Stratigraphy, geochemistry, syngenetic sulphide occurrences and tectonic setting of the lower Paleozoic Lardeau Group, northern Selkirk Mtns, B.C. In: Colpron, M., Nelson, J.L. (Eds.), Paleozoic Evolution and Metallogeny of Pericratonic Terranes at the Ancient Pacific Margin of North America, Canadian and Alaskan Cordillera: Geological Association of Canada, Special Paper 45, p. 361-382.

McCoy, D., Newberry, R., et al., 1997, Plutonic-Related Gold Deposits of Interior Alaska. Goldfarb, R.J., Miller, L.D. (Eds.), Mineral Deposits of Alaska. Econ. Geol. Monograph 9, p. 191-241.

McCoy, D., Newberry, R., Severin, K., Marion, P., Flanigan, B., Freeman, C., 2002, Paragenesis and metal associations in interior Alaska gold deposits: an example from the Fairbanks district. Mining Engineering 54, 33-38. (also Preprint number 00-036, presented at the SME Annual Meeting, Feb. 28 - Mar. 1 2001, Salt Lake City, UT http://me.smenet.org/200201/pdf/min0201_33.pdf)

McCoy, D.T., 2000, Mid-Cretaceous plutonic-related gold deposits of interior Alaska: metallogenesis, characteristics, gold associative mineralogy and geochronology. Ph.D. thesis, University of Alaska at Fairbanks AK. 245 pp.

Meinert, L.D., 2000, Gold in skarns related to epizonal intrusions. SEG Reviews in Economic Geology 13, 347-375.

Ray, G.E., 2003, Assessment Report on the Geology and Mineral Potential of the CLY1 & 2 claims (including the Bunker Hill & Mormon Girl Crown Grants), southeastern British Columbia, Canada (NTS 082F03)… 60 pp., 2 maps http://www.em.gov.bc.ca/DL/ArisReports/27513A.PDF

Roback, R.C., Sevigny, J.H., Walker, N.W., 1994, Tectonic Setting of the Slide Mountain terrane, southern British Colombia. Tectonics 13, 1242-1258. http://www.agu.org/pubs/crossref/1994/94TC01032.shtml

Rombach, C.S., Newberry, R.J., Goldfarb, R.J., Smith, M., 2002, Geochronology and Mineralization of the Liese Zones, Pogo Deposit, Alaska. Paper 52-15 Denver Annual Meeting The Geological Society of America http://gsa.confex.com/gsa/2002AM/finalprogram/abstract_45183.htm

Rombach, C.S., 2000, Genesis and Mineralization of the Shotgun Deposit, southwestern Alaska. In: Tucker, T.L., Smith, M.T. (Eds.), Gold Belt: Concepts, Exploration, and Discoveries, Special Volume 2, British Columbia and Yukon Chamber of Mines, Cordilleran Roundup Jan. 2000, p. 181-196.

Rombach, C.S., et al., 2004, Telluride-bearing deposits of the Tintina Gold Province, Alaska: Investigations of the Fort Knox and Pogo gold deposits. Oral Presentation in session: "G14.07 - Telluride and selenide minerals related to gold- and platinum-group element deposits" 32nd IGC, Florence Italy, Abstract volume CD-ROM, abstract 54-11 http://www.32igc.info/igc32/search/

Zachariáš, J., et al., 2001, Geology and Genesis of Variscan porphyry-style gold mineralization, Petráčkova hora deposit, Bohemian Massif, Czech Republic. Mineralium Deposita 36, 517-541.

Au-Ag-Bi-Te-Se vein mineralization at Roikonkoski, Karelia, northern Lake Ladoga region

V.I. IVASHCHENKO — Institute of Geology, KarRC, RAS, Russia, Republic of Karelia, Petrozavodsk, Pushkinskaya, 11, ivashche@krc.karelia.ru
O.B. LAVROV — Institute of Geology, KarRC, RAS Russia, Republic of Karelia, Petrozavodsk, Pushkinskaya, 11,
K. SUNDBLAD — Department of Geology, University of Turku, Finland, 20014 Turun yliopisto, krisun@utu.fi
A.N. TORITSIN — Karelprirodresurs, Russia, Republic of Karelia, Petrozavodsk, Varlamova, 72.

Summary: At set of Au-Ag-Bi-Te-bearing quartz-carbonate veins have been discovered in a Palaeoproterozoic metadolerite in Russian Karelia, 38 km north of Pitkäranta at Lake Ladoga. The metadolerite has intruded into carbonaceous shales of the Karelian Soanlahti suite (PR_1), which rests on top of the Jatulian Tulomozero dolomites and a crystalline basement consisting of an Archaean craton (AR_2). Sulphide mineralization has also been recognized in the Soanlahti carbonaceous shales. 41 ore minerals have been recognized in the quartz-carbonate veins and the carbonaceous shales, of which eleven are tellurides (hedleyite, pilsenite, tsumoite, tellurobismuthite, hessite, stutzite, racklidgite, joseite-B, altaite, volynskite and petzite); four bismuto-tellurides with the composition Bi_3Te, Bi_3Te_2, $BiTe_4$, PbBiTe; three selenides (clausthalite, tellurolaitakarite and selenium) and ten native metals and alloys (gold, silver, electrum, tellurium, copper, iron, lead, tin, bismuth and osmiridium). Ore mineralization was formed in the temperature range of 550 - <170°C, with very active Se and Te, beginning with medium temperatures (>300°C) - the complete miscibility of galena-clausthalite and galena-altaite. A wide temperature range (>400°C) of the evolution of the ore-forming process, together with the diversity of telluride and native-metal mineralization and the bizarre clustering of different-temperature associations, suggest that the Roikonkoski ore occurrence is a xenothermal type of deposit in the nomenclature of A.F. Baddington. The strong affinity to sheared parts of the metadolerite suggest that the veins were formed under "orogenic" conditions in the nomenclature of Groves, Goldfarb and others.

Key words: metadiabase, veins, black schists, tellurides, gold, silver, bismuth, tellurium, selenium, Paleoproterozoic, Roikonkoski, Republic of Karelia, Russian Federation

1. INTRODUCTION

The Roikonkoski Au-Ag-Bi-Te-Se occurrence is located 2 km southwest of the Roikonkoski village in the Leppäsyrjä gold prospect, Suojärvi area, Republic of Karelia. It occurs in a metadolerite that has intruded into a suite of Palaeoproterozoic Karelian supracrustal rocks (PR_1) close to the border to the Archaean Karelian craton (AR_2). Cu-Pb mineralization was first observed in 2004 in a quarry, operated for aggregate production by the Karelprirodresurs Open Joint-Stock Company. Subsequent joint studies, conducted by the Institute of Geology at the Karelian Research Center of the Russian Academy of Sciences in Petrozavodsk and the University of Turku, Finland, revealed a number of ore minerals and large quantities of several metals, e.g. Au (up to 25 ppm), Ag (up to 100 ppm), Bi (up to 350 ppm), Te (up to 171 ppm) and Se (up to 219 ppm).

2. GEOLOGICAL SETTING

The Roikonkoski ore-bearing carbonate-quartz veins occur in a metadolerite sill, which intruded at 2.1 Ga into a sequence of volcanic and sedimentary rocks belonging to the Karelian Soanlahti suite (PR_1), which at Roikonkoski is over 1750 m thick. It is subdivided into lower and upper subsuites. The lower subsuite ($\leq$ 750 m), consists of mottled dolomites, quartz-biotite-sericite-talc-chlorite schists, occasionally carbonaceous shales, less common basalt and metapophyrite bodies. The upper subsuite ($\geq$ 1000 m), is characterized by abundant carbonaceous biotite-sericite-talc-chlorite-amphibole schists, basalts and pyrite-pyrrhotite mineralization with anomalous contents of e.g. V, Mo, Ag, Au and Se. The Soanlahti suite is overlain by alumina-rich turbidites of the Kalevian Ladoga series.

3. ORE MINERALIZATION

a) vein mineralization in meta-dolerite

The Roikonkoski ore-bearing carbonate-quartz veins are cm-m-wide and occur as a swarm in a 300 wide NW-trending zone. The strike directions of the veins are predominantly NW (and NS) with steep dips towards NE (and E). This structure may be linked to the Au-bearing structures at Ilomantsi further 75 km towards NNW. The veins occur in dm- to m-wide shear zones with a visible length of up to 100 m. Dm-m-wide metasomatic alteration zones (including chloritization, carbonatization, silicification and tourmalinization) occur along the contact between the veins and the metadolerite, accompanied by sulphide disseminations. The ore minerals can be arbitrarily sub-divided into the following associations: pyritic, poly-sulphide, galena-bismutotelluride with silver and gold minerals as well as native metals and alloys. The two latter associations are the most important carriers of gold and silver. The abundance of ore minerals is generally c. 5-10%; metal contents are shown in Table 1. In addition to the common above-mentioned Bi-, Te-, Se-, Ag- and Au-rich mineral associations, an association that reflects the primary geochemical pattern of the altered meta-dolerite is also recognized. It occurs at the exocontacts of the carbonate-quartz veins and is composed of metasomatically altered dolerites that exhibit a distinct thinly-banded texture,

Table 1. Metal contents in ore samples collected from outcrop at the Roikonkoski quarry.

Sample №	Au ppm	Ag ppm	Te ppm	Se ppm	Bi ppm	Pb wt-%	Cu wt-%	Zn wt-%	As ppm	Sb ppm
1		460			320	>1.0	0.68	0.015		
3		100			220	>1.0	0.032	0.10		
3a	1.84	64								
3b	4.47	67								
R1	0.03	41								
2		>1000			2200	>1.0	>1.0	0.032		
KS0543	0.01	78.6	61	178	189.4	4.42	1.11	0.03	<0.5	2.8
4		>1000			>10000	>1.0	>1.0	>1.0		
5		>1000			10000	>1.0	>1.0	>1.0		
R1a	0.09	230	120							
6	0.03	3.0								
7	0.03	1.0								
KS0556	1.04	88.3	171	140	332.7	0.13	2.56	0.04	4.0	0.3
KS0557B	0.01	2.1		5.7	5.2	0.01	0.05		0.9	0.1
KS0557	25.28	23.9	17	49.8	43.0	0.05	1.37	0.02	<5	0.1
KS0558	18.72	91.6	155	219	318.4	0.20	4.85	0.09	0.5	0.1
KS0559		7.7		32.1	0.3	0.01	0.02		5.0	0.1

emphasized by the distribution of amphibole and quartz-carbonate aggregates that also contain chlorite, epidote and albite. The dolerites have been chloritized, carbonatized, silicified and locally tourmalinized. The ore mineralization in the zones consists dominantly of fine-grained pyrite (30-40%), pyrrhotite, magnetite, ilmenite, rutile, chalcopyrite and a later phase of sphalerite, bornite, chalcosine, anilite, galena, native Zn-bearing copper (up to 35% Zn), native copper with Sn impurity (20-30%), native copper with Ni impurity (3%), native iron, native lead with As impurity (1.5%) and native silver. The native metal particles vary in size from 1 to 20 μm. The carbonate-quartz veins are made up of quartz, calcite, chlorite, albite, sericite and ore minerals. The quartz is considerably broken down and granulated. Large quartz grains with cloudy, undulating extinction show fine polysynthetic twinning. Carbonate occurs dominantly at veinlet selvages as zones composed of xenomorphic grains, up to 2 mm in size, where twins often are deformed (indication of shears) and cut by quartz microveinlets. The ore mineralization is mainly restricted to the contact zone between the quartz and carbonate constituents of the veins. Chlorite is light-green, foliated, up to 0.5 mm in size and forms glomerogranular clusters. Albite occurs as

scarce grains and is associated with carbonate. Sericite is encountered as scarce scales in carbonate. Pyrite was formed before carbonate, whereas all other ore mineral associations were formed simultaneously with and after it. Carbonate-chalcopyrite microveinlets are characteristic; their filling varies repeatedly along the strike from carbonate to ore and combined.

Pyrite mineralization in the quartz-carbonate veins, like the mineralization of more recent associations and carbonate, typically shows a highly irregular distribution. Macroscopically, intervals of several meters along the dip of the veins often look as if they are barren or only contain pyrite. However, detailed instrumental studies show that they contain galena, chalcopyrite, sphalerite, bismutotellurides and native metals, such as silver and copper, but their content is typically small.

The polysulphide mineral association (chalcopyrite, cubanite, bornite, sphalerite, galena etc.) dominates in the ore occurrence. It forms disseminations, veinlets, nests and massive aggregates. Chalcopyrite is intergrown with galena, sphalerite, hessite and bismutotellurides. It often contains graphic cubanite units and sphalerite microinclusions with stellar morphology, galena and less common pyrrhotite with the composition $(Fe_{0,75}Co_{0,15}Ni_{0,02}Cu_{0,07})_{0,99}S_{1,01}$. It is cross-cut by pyrite microveinlets that contain Cu (5.73%) and Ni (0.94%). Sphalerite is Fe-poor but Cd-rich (2.34-4.35%). The cubanite contains 0.74-1.08% Ni and 3.83-5.45% Co.

The galena-bismutotelluride mineral association is the most extensive from a mineral diversity point of view (>20 minerals) at Roikonkoski. The composition of galena varies almost continuously from proper galena (<1% Se) to clausthalite (>20% Se). Intermediate phases between clausthalite and altaite also occur: $(Pb_{0.80}Bi_{0.23})_{1,03}(Se_{0.73}Te_{0.24})_{0.97}$, $Pb_{1.10}(Se_{0.80}Te_{0.10})_{0.90}$. It has often increased contents of bismuth (up to 6%) and silver (up to 0.5%).

Bismutotellurides with occassional contents of selenium and lead and less common silver and copper (Table 2) are fully represented in the Bi-Te system (hedleyite, pilsenite, tsumoite and tellurobismuthite). Furthermore, phases with similar compositions to Bi_3Te, Bi_3Te_2, $BiTe_4$ and PbBiTe, were detected. Characteristic for bismutotellurides are graphic < 1 mm intergrowths with galena and hessite (Fig. 1d). This mineral triad is sometimes accompanied by volynskite - $Ag(Bi_{0,88}Pb_{0,22})_{1,00}Te_{1,48}Se_{0,39}$, $AgBi_{1,05}Te_{1,95}$ or occurs instead of galena. In other associations, volynskite often occurs at the boundary of galena and chalcopyrite grains or is incorporated in galena units. More complex symplectitic aggregates with dominant bismuth telluride (pilsenite-tsumoite), chalcopyrite, galena, hessite and greenockite - $(Cd_{0.94}Te_{0.03}Fe_{0.03})_{1.00}(S_{0.99}Se_{0.01})_{1.00}$ also occur (Fig. 1 e, f) presumably formed by decomposition of complex sulphosalts. In addition to graphic and symplectitic intergrowths with the above minerals, hessite is encountered in association with petzite, electrum and gold and as independent units (up to 1 mm in size) and microinclusions in pyrite and quartz. Regardless of association, hessite has not wide compositional variations (Table 2), but can contain up to 3% gold. Stützite ($Ag_{4,35}Te_3$) is far less common. Petzite ($Au_{1,18}Ag_{2,83}Cu_{0,10}Te_{1,88}$; $Au_{1,20}Ag_{2,88}Te_{1,92}$; $Au_{1,06}Ag_{2,96}Te_{1,97}$) typically occurs only in the presence of electrum or native gold, forming a zone that separates them from hessite (Fig. 1 a,b).

The compositions of some mineral phases of the bismutotelluride association are similar to those of rucklidgeite – $Pb_{0,91}Bi_{2,74}(Te_{2,82}Se_{0,53})_{3,35}$, joseite-B - $Bi_{2,51}Cd_{0,05}Te_{1,44}Se_{0,37}S_{2,64}$, a tellurium variety of laitakarite $(Bi_{2,51}Te_{1,44}Cd_{0,05})_{4,00}$ $(Se_{0,36}S_{2,64})_{3,00}$, while others, even in rough approximation, $PbBi_{2,11}(Te_{1,72}Se_{0,34})$ (?), $AgBi_{2,36}Te_{2,91}Se_{0,79}$ (?) do not correspond to any known mineral of the system discussed.

Native metal minerals (and alloys) include those of gold, silver, electrum, bismuth, tellurium, selenium, copper, lead, tin, and iron. The units, formed by most of them, except bismuth and tellurium, are not more than 20 μm in size. Native gold that dominantly shows lamellar morphology is encountered in vein quartz, chalcopyrite and galena, and is associated with bismutotellurides, petzite and hessite (Fig.1a, b). It varies slightly in composition, Au (64.16-81.79), Ag (18.21-35.84) and sometimes contains 7.76% Hg, 0.94% Se and 4.99% Te. Native silver occurs as dendrite-like microinclusions in most ore minerals and quartz. Acanthite, one of the latest minerals, is

encountered as skeletal micro-inclusions in quartz and carbonate and as numerous idiomorphic crystals in carbonate microgeodes (Fig. 1c).

Table 2. Electron microprobe analyses in wt.% of ore minerals from the Roikonkoski ore occurrence.

Mineral	Au %	Ag %	Te %	Se %	Bi %	Pb %	Cu %	Fe %	S %	Total%
Gold	71.21	28.79								100.00
	71.05	28.95								100.00
	81.79	18.21								100.00
Petzite	29.72	38.87	30.60				0.82			100.00
	26.50	40.22	31.53				1.74			100.00
Volynskite		19.34	33.95	5.52	33.04	8.14				100.00
		18.81	43.34		37.85					100.00
		18.72	43.35		37.93					100.00
		16.62	41.25	3.03	33.42		5.68			100.00
Hedleyite			26.23		73.77					100.00
Pilsenite			27.92	2.43	67.90		1.06	0.68		100.00
			31.99		68.01					100.00
			34.33		65.67					100.00
			25.88	3.20	70.25		0.67			100.00
Tsumoite			39.34		56.79	3.87				100.00
		2.25	39.94		57.81					100.00
			34.36		62.46	3.16				100.00
		2.25	38.43		54.65	4.67				100.00
Tebismuthite		1.86	35.33	1.11	49.19					100.00
Tellurium			75.57		24.43					100.00
		1.44	84.05		14.51					100.00
Hessite		61.33	38.67							100.00
		62.51	37.49							100.00
	4.02	57.89	36.98				1.11			100.00
Stützite		55.11	44.89							100.00
	1.17	56.30	42.53							100.00
Joseite B			22.24	3.49	67.03				7.24	100.00
Laitakarite			21.20	3.61	64.43				10.12	100.00
Galena				1.96		85.17			12.87	100.00
				5.70		82.63			11.67	100.00
				8.78		80.95			10.27	100.00
			2.75	10.72		78.31			8.22	100.00
				13.39		79.93			7.65	100.00
				15.30		78.58			6.12	100.00
				17.41		78.83			7.78	100.00
Clausthalite			4.40	20.64		74.95				100.00
				21.20		78.80				100.00
				28.10		71.90				100.00
Rucklidgeite			30.97	3.63	49.95	16.14				100.00

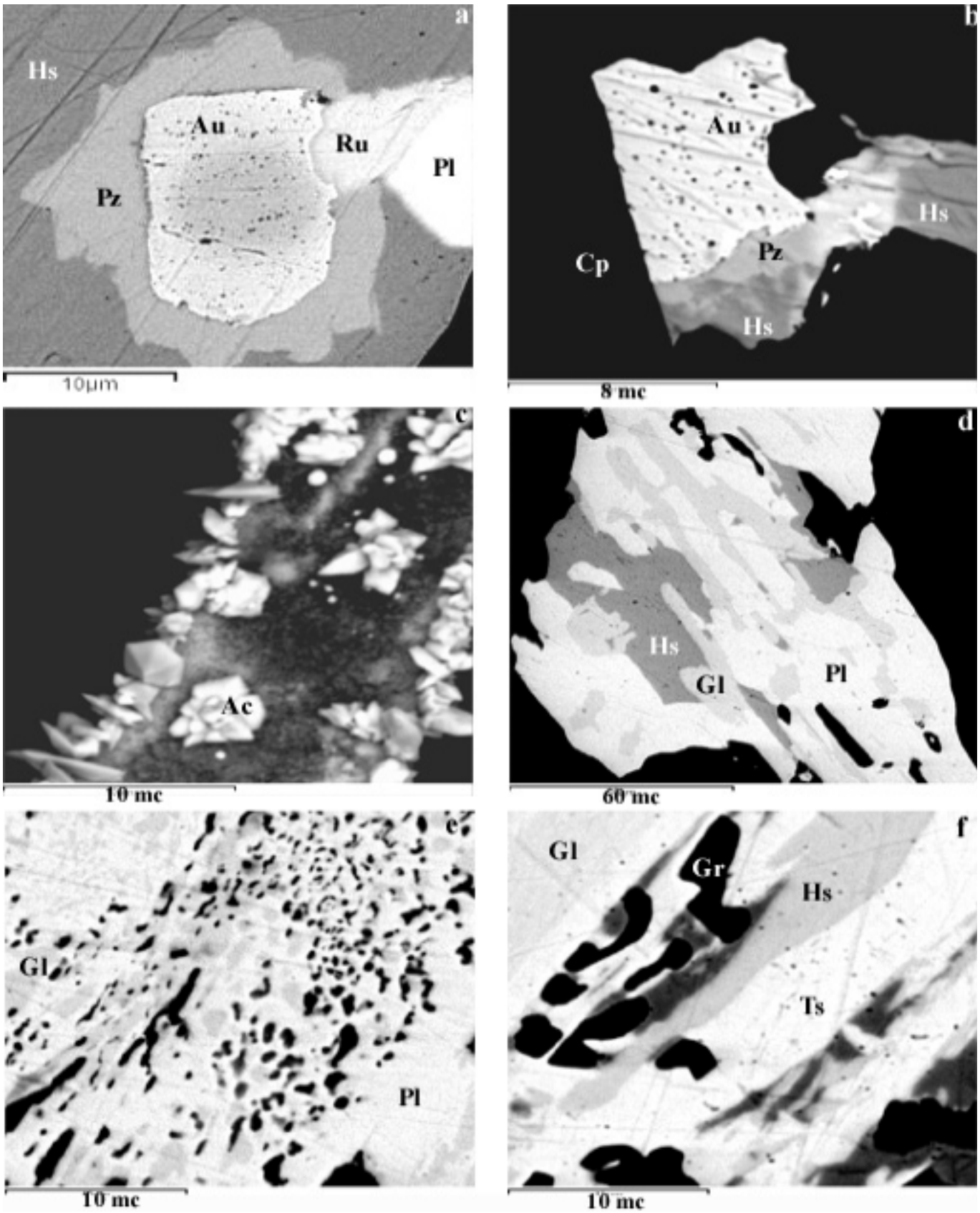

Fig. 2. Electron photomicrographs of ore minerals of the Roikonkoski ore occurrence: **a**) native gold (Au), petzite (Pz), rucklidgeite (Ru) and pilsenite (Pl) in hessite (Hs); **b)** native gold (Au), petzite (Pz) and hessite (Hs) in chalcopyrite (Cp); **c)** acantite (Ac) in calcite; **d)** graphic intergrowths pilsenite (Pl) with galena (Gl) and hessite (Hs); **e)** symplectitic intergrowths pilsenite (Pl), galena (Gl) and greenockite (black); **f)** graphic intergrowths tsumoite, galena (Gl), hessite (Hs) and greenockite.

Native bismuth forms scarce grains, c. 5 μm in size, in vein quartz and grows on galena faces to form inclusions. Native tellurium with up to 25% bismuth impurity occurs in subgraphic intergrowths with galena and hessite. Selenium is a scarce microinclusion in pyrite.

b) mineralization in the Soanlahti suite

Drill core data show that carbonaceous shales, which underlie the vein-bearing dolerites, are highly brecciated, are pierced by numerous quartz veinlets and are rich in Mo (0.022-0.046%), Cu (0.05%), Pb (0.032%), Zn (0.05%), V (0.1-0.15%) and Ag (1-3 ppm). They host irregularly distributed ore mineralization: pyrite, rutile, ilmenite, molybdenite, chalcopyrite, covelline, galena, clausthalite, cobaltine, sphalerite, pyrrhotite, osmiridium, native copper, zinc copper (Zn ~35%), nickel, iron, tin (Pb – 5%), lead (Sb - 7%, Sn - 5%) and silver. Two generations of pyrite, chalcopyrite and galena can be recognized: Galena-1 (without Se) occurs as small inclusions in chalcopyrite. Galena-2 (with 5-20 % Se) occurs as bigger independent units restricted commonly to quartz veinlets. 5-10 μm grains of clausthalite and 0.5 mm sized grains of osmiridium (Ir_3Os_2) make up clusters of fine xenomorphic grains in graphite. Native metals in black shales are represented dominantly by fine (2-20 μm) xenomorphic grains, zinc and copper being most common among them.

4. CONCLUSIONS

The formation of ore mineralization spanned a wide temperature range - from 550°C (as shown by the occurrence of stellar sphalerite inclusions in chalcopyrite) to <170°C (as indicated by the presence of acanthite, hessite etc.). Gold-telluride associations were formed chiefly at the final stages of ore formation, although selenium and tellurium were also fairly active in solutions at medium temperatures. Evidence for that is provided by the practically complete miscibility of galena-clausthalite and galena-altaite observed at a temperature over 300° (Afifi et. al., 1988). The abundance of the symplectitic intergrowths of the minerals of the system Bi-Te-Ag-Se-Pb in the Roikonkoski prospect indicates high-gradient changes in mineral crystallization conditions. This, together with the wide temperature range (> 400°C) of the evolution of ore formation and the diversity of telluride (14 minerals) and native metal (13 minerals) mineralization and the bizarre clustering of different-temperature associations, suggests that the Roikonkoski is a xenothermal type of deposits, according to A.F. Baddington (Park & MacDiarmid, 1966). A more recent approach, applying the "orogenic" or "mesothermal" concepts of Goldfarb et al. (2001) is even more relevant for the Au-Ag-Bi-Te-Se-bearing quartz-carbonate veins at Roikonkoski implying that a genetic link to the Au-bearing structures at Ilomantsi cannot be excluded.

The ore mineralization in the black shales has several identical rare minerals (selenian galena, clausthalite, native zinc copper, tin, lead and silver). It is still an open question whether this ore type is genetically related to the ore-bearing quartz-carbonate veins or whether they are part of a stratabound mineralized system.

REREFENCES

Afifi, A.M., Kelly, W.C. & Essene, E.J., 1988, Phase relations among tellurides, sulfides, and oxides: I. Thermo-chemical data and calculated equilibria. Economic Geology 83, 377-394.

Goldfarb, R.J., Groves, D.I. and Gardoll, S., 2001, Orogenic gold and geological time: a global synthesis. Ore Geology Reviews 18, 1-75.

Park C.F. & MacDiarmid, R.A., 1966, Ore deposits. Moscow, Meer, Russia, 546 p.

Geochemistry of Se and Te in Arsenian Pyrite: New Evidence for the Role of Se and Te Hydrothermal Complexes in Carlin and Epithermal-type Deposits

Stephen E. KESLER — Department of Geological Sciences, University of Michigan, Ann Arbor, MI 48109-1005, USA – skesler@umich.edu

Artur P. DEDITIUS — Department of Geological Sciences, University of Michigan, Ann Arbor, MI 48109-1005, USA – deditius@umich.edu

Stephen CHRYSSOULIS — Amtel, 100 Collip Circle, Suite 205, UWO Research Park, London, Ontario, N6G 4X8, Canada –amtel@skynet.ca

Summary: Analyses by electron microprobe and secondary-ion mass spectrometry provide information on the relation of Se and Te to other trace elements in arsenian pyrite from Carlin-type and low-sulfidation type epithermal deposits. Correlations between abundances of Se and Te and the other trace elements probably reflect similar behavior in hydrothermal solution and possibly the presence of as yet unknown complexes. Strongest correlations are seen between Te and both Au and Ag in Carlin-type deposits and between Te and Ag in epithermal-type deposits; correlations of Au and Ag with Se are uniformly poor. Although correlations with Te are strong, crossplots indicate low Te:Au and Te:Ag ratios of ~0.1 or less, suggesting that Te was not sufficiently abundant to complex either Au or Ag. These results suggest that Se complexes are not present and that Te complexes, though present, are of secondary importance as an agent of metal transport.

Key words: pyrite, arsenic, trace elements, selenium, tellurium, gold, silver, ore-forming fluids

1. INTRODUCTION

Arsenian pyrite is an important constituent of many hydrothermal deposits that contain Se and Te. In most Carlin and low-sulfidation epithermal deposits, the arsenic in arsenian pyrite has an oxidation state of -1 and substitutes for sulfur (Palenik et al., 2004; Simon et al., 1999). In high-sulfidation epithermal deposits, some arsenian pyrite contains arsenic with an oxidation state of 3+, which substitutes for Fe (Deditius et al., 2007). The two types of pyrite are commonly distinguished as As^{1-}-pyrite and As^{3+}-pyrite, respectively.

The presence of As^{3+}-pyrite in high-sulfidation deposits appears to reflect the relatively high oxidation states of fluids that form this mineral. Under these conditions, hydrothermal solutions contain oxidized (3+) arsenic, which substitutes for Fe in the structure of the pyrite, and the pyrite coexists with barite, alunite and similar phases.

2. TRACE ELEMENT CONTENTS OF ARSENIAN PYRITES

Trace element analyses have been carried out on As^{1-} and As^{3+}-pyrites using both secondary-ion mass spectrometry (SIMS) and electron microprobe (EMPA). EMPA analyses show that Se varies inversely with S in both types of deposits, indicating that it substitutes for S. EMPA detection limits are too high to provide information on the setting of Te, although Chouinard et al. (2005) have shown that Te follows Se in arsenian pyrite.

SIMS analyses provide information on concentrations of trace elements, but were not carried out on S or Fe (thus limiting our ability to determine whether the trace elements substitute for S or Fe). In general, Se and Te from the SIMS analyses are more abundant in As^{1-} pyrites than in As^{3+} pyrites.

Systematic behavior of trace elements relative to Se and Te was observed in our analyses, particularly in the As^{1-} pyrites. Specifically, Se shows weak to no correlations with all elements

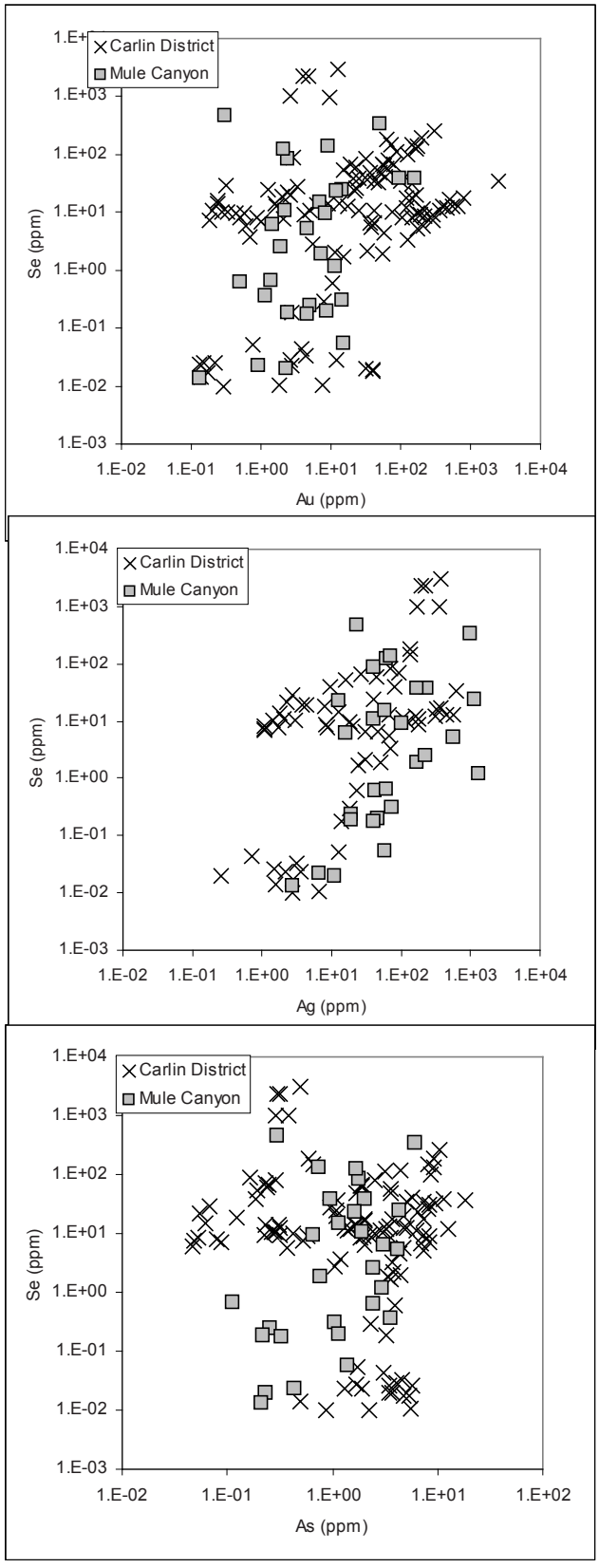

Figure1. Relation of Se to Au, Ag and As in SIMS analyses of As^{1-} pyrite from Carlin-type and Mule Canyon low-sulfidation epithermal type deposits.

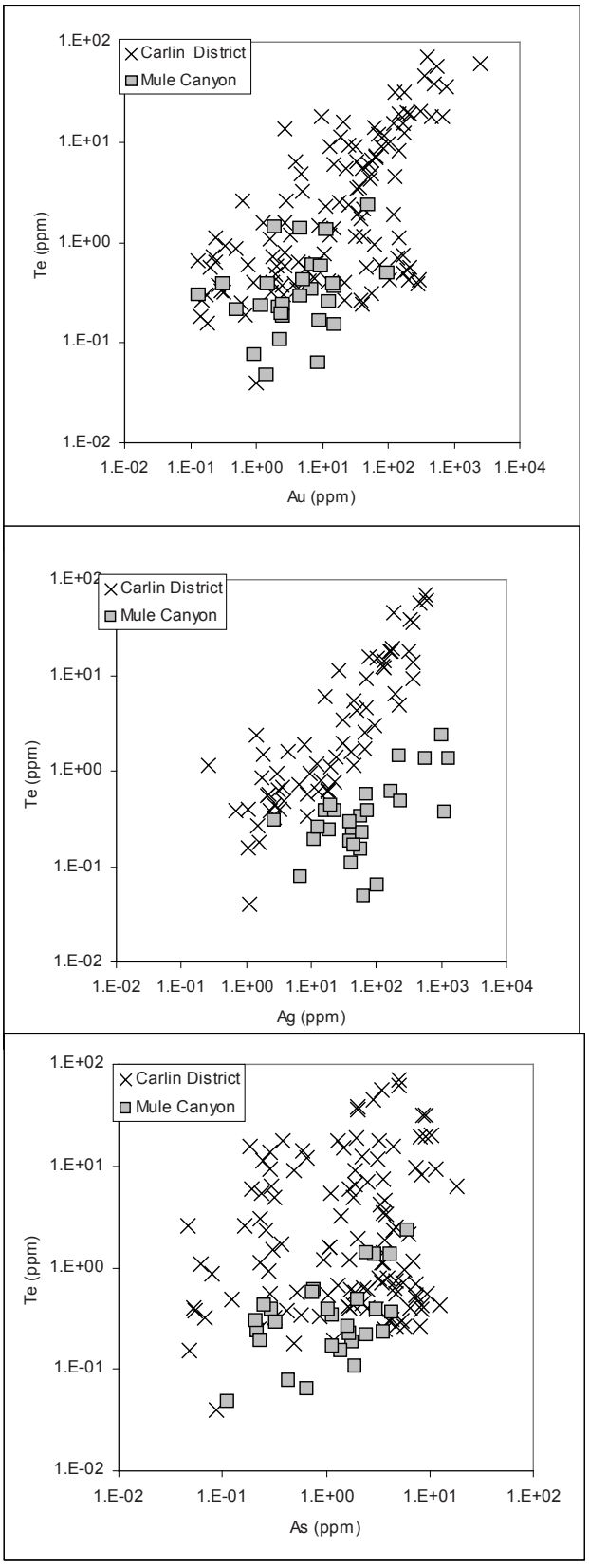

Figure 2. Relation of Te to Au, Ag and As in SIMS analyses of As^{1-} pyrite from Carlin-type and Mule Canyon low-sulfidation epithermal type deposits.

Table 1 – Correlation coefficients for Se and Te with other elements in As^{1-} arsenian pyrites from Carlin-type deposits in the Carlin district (including Betze-Post-Screamer, Rodeo, Griffin, Carlin and the Mule Canyon low-sulfidation epithermal deposit. All analyses by SIMS.

Carlin-type Deposits									
	Ag	*As*	*Au*	*Co*	*Cu*	*Ni*	*Sb*	*Se*	*Te*
Se	0.350	-0.142	-0.059	-0.093	0.299	0.118	-0.020	1.000	0.062
Te	0.880	0.138	0.678	-0.165	0.379	-0.092	0.390	0.062	1.000
Mule Canyon Low-Sulfidation Epithermal Deposit									
Se	0.164	0.190	0.094	0.012	-0.167	0.036	0.181	1.000	0.358
Te	0.685	0.679	0.049	0.177	0.083	0.207	0.676	0.358	1.000

3. SIGNIFICANCE OF THE TRACE ELEMENT CORRELATIONS

Correlations between trace elements in arsenian pyrite could reflect similar substitutional behavior. For instance, As occupies the S site in As^{1-} pyrite and therefore correlations might be expected between As and Se or As and Te if their presence in pyrite was governed only by the availability of substitutional sites. However, only one such correlation is seen in epithermal pyrite from Mule Canyon, between As and Te; all other correlations of As with Te or Se are very poor. This suggests that correlations between trace elements reflect external factors such as relations between elements in the source region from which they were derived (wallrocks, magmas), similar response to depositional processes, or existence of soluble complex ions involving the two elements.

Inheritance of correlations from possible source regions is unlikely, but there has been continued speculation about the degree to which Au or Ag might complex with Se or Te in hydrothermal solutions. Reich et al. (2004) have shown that Au probably occupies the Fe site in As^{1-} arsenian pyrite, and a similar setting is likely for Ag. Thus, Au and Ag do not substitute in the same site as Se and Te, and their abundances in pyrite should vary independently. The strong correlations shown by Te with Au in both Carlin-type and epithermal-type deposits argues strongly for a close relation between these two elements in the parent hydrothermal solutions. A similar conclusion can be reached for Ag and Te in Carlin-type deposits where the correlation is strong, but epithermal deposits do not show a similar correlation.

The key question is whether these relations indicate that Au and Ag are complexed with Te in hydrothermal solutions and, if so, whether these Te-complexes are important or simply minor, ancillary agents of metal transport. The likely answer is that the Te-precious metal complexes, if they exist, are not the dominant complexing agent. This is suggested by the fact that slope and position of the trends in Figures 1 and 2 suggest Te:Me ratios of 1:10 or less. This amount of Te is much less than would be needed to complex the metals and less than is suggested for most Te-complexes (Wood and Samson, 2000). Thus, although Te-complexes probably played a role in formation of these deposits, they were not the main agent of metal transport.

REFERENCES

Chouinard, A., Paquette, J. and Williams-Jones, A., 2005, Crystallographic controls on trace-element incorporation in auriferous pyrite from the epithermal high-sulfidation Pascua Deposit, Chile-Argentina: Canadian Mineralogist, 43, 951-963.

Deditius, A.P., Utsunomiya, S., Ewing, R.C., Ramana, C.V., and Kesler, S.E., 2007, New Form of Arsenian Pyrite, $(Fe,As^{3+})S_2$: Frontiers in Mineral Sciences, Cambridge, England.

Palenik, C.S., Utsunomiya, S., Reich, M., Kesler, S.E., Wang, L. and Ewing, R.C., 2004, "Invisible" gold revealed: Direct imaging of gold nanoparticles in a Carlin-type deposit: American Mineralogist, 89, 1359-1366.

Reich, M., Becker, U. and Kesler, S.E., 2004, Quantum-mechanical and Monte Carlo simulations of Fe-As-S solid solution properties and the energetics of Au incorporation into arsenian pyrite: Geochimica Cosmochimica Acta, Abstracts of the 13th Annual Goldschmidt Conference, Copenhagen, Denmark, A81.

Simon, G., Huang, H., Penner-Hahn, J.E., Kesler, S.E., and Kao, L-S., 1999, Oxidation state of gold and arsenic in gold-bearing arsenian pyrite: American Mineralogist, 84, 1071-1079.

Wood, S.A. and Samson, I.M., 2000, Solubility of ore mineals and complexation of ore metals in hydrothermal solutions *in* Reviews in Economic Geology, 10, 33-80.

Au-Ag telluride-selenide minerals and their diagnostic features

Kari K. KOJONEN, Geological Survey of Finland, P.O. Box 96, FI-02151 Espoo, Finland (Kari.Kojonen@gtk.fi)

Abstract: The most important Au-tellurides belong to the kostovite-sylvanite group and consist of kostovite $CuAuTe_4$, calaverite $AuTe_2$, krennerite $AuTe_2$, and sylvanite $(Au,Ag)_2Te_4$. The cameronite-montbrayite group consists of cameronite Cu_7AgTe_{10} and montbrayite $(Au,Sb)_2Te_3$. The Ag tellurides belong to the henryite-hessite and petzite groups: henryite $CuAg_3Te_4$, cervelleite Ag_4TeS, hessite α-Ag_2Te, kurilite $Ag_2(Te,Se)$, stützite $Ag_{5-x}Te_3$, benleonardite $Ag_8Te_2(Sb,As)S$ and tsinigriite $Ag_9(Te,Sb,S)_3$; fischesserite Ag_3AuSe_2, and petzite $AgAuTe_2$. Volynskite $AgBiTe_2$ belongs to the matildite group. The vulcanite-empressite group contains empressite AgTe and muthmannite $(Ag,Au)Te_3$. The Cu-bearing Au-Ag tellurides belong to the bezmertnovite group: bezmertnovite $Cu(Au,Ag)_4(Te,Pb)$, bogdanovite $(Cu,Fe)_3Au_5(Te,Pb)_2$, and bilibinskite $Cu_2Au_3PbTe_2$. Nagyágite $[(Pb_3(Pb,Sb)_3)S_6][(Au,Te)_3]$ and buckhornite $[(Pb_2Bi)_3S_3][(Au,Te_2)_3]$ belong to the nagyágite–buckhornite series of nesosulfarsenites; museumite $[Pb_2(Pb,Sb)S_8](Te,Au)_2$ is structurally related. Au-Ag selenides are eucairite CuAgSe, aguilarite Ag_4SeS and naumannite α-Ag_2Se (eucairite-naumannite group of simple sulfides and selenides), bohdanowiczite $AgBiSe_2$ (matildite group), geffroyite $(Cu,Fe,Ag)_9(Se,S)_8$ (pentlandite group), chrisstanleyite $Pd_3Ag_2Se_4$ of unknown structure, penzhinite $(Ag,Cu)_4Au(S,Se)_4$, and petrovskaite Au,Ag(S,Se) of the petzite group.

Keywords: tellurides, selenides, gold, silver, classification, optical properties

1. INTRODUCTION

The Au-Ag tellurides and selenides have an important role in many epi- and mesothermal gold deposits worldwide. The deposits range in age from Precambrian shear-zone hosted mesothermal lode gold deposits to younger subvolcanic near surface intrusion-related epithermal deposits (Evans, 1993). The tellurides are often accompanied with base metal sulfides, arsenides, bismuthinides and other tellurides and selenides of Pb, Fe, Bi and Ni. With high tellurium fugacity, Ag and Au form specific telluride minerals, which are often texturally intergrown with native gold and have probably crystallized simultaneously with native gold grains. This paper aims to point out the most important Au-Ag tellurides and selenides and describe their identification diagnostics, especially using the polarizing microscope in reflected light to study polished ore specimens.

2. CLASSIFICATION OF Au-Ag TELLURIDES AND SELENIDES

The tellurides and selenides are thoroughly classified by Strunz and Nickel (2001). In the mineralogical tables, most of the Au-tellurides are in the kostovite-sylvanite group of class 2.E: metal sulfides with M:S≤1:2. These include kostovite $CuAuTe_4$, calaverite $AuTe_2$, krennerite $AuTe_2$, and sylvanite $(Au,Ag)_2Te_4$. The cameronite-montbrayite group belongs to class 2 DB; M:S = 2:3 and consists of cameronite Cu_7AgTe_{10} and montbrayite $(Au,Sb)_2Te_3$. Nagyágite $[(Pb_3(Pb,Sb)_3)S_6][(Au,Te)_3]$ and buckhornite $[(Pb_2Bi)_3S_3][(Au,Te_2)_3]$ belong to the nagyagite–buckhornite series 2.GB.35 of the sulfosalts 2G to 2K; museumite, $[Pb_2(Pb,Sb)S_8](Te,Au)_2$ is structurally related. Most Ag- and Ag-Au tellurides are in the henryite-hessite group (2.B.40) and petzite group (2.BA.50) of the class of simple sulfides, selenides etc. 2.B to 2.F with M:S>1:1. These include henryite $CuAg_3Te_4$, cervelleite Ag_4TeS, hessite α-Ag_2Te, kurilite $Ag_2(Te,Se)$, stützite $Ag_{5-x}Te_3$, benleonardite $Ag_8Te_2(Sb,As)S$, tsinigriite $Ag_9(Te,Sb,S)_3$ and petzite $AgAuTe_2$. The silver-bearing telluride volynskite $AgBiTe_2$ belongs to the matildite group 2.CD.15, whereas empressite AgTe and muthmannite $(Ag,Au)Te_3$ belong to the vulcanite-empressite group 2.CB.75 of class 2.C metal sulfides with M:S=1:1. The copper-bearing Au-Ag tellurides belong to the bezmertnovite group 2.BA.55 of the class simple sulfides, selenides, etc. with M:S>1:1: bezmertnovite $Cu(Au,Ag)_4(Te,Pb)$, bogdanovite $(Cu,Fe)_3Au_5(Te,Pb)_2$, and bilibinskite $Cu_2Au_3PbTe_2$.

Au-Ag selenides consist of eucairite CuAgSe, aguilarite Ag_4SeS and naumannite α-Ag_2Se of the eucairite-naumannite group of simple sulfides and selenides, bohdanowiczite $AgBiSe_2$ of the matildite group, geffroyite $(Cu,Fe,Ag)_9(Se,S)_8$ of the pentlandite group, chrisstanleyite $Pd_3Ag_2Se_4$ of 2.BC. group, fischesserite Ag_3AuSe_2, penzhinite $(Ag,Cu)_4Au(S,Se)_4$, and petrovskaite AgAu(S,Se) of the petzite group.

3. DIAGNOSTIC FEATURES OF Au-Ag TELLURIDES AND SELENIDES

In hand specimen, the Au-tellurides are soft, silvery white to brass yellow (calaverite, krennerite, sylvanite) to tin-white and pale yellow (montbrayite), dark lead-gray (nagyágite) or grayish white (kostovite). The Ag-tellurides are macroscopically steel gray to black (petzite) or lead gray (hessite) in color. Mostly, the tellurides occur as very small grains not even visible in the hand specimen. In such cases, an ore microscope study is absolutely necessary. Even under medium microscope magnification (10x or 20x), the tellurides may be difficult to observe because of their small grain size (Fig. 1).

Furthermore, they often occur in the intergranular spaces of the gangue minerals, as inclusions in the sulfides or arsenides and as very soft minerals (Table 1) they are poorly polished. However, if one knows of the presence of Te in the sample that usually far exceeds the amount of Au and Ag, the small inclusions in the sulfides and within the gangue minerals will have more attention and will be found using higher magnification objectives (50x, 100x) and oil immersion.

The Au-Ag selenides are macroscopically bronze, gray, silver white or tin white (eucairite); gray, iron gray, black (aguilarite); grayish black, iron black (naumannite); gray to silver gray (chrisstanleyite), gray white to steel gray (penzhinite), silver white (fischesserite), lead gray to darkish gray black (petrovskaite).

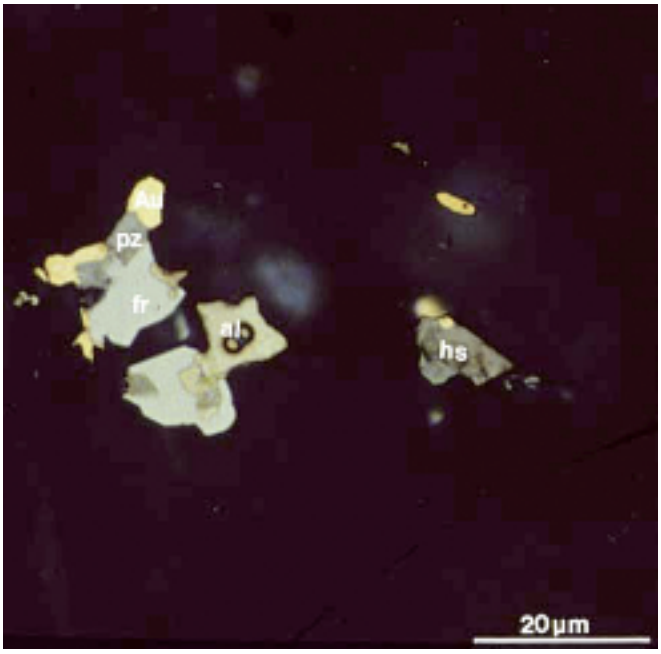

Fig. 1. Telluride minerals and gold with a very fine grain size in gangue minerals, Korvilansuo, Ilomantsi, Finland, reflected light, 1 polarizer. Abbreviations: Au = native gold, Hs = hessite, al = altaite, fr = frohbergite, pz = petzite

In general, the gold tellurides have high reflectance values ca. 60-65 % and are white or yellowish white in color.

Table 1. Vickers hardness number (VHN) of Au-Ag tellurides and selenides (Uytenbogaardt and Burke, 1971)

Hessite	23-35
Eucairite	23-94
Tellurium	25-87
Aguilarite	25-35
Naumannite	27-56
Fischesserite	32-55
Kostovite	35-43
Petzite	35-74
Krennerite	36-130
Petrovskaite	39-47
Nagyagite	39-129
Volynskite	55-103
Sylvanite	60-250
Geffroyite	67-70
Stützite	75-90
Empressite	108-133
Montbrayite	198-228
Calaverite	198-297
Chrisstanleyite	371-395

The silver tellurides are gray in color and have lower reflectance values of ca.40 %. The Au-Ag selenides have even lower reflectance values <35% (Table 2).

Table 2. Reflectance values (λ=589 nm) of Au-Ag tellurides and selenides (Criddle and Stanley, 1993)

Isotropic or weakly ansitropic

Fischhesserite	31.5
Aguilarite	33.5
Petzite	38.25
Nagyagite	40.65-38.9
Montbrayite	58.3-60.55
Calaverite	61.5

Distinctly to strongly anisotropic

Naumannite	33.55-35.3
Eucairite	36.95-36.5
Stützite	40.6-39.3
Hessite	39.3-42.2
Empressite	40.05-52.85
Sylvanite	52.55-62.95
Kostovite	51.9-61.3
Krennerite	59.35-62.6

According to Ramdohr (1980), calaverite is white with a light tinge to brownish-yellow, tarnishing a little (Fig. 2). Reflection pleochroism is weak, and the anisotropy is distinct, but weak. Krennerite has very similar optical properties, but has clearly stronger anisotropy and better cleavage. Sylvanite has marked reflection pleochroism, strong anisotropism and pronounced twinning. In comparison with calaverite, it appears darker whereas in comparison with nagyágite it is lighter. Nagyágite is grayish-white, similar to galena. Reflection pleochroism is weak, but distinct and has undulating extinction. Montbrayite has similar reflection as krennerite and calaverite, and may be difficult to distinguish from these. The anisotropy color effects are quite distinct: light-gray, yellowish brown, bluish-gray.

The silver telluride hessite is according to Ramdohr (1980) grayish-white (Fig. 3), in oil immersion brownish. It is clearly anisotropic and has a very low hardness.

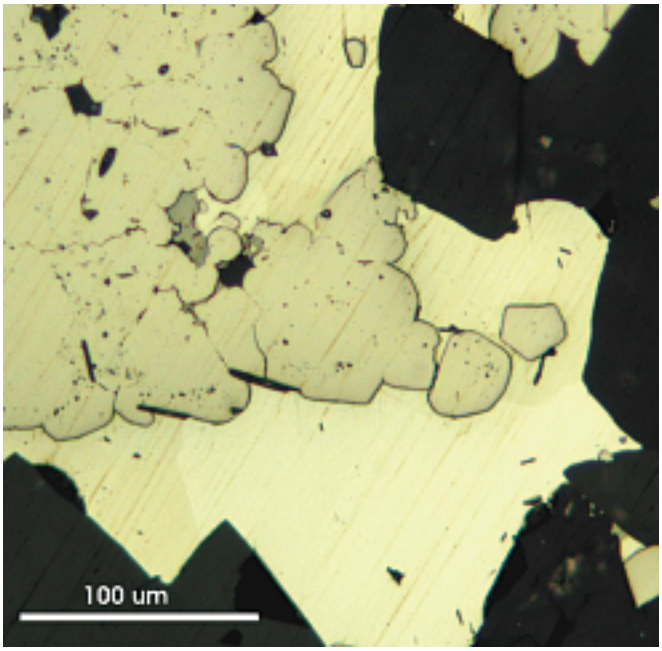

Fig. 2. Calaverite intergrown with pyrite, Kalgoorlie, Eastern Goldfield, Western Australia, reflected light, 1 polarizer.

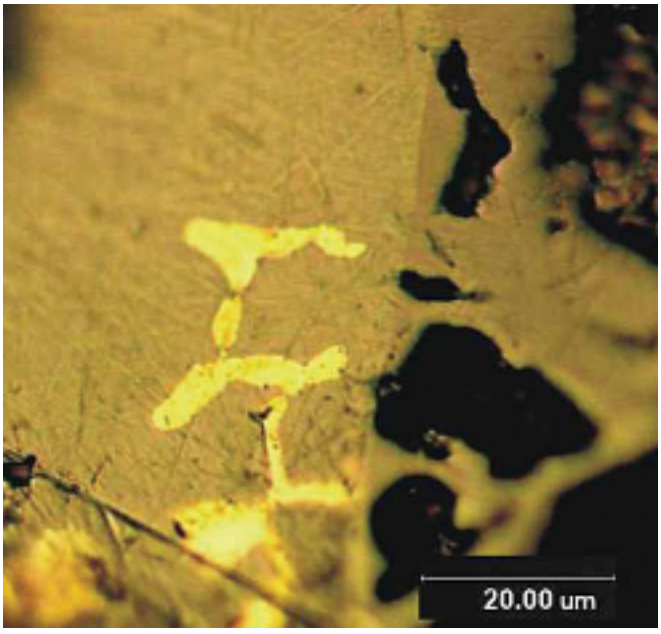

Fig. 3. Native gold in hessite, Kylmäkangas deposit, Oijärvi, Finland. Reflected light, 1 polarizer.

Petzite is light gray (Fig. 4) with a pinkish hue and is weakly anisotropic, sometimes isotropic. Stützite and empressite are bluish white in color in comparison with galena. The reflection pleochroism is strong: light-gray, cream white. Anistropy is very strong.

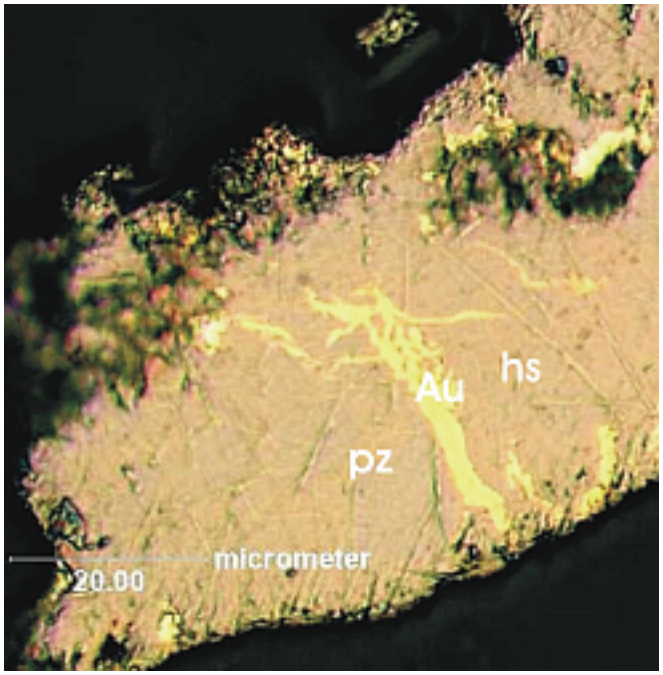

Fig. 4. Petzite-hessite intergrowth, Kylmäkangas deposit, Oijärvi, Finland, reflected light, 1 polarizer.

Volynskite is white with a slight rose tint in air and in oil not very different. Reflectivity is higher than in galena. Anisotropy between crossed polarizers is distinct, the extinction straight.

The Au-Ag selenides are even more rare than the tellurides and information about their optical properties is sparse. According to Ramdohr (1980) eucairite is light yellow, with weak reflection pleochroism, the anisotropy is distinct under crossed polarizers. The polarization colors are bluish and olive brown tints in air in the 45° position. Naumannite and aguilarite are white, in contrast to the grayish-bluish green tint of clausthalite. Reflection pleochroism is not recognizable in air, whereas in oil it is clear with brownish gray to greenish gray tones. Naumannite is strongly anisotropic under crossed polarizers with rather lively colors, aguilarite has only weak anisotropism. Bohdanowiczite is the Se-analogue of schapbachite. It is very similar to matildite but a bit higher reflectivity with galena-like appearance and color, but with rather distinct anisotropy. It is often intergrown with clausthalite. Geffroyite is isotropic and is brown with a creamy tint in reflected light. Fischhesserite is isotropic, with a rose red color between chalcopyrite and bornite or enargite.

4. SUMMARY AND DISCUSSION

The Au-Ag tellurides and selenides are rare ore minerals which occur in hydrothermal gold deposits with other tellurides and selenides, base metal sulfides, arsenides and sulfosalts.

Their identification is macroscopically and optically very difficult, and only with experience and in specific ore deposits and paragenesis may one identify them without using more sophisticated methods like SEM/EDS, electron probe microanalysis, XRD, hardness and reflectance measurements. It may often be possible to recognize the tellurides in general because of their high reflectivity, color and mode of occurrence, but final identification has to be made certain using the electron microprobe.

5. REFERENCES

Criddle, A.J., Stanley, C.J., 1993. Quantitative Data File for Ore Minerals. Chapman and Hall, 635 pp.

Evans, A.M., 1993. Ore Geology and Industrial Minerals. Blackwell Science, 389 pp.

Ramdohr, P., 1980. The Ore Minerals and their Intergrowths, 2nd ed. Pergamon Press, 1205 pp.

Strunz, H., Nickel, E.H., 2001. Strunz Mineralogical Tables. E. Schweizerbartsche Verlagsbuchhandlung, Stuttgart, 870 pp.

Tarkian, M., 1974. A key-diagram for optical determination of common ore minerals. Minerals Science and Engineering, 6 (2), 101-105.

Tarkian, M., Liessman, W. 1991. A guide for optical and analytical identification of ore minerals. Clausthaler geologische Abhandlungen 47, 78 pp.

Uytenbogardt, W., Burke, E.A.J., 1971. Tables for Microscopic Identification of Ore Minerals. Elsevier, 430 pp.

The Secret Lives of Immiscible Metal-Rich Melts: Two Liquid Immiscibility in the Sulfide-Antimony System

Heather A. SPARKS — Research School of Earth Sciences, Australian National University, Canberra, ACT, 0200 AUSTRALIA
Heather.Sparks@anu.edu.au

John A. MAVROGENES — Research School of Earth Sciences, Australian National University, Canberra, ACT, 0200 AUSTRALIA
John.Mavrogenes@anu.edu.au

B. Ron FROST — Department of Geology and Geophysics, University of Wyoming, Laramie, WY, 82071 USA

Summary: It is generally accepted that magmatic ore deposits form by the segregation of immiscible sulfide melts from silicate melts. However, very little is known about how sulfide melts evolve chemically. Recent experimental work has revealed some rather unexpected results. Polythermal isobaric silicate trap experiments demonstrate *in situ* sulfide melt evolution. Experiments were conducted at a pressure of 0.5 GPa and temperatures between 380-820 °C in an internally heated piston cylinder. Rapid quenching revealed that as initially homogenous sulfide melts cool, they un-mixed into two or more immiscible melts. Based on these observations we contend that the sulfide melts that formed at Broken Hill, Australia during peak metamorphic conditions were enriched in Sb, As, Ag, Bi and Au. Differentiation lead to extreme enrichment of 'dropper ores' which accounts for the very high Au grades (1 gram/ton) as well as high grades of Sb, As, Ag, and Bi in the garnetites surrounding the Pb-lodes. This process may have occurred at numerous deposits worldwide, but is generally unrecognized. Therefore, deposits that sit in or near high metamorphic grade terranes should be reconsidered in light of these new results.

Key words: metal ores, sulfides, melts, immiscibility, annealing, quenching, experimental studies, Broken Hill, Australia

1. INTRODUCTION

Liquid immiscibility is not easily documented in nature due to its fleeting nature and unclear crystallization record (Bowen, 1928 and Roedder, 1951). Morphological evidence of immiscibility consists of droplets or globules of one phase within another of contrasting composition. However, such direct evidence might be blurred by further evolution of the un-mixed melts, notably "epitaxial" crystallization of mineral phases (e.g. Roedder, 1984). In the early 1950's Roedder (e.g. 1951) showed clear evidence of silicate-silicate immiscibility in experimental systems, however, that work was largely ignored until the first clear case of confirmed immiscibility was recognized in lunar samples, where perfect immiscible droplets were quenched in silicate glasses (Roedder and Weiblen, 1971). Immiscibility is an established process in hydrothermal systems and is known to play a significant role in many low pressure ore deposits (e.g. Hedenquist and Lowenstern, 1994). In these systems, entrapment of high density brine and coeval low density vapor fluid inclusions are clear evidence of immiscibility. Furthermore, segregation of immiscible sulfide melts from mafic silicate melts is the process that leads to many of the world's major nickel and/or PGE deposits (e.g. Sudbury, Kambalda and Noril'sk; Naldrett, 2005). But little is known about how sulfide melts evolve chemically, other than the ground breaking work of Mungall and Brenan (2003), who experimentally mapped out possible fractionation paths for Sudbury ores.

Sulfide melts are generated whenever orebodies are subjected to temperatures exceeding approximately 500 °C (Frost et al., 2002). With the onset of sulfide melting, sulfides become enriched in low melting point chalcophile elements (LMCE) to levels well above average ore grades and

transport into pockets of low strain (e.g. Hemlo; Tomkins et al., 2004). Recent experimental evidence has revealed that as the sulfides within these pockets cool they un-mix into immiscible sulfide-sulfosalt-metal phases allowing for further transportation and concentration of ore. We propose here that zones of enriched sulfosalts and metals are not primary features, but are late stage events. The common occurrence of low-sulfur ore minerals such as antimonides and native alloys are typical of metamorphosed ore deposits (for example, Sulitjelma, Tunaberg and Hemlo; Frost et al., 2002), suggesting that this process may be more common in differentiating sulfide melts than first thought. Being able to understand the processes which cause this type of re-mobilization will enable us to better predict metal distribution and allow us to better resolve primary features from those features created after ore deposition. Furthermore, a metamorphic origin should be considered for any deposit rich in the LMCE (e.g. Sb, As, Ag, and Bi) that are in or near high metamorphic grade terranes.

2. BACKGROUND

The isolated concentration of sulfosalts and LMCE can occur during the differentiation of polymetallic melts. Frost et al., (2002) suggest that finding these mineral assemblages within an orebody is strong evidence for the presence of melt. As recorded by Lawrence (1968) the Broken Hill orebody is riddled with such occurrences (Fig. 1). He suggested that some of the ore assemblages seen at Broken Hill formed via the breakdown of tetrahedrite. For example tetrahedrite can breakdown to produce pyrargyrite (Ag_3SbS_3), polybasite ($(AgCu)_{16}Sb_2S_{11}$), stephanite (Ag_5SbS_4) and argentite (Ag_2S). Further "break down" produces antimonial silver (Ag+Sb), allargentum (Ag_6Sb), dyscrasite (Ag_3Sb) and native silver (Ag). All of these assemblages are abundant at Broken Hill, and in light of our recent experimental work we suggest that these assemblages are the last crystallization stages of sulfur poor immiscible melts. The main lodes at Broken Hill are dominated by the high sulfur immiscible melt which finally crystallizes at much higher temperature.

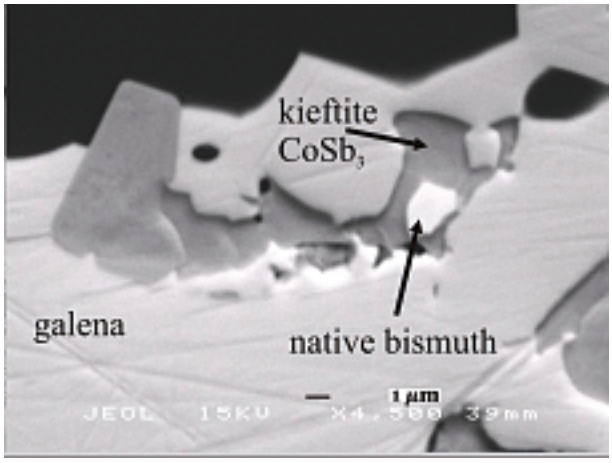

Figure 1. Backscattered electron image of a sulfosalt in association with a LMCE taken from the zinc lode at Broken Hill. These assemblages are likely to be the last remnants of an evolved sulfide melt.

A curious feature of the Broken Hill orebody is the grade and distribution of Au within and around the ore. Stillwell (1940) reports average Au grades for run of the mill sulfides of 2 grams/ton, while Peryilla mine records show that the garnetites associated with the ore contain up to 1 gram/ton of Au. Comparison of 2 grams/ton Au in 100% sulfide ore and garnetite that contains <2% sulfide yet contains up to 1 gram/ton Au leads to the conclusion that something unusual is occurring within the garnetites. Relative to run of the mill ore, sulfides (and metal alloys) within the garnetites are enriched in Au up to 300% (2 ppm in 100% vs 1 ppm in <2%). We suggest that this enrichment must be the result of extreme melt fractionation, likely through immiscibility.

Clear evidence of the presence of a sulfide melt as suggested by Frost et al. (2002) is the occurrence of polyphase sulfide melt inclusions (SMINCs). SMINCs are solidified microscopic samples of liquid sulfide melt that have become trapped in defects of crystallizing minerals. In a thorough study of SMINCs found within garnetites and quartz veins in garnetites surrounding 'droppers' and large masses of the Broken Hill orebody, Sparks and Mavrogenes (2005) showed that these samples are trapped remnants of sulfide melt which provide clues to the melt history (Fig. 2). Not only do

SMINCs sample melts at a given moment during melt evolution, but once trapped, SMINCs continue to evolve in a manner similar to the main melt mass. Figure 2, a cross section of a primary SMINC hosted in a garnet grain shows suspicious characteristics of immiscibility. Taken from the alteration package surrounding a 'dropper' at Broken Hill, it contains eight different daughter crystals. If daughter crystals represent a single trapped evolving sulfide melt, then it would be expected that all early crystallizing phases would have been Ag saturated. For example, tetrahedrite, a major Ag source within the orebody would be expected to contain a significant amount of Ag in the SMINC. However, this is not the case. Tetrahedrite does not contain any Ag, rather all the Ag was partitioned into a metal Sb alloy. One explanation for the lack of Ag within tetrahedrite might be that this SMINC resulted from a trapped homogenous sulfide melt that upon cooling un-mixed into immiscible S-rich melt and a S-poor melt. This is, however, difficult to prove. The Broken Hill orebody, was once partially molten during metamorphism (810 ºC, 0.5 GPa), has left a cryptic record of sulfide melt evolution. It is clear that melting occurred, but its fractionation history is not yet well understood.

If immiscibility is occurring, it must be confirmed through experimental investigation. Faced with this dichotomy, a series of polythermal isobaric silicate trap experiments were developed.

3. POLYTHERMAL ISOBARIC SILICATE TRAPS

To understand the observed sulfide-sulfosalt-metal mineral assemblages in SMINCs and parts of the Broken Hill orebody, a series of novel experiments were developed. A technique whereby either quartz or garnet aggregates were used to trap sulfide melts as they trickle down a temperature gradient while kept at constant pressure have been used to view sulfide melt evolution.

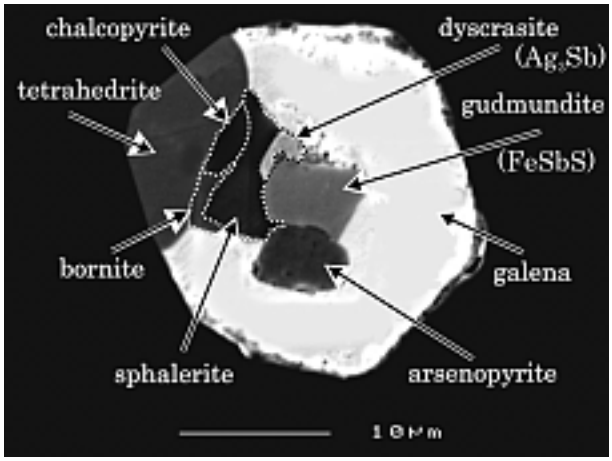

Figure 2. Backscattered electron image of primary SMINC hosted in garnet taken from the alteration package around a 'dropper' at Broken Hill, Australia. It contains eight different daughter minerals representing a trapped evolving sulfide melt (Sparks and Mavrogenes, 2005).

Graphite rods were machined into 2 cm long capsules with an internal diameter of 4 mm. Capsules were lightly packed with either chipped clear quartz crystals or natural garnet grains all of approximately 100 µm in diameter. A homogenous pressed sulfide pellet was then placed on top of the aggregate (Fig. 3.). Pressed sulfide pellets were composed of a combination of either synthetic or natural minerals and elements, powdered and pressed into a 2 mm long pellet. A graphite lid was used to close the capsule. A talc outer sleeve was fitted over the graphite capsule and MgO spacers were placed on either end of the capsule to position the pressed pellet at the hot spot in the apparatus. Temperature ranges have been calibrated from the top of the capsule at 820 °C all the way to the bottom of the capsule at 380 °C, creating a smooth temperature gradient. As the melt traverses the capsule, phases crystallize at an appropriate temperature. This allows melts to evolve to very low temperatures.

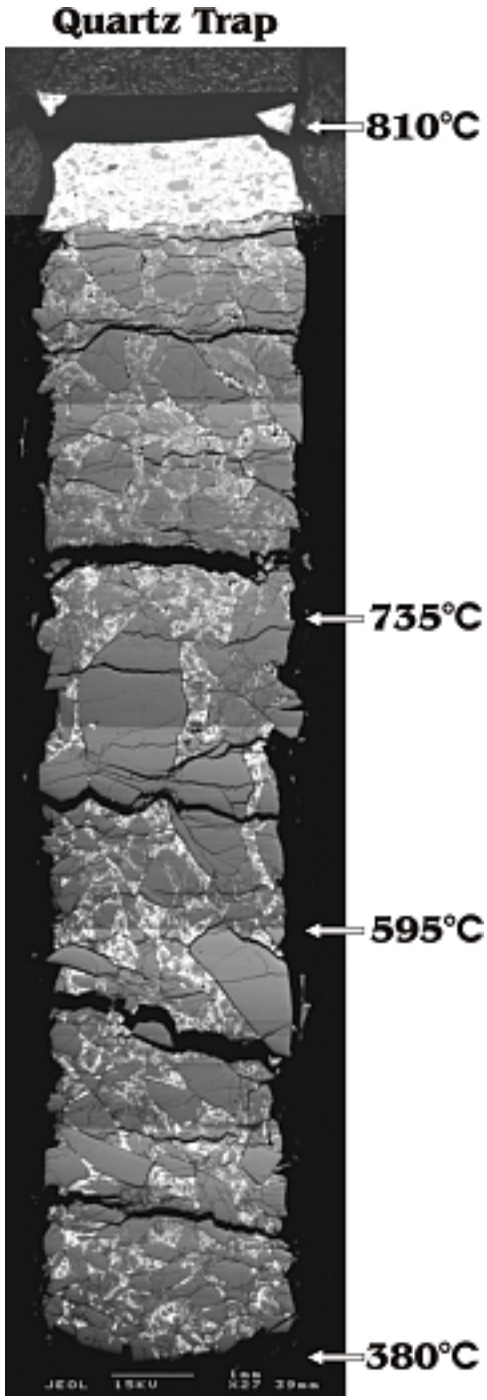

Figure 3. Backscattered electron image of a post run quartz trap experiment. The homogenous sulfide pellet at the top of the capsule partially melted and the resulting melt trickled down between the quartz grains, trapping immiscible melts as a function of temperature.

Experimental Conditions

All experiments were conducted using a 12.7 mm end-loaded piston cylinder apparatus located at the Research School of Earth Sciences, Australian National University. In a typical 0.5 GPa experiment, all the pressure was applied to the sample before the furnace was connected. The sample was then heated at a rate of 50 °C per minute. Each experiment was run for a duration of 2 hours and continually monitored to ensure pressure was maintained at 0.5 GPa. Temperature at the top of the capsule was monitored using a Type B, $Pt_{94}Rh_6$-$Pt_{70}Rh_{30}$ thermocouple, cased in two bore mullite tubing, and believed to be accurate to ±10 °C. Runs are quenched by disconnecting the power supply to the graphite capsule. Cooling rates from 820 °C to below 50 °C occur within 10-20 seconds.

Analytical Technique

Capsules were removed from the assembly and placed in epoxy resin. Once hardened, 2 mm holes are drilled along one length of the capsules to breach the inside of the capsule. Further epoxy resin was poured into the holes and vacuum impregnated. Samples were then mounted on a small diamond saw and sectioned longitudinally using ethanol. Dry polishing using successive grit paper followed by mechanized laps using 3-0.25 micron diamond paste were used on one half of the experiment.

Both graphite capsule and silicate trap material were examined on the JEOL 6400 SEM equipped with EDS at the Research School of Biological Sciences, Australian National University, and were shown not to have participated in the experiment.

Results

As the capsules were heated, the sulfide pellet began to melt. Initially a homogenous sulfide melt was generated from the pellet and trickled down through the aggregate, solidifying over a range of temperatures, from 820 to 380°C at 0.5 GPa. In these experiments, melts evolved from sulfur-rich to metal-rich and appear to contain at least two immiscible melts: one dominated by galena and the other an alloy melt with Sb, As and Ag. Only those melts which can exist at low temperatures migrate to the bottom of the capsule. These relations are seen both within the main orebody and within individual SMINCs, at Broken Hill.

Once immiscibility was established in this system, isothermal experiments were conducted to demonstrate that immiscibility occurs during equilibrium conditions. A calculated bulk composition representative of the pre-immiscible compositions found in the polythermal experiments were run at 700 ºC and 0.5 GPa with no temperature gradient. These experiments showed two melts (Fig. 4), one a metal alloy (rich in Sb and Ag) and the other more S-rich (low in Sb, high in Pb). This we believe is how sulfosalts and metal alloy rich melts form.

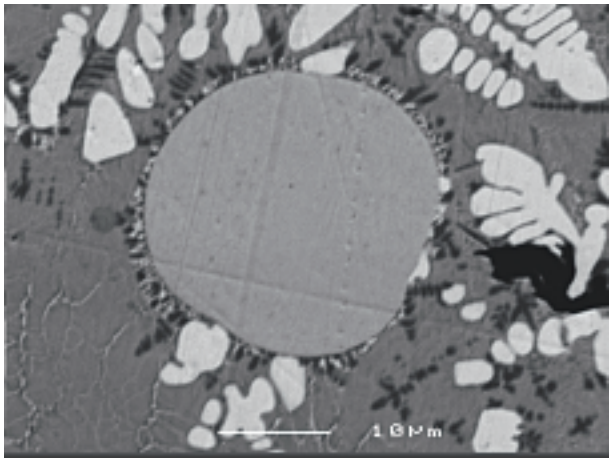

Figure 4. Backscattered electron image of quenched immiscible melts. The large bleb in the center is a metal rich alloy in equilibrium with a relatively sulfur rich matrix.

4. CONCLUSION

Polythermal isobaric silicate trap experiments demonstrate *in situ* sulfide melt evolution. Rapid quenching of the experiments preserves clear textural evidence for sulfide immiscibility. Based on these observations we contend that enrichment in Sb, As, Ag and Au during differentiation, combined with cooling, caused the sulfide melt at Broken Hill to un-mix into two or more immiscible melts. Melt compositions inferred from SMINCs indicate that during differentiation the melt becomes depleted in Zn, Pb and S and enriched in Cu, Sb As, Ag and Au. This process of sulfide melt fractionation eventually leads to extremely high Sb, As and Ag contents in 'dropper ores' and accounts for the very high Au grades (1 gram/ton) in the garnetites surrounding the Pb-lodes at Broken Hill. Alloys and sulfosalts are common not only in SMINCs but within the Broken Hill orebody.

Furthermore, if water and halogens are soluble in sulfide melts (as documented experimentally by Mungall and Brenan, 2003; and Wykes and Mavrogenes, 2005) then veins that appear to be of hydrothermal origin may in fact be late stage polymetallic melts.

The results presented here are not only applicable to Broken Hill, but may apply to all polymetallic orebodies associated with high temperature environments, even if high metamorphic grade rocks are not exposed in the region. The common occurrence of low-sulfur ore minerals such as antimonides and native alloys are typical of metamorphosed ore deposits, such as Sulitjelma, Norway (Cook, 1996) and Hemlo, Ontario (Tomkins et al., 2004), which suggests that this process may be the major control on differentiating sulfide melts. Any system near metamorphic terranes could contain ore deposits that contain only the low temperature end of an evolved high temperature system. In fact, any deposit rich in sulfosalts and alloys may have formed in this way.

REFERENCES

Bowen, N.L., 1928, The Evolution of Igneous Rocks. Princeton University Press, Princeton.

Cook, N.J., 1996, Mineralogy of the sulphide deposits at Sulitjelma, northern Norway. Ore Geology Reviews, v. 11, p. 303-338.

Frost, B.R., Mavrogenes, J.A. and Tomkins, A.G., 2002, Partial melting of sulfide ore deposits during medium- and high-grade metamorphism. Can. Mineral., 40, 1-18.

Hedenquist, J.W. and Lowenstern, J.B., 1994, The role of magmas in the formation of hydrothermal ore-deposits. Nature, 370, 519-527.

Lawrence, L.J., 1968, The minerals of the Broken Hill district. *In* Radmanovich, M. and Woodcock J.T. (ed.), Broken Hill Mines 75th anniversary monograph 3, The Australasian Institute of mining and metallurgy, Victoria, 161-169.

Mungall, J.E. and Brenan, J.M., 2003, Experimental evidence for the chalcophile behaviour of the halogens. Can. Mineral., 41, 207-220.

Naldrett, A.J., 2005, A history of our understanding of magmatic Ni-Cu sulfide deposits. Can. Mineral., 43, 2069-2098.

Roedder, E., 1951, Low temperature liquid immiscibility in the system K_2O-FeO-Al_2O_3-SiO_2. Am. Mineral., 36, 282-286.

Roedder, E., 1984, Fluid inclusions. Rev. in Mineral., 12. Mineral. Soc. of Am., 644.

Roedder, E., and Weiblen, P. W., 1971, Petrology of silicate melt inclusions, Apollo 11 and Apollo 12 and some terrestrial equivalents. Proc. Second Lunar Sci. Conf. Geochim. Cosmochim. Acta Suppl., 2, 507-528.

Sparks, H.A. and Mavrogenes, J.A., 2005, Sulfide melt inclusions as evidence for the existence of a sulfide melt at Broken Hill, Australia. Econ. Geol., 100, 773-779.

Stillwell, F.L., 1940, The occurrence of gold in the Broken Hill lode. The Australasian Institute of mining and metallurgy. Bd., 117.

Tomkins, A.G., Pattison, D.R.M. and Zaleski, E., 2004,

The Hemlo gold deposit, Ontario: An example of melting and mobilization of a precious metal-sulfosalt assemblage during amphibolite facies metamorphism and deformation. Econ. Geol., 99, 1063-1084.

Wykes, J.L. and Mavrogenes, J.A., 2005, Hydrous sulfide melting: Experimental evidence for the solubility of H_2O insulfide melts. Econ. Geol., 100, 157-164.

Tectonic evolution of the Paleoprotezoic Tampere Belt during the Svecofennian orogeny, with reference to hydrothermal alteration at Kutemajärvi

Matti TALIKKA

Polar Mining Oy, Käärmesaarentie 3B, 02160 Espoo, Finland
matti.talikka@dragonmining.fi

Summary: The Paleoproterozoic, volcano-sedimentary Tampere Belt lies in the centre of the Svecofennian domain between the Central Finland Granitoid Complex and the Pirkanmaa Belt. The east-west striking greenstone belt is dominated by turbiditic metasedimentary rocks, metavolcanic rocks of island-arc type and granitoids. Metamorphic and structural features and age data evidence the rapid tectonic evolution of the Tampere Belt during the Svecofennian orogeny.

The subvolcanic Pukala intrusion, which was emplaced into volcanic sequence of the Tampere Belt before or during the early stages of the main regional deformation, can be linked to the hydrothermal alteration observed at Kutemajärvi. The mineral assemblage of the alteration, geometry of the area, isotope data and presence of the comb quartz banding suggest that the hydrothermal system was driven by the Pukala intrusion. Later on, the hydrothermally altered area was subjected to deformation and metamorphism.

Key Words: greenstone belts, Tampere Belt, tectonics, Svecofennian Orogeny, intrusions, hydrothermal alteration, gold ores, Paleoproterozoic, Tampere, Orivesi, Pukala, Kutemajärvi, Finland

1. INTRODUCTION

Tampere region has been in focus of geological interest since the 19th century after Sederholm (1897) released his study on the sedimentary rocks of southwestern Finland. The contributions of a number of distinguished researchers have highlighted the Tampere Belt as a first-class example of a Proterozoic greenstone belt and an integral part in understanding the tectonic evolution of the Svecofennian domain.

The Proterozoic greenstone belts around the world are considered to be highly potential regions for metal exploration and they host a vast amount of the Earth's premier ore deposits. In orogenic belts, intrusives at subvolcanic depths, e.g. magma chambers of volcanoes, often create hydrothermal systems that may carry constituents to and cause mineralisations in the intrusions or their country rocks.

The purpose of this extended abstract is to present a simplified tectonic model for the Tampere Belt (TB) during the Svecofennian orogeny that summarises the investigations of numerous researchers. In addition, the model is intimately linked to the hydrothermal alteration phenomena observed at Kutemajärvi in the eastern flank of the Tampere Belt.

2. GEOLOGIC SETTING

The bedrock in Finland belongs to the Precambrian Fennoscandian craton. The two major tectonic collisions that led to the formation of the Finnish crystalline bedrock occurred at 2.8-2.7 Ga and 1.9-1.8 Ga ago. Since the Paleoproterozoic, no major tectonic events have taken place, and the bedrock has been subjected to erosion for an extensive period of time. Therefore, mainly Archean and Paleoproterozoic rocks are exposed at the current erosional level in Finland.

The Tampere Belt (TB) is located in the middle of the Paleoproterozoic Svecofennian domain that formed 1920-1870 Ma ago as a result of orogenic and extensional events (Lahtinen et al., 2005). The bedrock of the domain is mainly composed of metasedimentary rocks, metavolcanic rocks of island-arc type and plutonic rocks that cut the supracrustal sequence (Korsman et al., 1997).

The east-west striking, volcano-sedimentary TB (Fig. 1) extends over 200 km and lies between the Central Finland Granitoid Complex (CFGC) and the Pirkanmaa Belt (PB). The CFGC mainly comprises tonalites, granites and granodiorites with minor proportions of supracrustal rocks and mafic plutonic rocks (Korsman et al., 1997). The collision-related intrusions are 1.89-1.88 Ga and the intrusions post-dating the main stage of crustal thickening 1.88-1.87 Ga old (Korsman et al., 1997). The PB is dominated by migmatitic metasedimentary rocks that are intruded by granitoids and mafic plutons (Nironen et al., 2002).

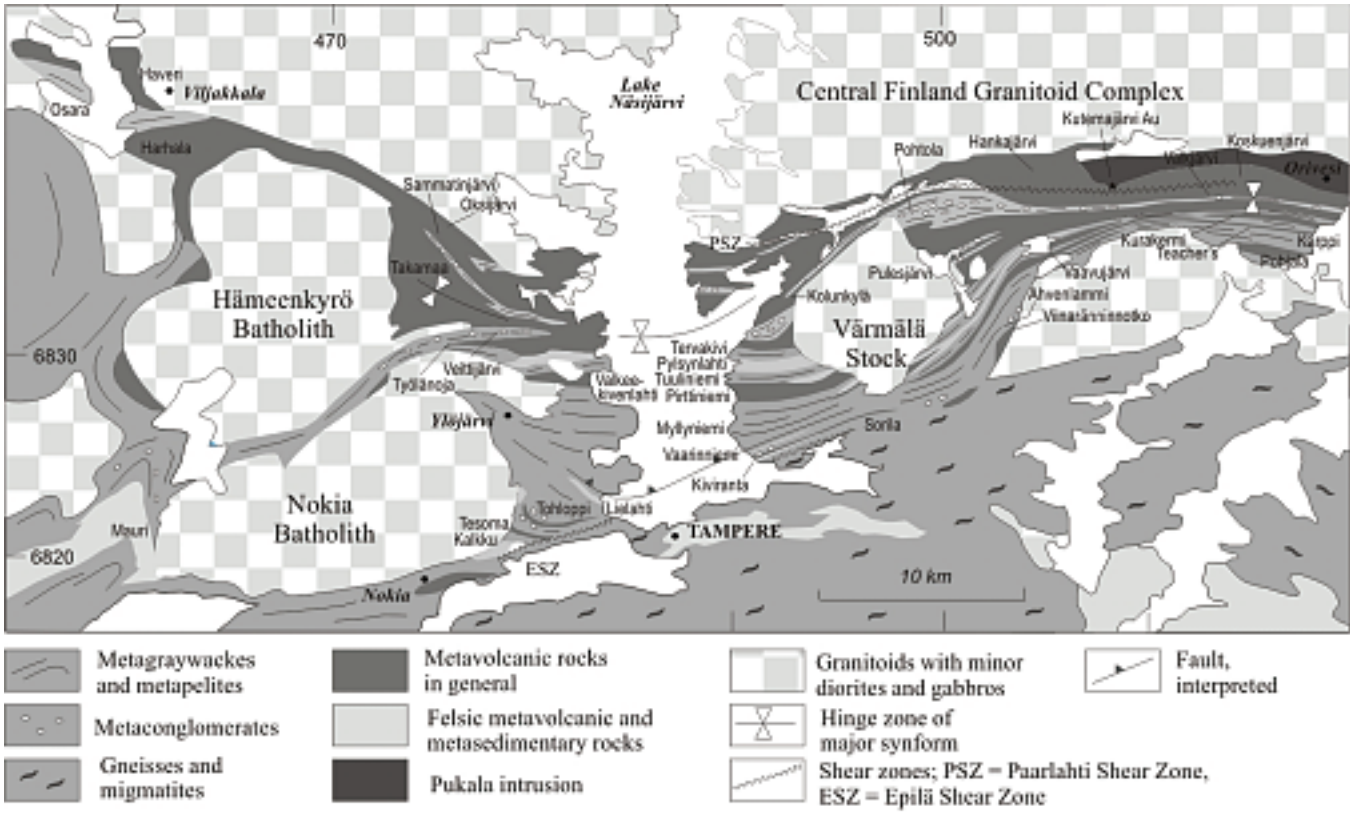

Figure 1. Lithological map of the Tampere Belt. Modified from Kähkönen 1999, Kähkönen 2005 and references therein.

3. TAMPERE BELT (TB)

Seitsaari (1951), Ojakangas (1986) and Kähkönen (1989, 1999, 2005) among others have studied the stratigraphy and rock types of the TB. Accordingly, the main rock types are turbiditic metasedimentary rocks, felsic-intermediate arc-type metavolcanic rocks and granitoids (Ojakangas, 1986; Kähkönen, 1989; Kähkönen & Leveinen, 1994; Nironen, 1989). On the basis of the geochemical data, the metavolcanic rocks of the TB were formed in an island-arc or active continental setting, and the absence of carbonate rocks and iron formations, and the presence of turbidites indicate a steep convergent plate margin (Kähkönen, 1989,1999; Luukkonen, 1994) (Fig. 3). In addition, a mantle reflector dipping to the north indicates a norward subduction under a microcontinent (Lahtinen et al., 2005).

The zircon U-Pb ages of the metavolcanic rocks of the TB are 1904-1889 Ma (Kähkönen et al., 1989; Kähkönen et al., 2004). In comparison, zircons from the metasedimentary rocks are mainly 2.0-1.91 Ga old (Huhma et al., 1991), and the U-Pb ages of the synorogenic granitoids within the TB are 1885±2 and 1878±3 Ma (Nironen, 1989). The zircon U-Pb age for the Pukala subvolcanic intrusion, which is located in the northern flank of the TB, is 1896±4 Ma (Talikka & Mänttäri, 2005).

During the Svecofennian orogeny, the supracrustal rocks of the TB were deformed and metamorphosed under low-pressure, greenschist to lower amphibolite facies conditions (Campbell, 1978; Mäkelä, 1980; Kilpeläinen et al., 1994; Kilpeläinen, 1998). According to Mouri et al. (1999), the regional metamorphic peak occurred at ca. 1880 Ma.

4. PUKALA INTRUSION AND HYDROTHERMAL ALTERATION AT KUTEMAJÄRVI

The data on the Pukala intrusion is based on publications by Talikka (2003) and Talikka and Mänttäri (2005).

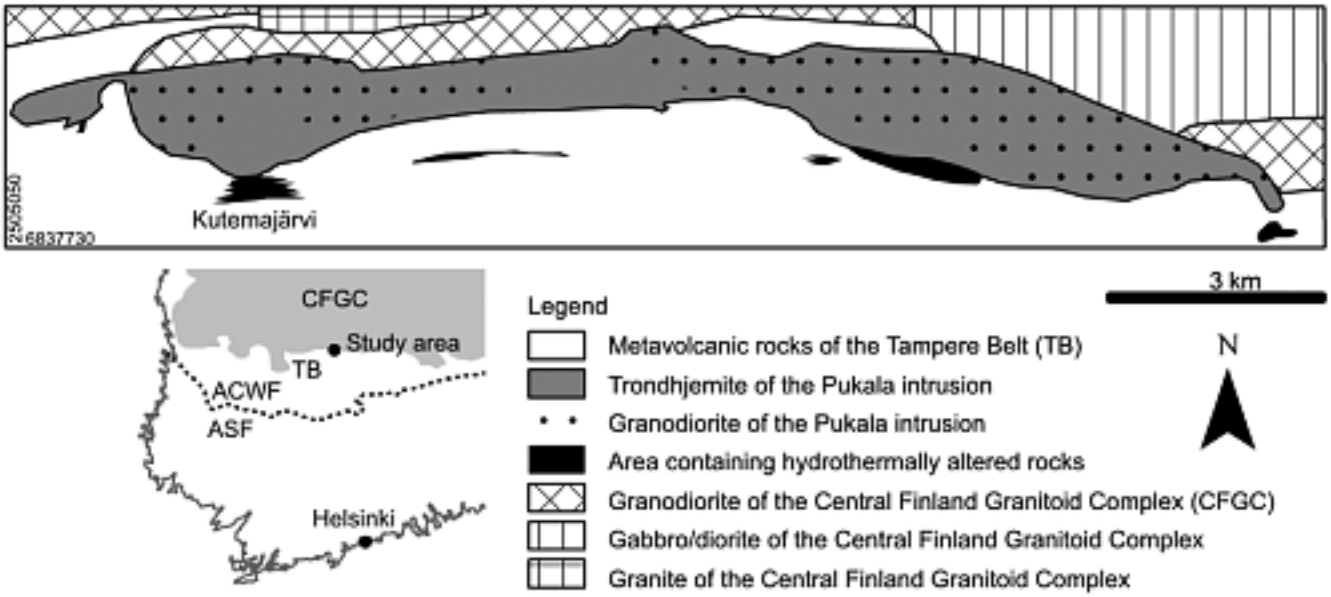

Figure 2. Generalised geological map of the Pukala intrusion (Talikka & Mänttäri 2005 and references therein). ACWF = arc complex of central and western Finland, ASF = arc complex of southern Finland. Inset after Korsman et al. (1997).

According to Kähkönen (1989) and Nironen (1989), the TB forms a large synform whose northern limb is dominated by metavolcanic rocks and the southern limb by metasedimentary rocks. On the basis of the recent age data, Kähkönen et al. (2004) suggested a folded early thrust as a more compatible explanation for the large-scale structure of the TB.

Several east-west striking faults cut the TB (Kähkönen, 1989). The striking mappable structural feature within the TB is the east-west striking, subvertical foliation that formed during the main deformation phase (Kähkönen, 1989; Nironen, 1989; Kilpeläinen, 1998). Latter deformational features include fracturing, kink-folding and movement along narrow shear zones (Nironen, 1989; Kilpeläinen, 1998).

The Pukala intrusion lies in the eastern side of the TB in the contact region between the TB and the CFGC (Fig. 2). The acid, subvolcanic intrusion extends over 20 km in east-west and 1-2 km in north-south direction. The main rock types are porphyritic granodiorite and trondhjemite. The granodiorite has a zircon U-Pb age of 1896±4 Ma and titanite age of 1851±4.6 Ma. Geochemically, the intrusion is a peraluminous, volcanic-arc granitoid.

The Pukala intrusion was emplaced as a sheet-like pluton at subvolcanic depths before or during the early stages of the main regional deformation phase and ca. 15 Ma before the regional metamorphic peak. The main regional foliation is observed in all rock types within the intrusion. On the basis of the stratigraphy observed today, the thickness of the volcanic strata above the Pukala intrusion at 1.9 Ga ago was 1.5-2.5 km. During the Svecofennian orogeny, the intrusion tilted slightly

to the west and steeply to the south along with the adjoining volcanic rocks. This is evidenced by the grain size variations, the presence of abundant xenoliths near the southern margin, and the evidence of magmatic-hydrothermal activity, e.g. comb quartz banding in the contact between the hydrothermally altered metavolcanic rocks and the intrusion at Kutemajärvi.

Several hydrothermally altered domains are located within the metavolcanic rocks of the TB less than one kilometre south of the Pukala intrusion. The largest of the hydrothermally altered areas, Kutemajärvi, is in contact with the Pukala intrusion and hosts a gold deposit, which was mined during 1994-2003 by Outokumpu Mining Oy and Polar Mining Oy. The Kutemajärvi area has been studied by Nurmi et al. (1984), Grönholm (1992), Luukkonen (1994), Poutiainen & Grönholm (1996), Kojonen et al. (1999) and Poutiainen et al. (1999) among others. The continuous hydrothermally altered domain is formed by an outer rim of chlorite-sericite±quartz schist and a centre dominated by sericite-quartz schist, which hosts the pipe-shaped ore deposits (Grönholm, 1992). In addition, massive andalusite, quartz and topaz rocks exist in the centre of the altered area. Monazite from the chlorite schist has a U-Pb age of 1.88 Ga, and a galena with small crustal component in Pb-composition has a model age of 1888 Ma (Mänttäri et al., 1997).

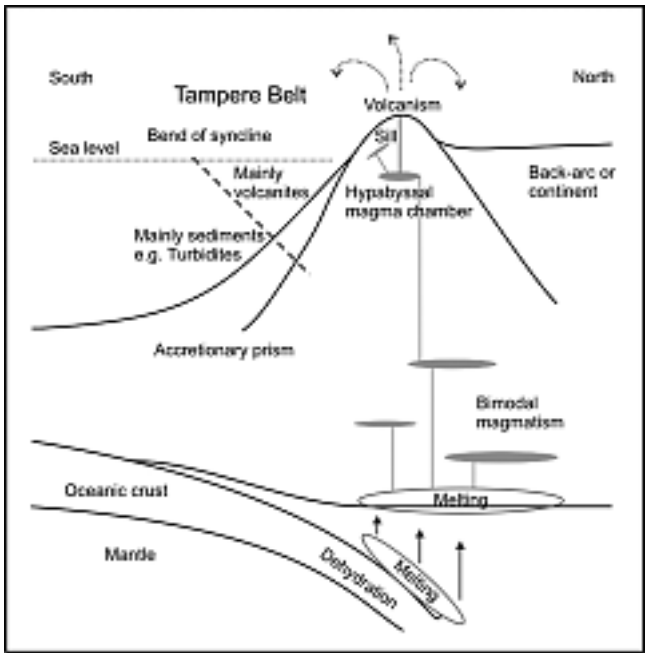

Figure 3. Tectonic setting at ~1.9 Ga. Oceanic crust is subducting under island-arc or active continental margin. The Pukala intrusion may represent a hypabyssal magma chamber. Modified from Talikka (2003).

The intense sericitisation, comb quartz banding, age data and geometry of the area suggest that the pervasive alteration at Kutemajärvi was a resultant of acid hydrothermal fluids of magmatic origin at 1895-1890 Ma ago. After the pervasive alteration, the rocks were deformed and metamorphosed during the Svecofennian orogeny.

5. TECTONIC EVOLUTION OF THE TAMPERE BELT

The model for the tectonic evolution of the Tampere Belt during the Svecofennian orogeny is based on the lithologic data, age data and structural and metamorphic features. The tectonic evolution is divided into four stages in relation to the collision between island-arcs or an island-arc and continental margin (Figs. 3 & 4).

Pre-collision, ←1900 Ma
- Deposition of turbiditic sedimentary rocks
- Active volcanism
- Structural features include primary features e.g. bedding
- Steep convergent plate margin
- Island-arc or active continental margin

Early-collision, 1900-1890 Ma
- Active volcanism
- Compressional deformation → foliation, folding
- Metamorphism
- Emplacement of Pukala intrusion
- Pervasive hydrothermal alteration at Kutemajärvi

Syn-collision, 1890-1878 Ma
- Minor volcanism
- Compressional deformation → main foliation, folding, large shear zones
- Main metamorphic phase, metamorphic peak
- Emplacement of synorogenic granitoids
- Deformation and metamorphism of the Kutemajärvi alteration domain

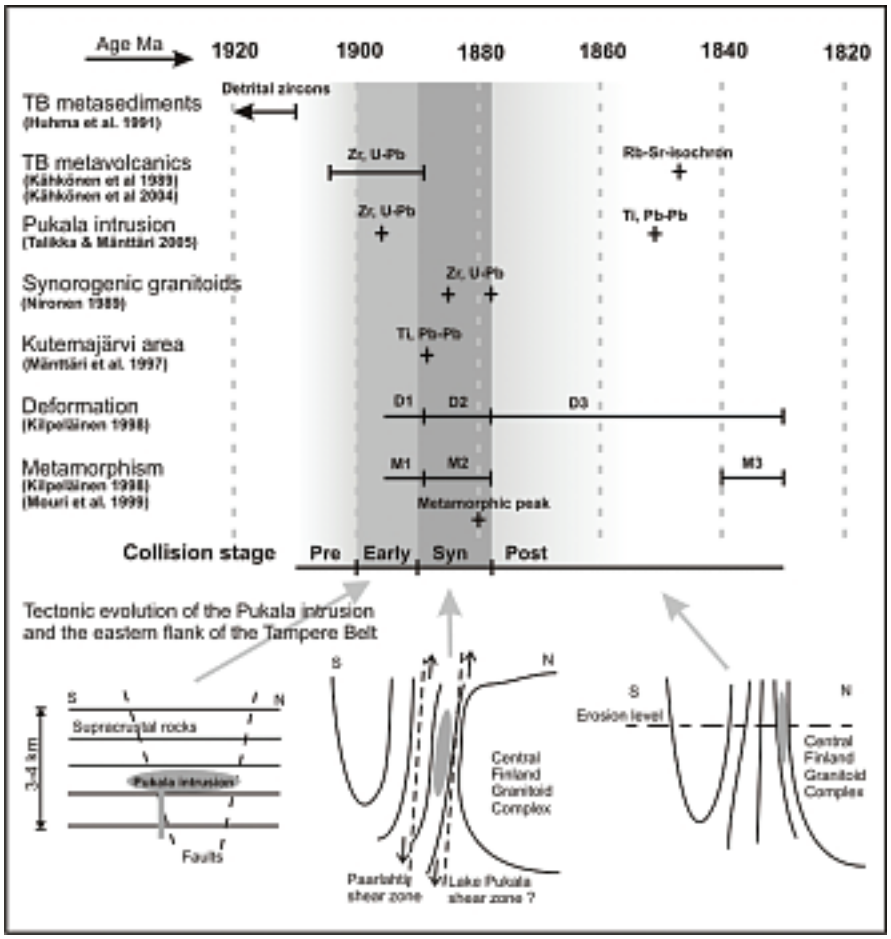

Figure 4. Age data of the rock types, metamorphism and deformation of the Tampere Belt linked to the stages of the tectonic collision. Lower part of the figure illustrates the tectonic evolution of the Pukala intrusion and the adjoining metavolcanic rocks. (Modified from Talikka, 2003).

Post-collision, 1878-1830 Ma

- Extensional deformation → shear zones, kink-folding, fracturing
- Retrograde metamorphism, cooling

6. CONCLUSIONS

The volcano-sedimentary Tampere Belt mainly comprises turbiditic sedimentary rocks, volcanic rocks of island-arc type and synorogenic granitoids. The range of the isotopic ages of the volcanic rocks and the synorogenic granitoids is ca. 25 Ma, and the main regional metamorphic and deformational phase lasted ca. 10 Ma. Accordingly, the tectonic evolution of the Tampere Belt during the Svecofennian orogeny has been a rapid, continuous process.

The expeditious orogenic processes are also evidenced in the Kutemajärvi hydrothermally altered domain that hosts an economic gold deposit. The Kutemajärvi area is located in the northern flank of the TB and is in contact with the subvolcanic Pukala intrusion, which was emplaced within the metavolcanic rocks before or during the early stages of the Svecofennian orogeny. It is suggested that the magmatic fluids from the Pukala intrusion caused the pervasive alteration including sericitisation and silicification observed at Kutemajärvi. The pervasive alteration preceded the main regional deformation and metamorphic processes that led to changes in geometry and mineralogy of the gold deposit.

REFERENCES

Cambell, D.S., 1980, Structural and metamorphic development of migmatites in the Svekokarelides, near Tampere, Finland. Transaction of the Royal Society of Edinburg. Earth Sciences 71, 185–200.

Grönholm, P., 1992, Oriveden Kutemajärven kultaesiintymän ja sen ympäristön geologia. M.Sc. Thesis, University of Helsinki, 115 p.

Huhma, H., Claesson, S., Kinny, P.D., Williams, I.S., 1991, The growth of Early Proterozoic crust: New evidence from Svecofennian detrital zircons. Terra Nova 3, 175–179.

Kähkönen, Y., 1989, Geochemistry and petrology of the metavolcanic rocks of the early Proterozoic Tampere Schist Belt, southern Finland. Geological Survey of Finland, Bulletin 345, 104 p.

Kähkönen, Y., Huhma, H., Aro, K., 1989, U-Pb zircon ages and Rb-Sr whole rock isotope studies of early Proterozoic volcanic and plutonic rocks near Tampere, southern Finland. Precambrian Research 45, 27–43.

Kähkönen, Y., Leveinen, J., 1994, Geochemistry of metasedimentary rocks of the Paleoproterozoic Tampere Schist Belt, southern Finland. Geological Survey of Finland, Special paper 19, 117–136.

Kähkönen, Y., 1999, Stratigraphy of the central parts of the Paleoproterozoic Tampere Schist Belt, southern Finland: review and revision. Bulletin of the Geological Society of Finland 71, 13–29.

Kähkönen, Y., Huhma. H., Mänttäri, I., 2004, TIMS and SIMS U-Pb zircon ages and Rb-Sr whole.rock isotope studies of early Proterozoic volcanic rocks bear Tampere, southern Finland. In: J. Mansfield. Ed., The 26th Nordic Geological Winter Meeting, Abstract Volume, GFF 126, 25.

Kähkönen, Y., 2005, Svecofennian supracrustal rocks. In: Lehtinen, M., Nurmi, P., Rämö, O.T. eds., Precambrian Geology of Finland – Key to the Evolution of the Fennoscandia Shield. Elsevier Science B.V., Amsterdam, 343–406.

Kilpeläinen, T., Korikovski, S., Korsman, K., Nironen, M., 1994, Tectono-metamorphic evolution in the Tampere-Vammala are. Geological Survey of Finland, Guide 37, 27–34. In: J., Mansfield, ed., The 26th Nordic Geological Winter Meeting, Abstract Volume, GFF, 25 p.

Kilpeläinen, T., 1998, Evolution and 3D modelling of structural and metamorphic patterns of the Palaeoproterozoic crust in the Tampere-Vammala area, southern Finland. Geological Survey of Finland, Bulletin 397, 124 p.

Kojonen, K., Sorjonen-Ward, P., Saarnio, H., Himmi, M., 1999, The early Proterozoic Kutema gold deposit, Southern Finland. In: Stanley et al. eds., Mineral Deposits: Processes to Processing. Proceedings of the Fifth Biennal SGA Meeting and 10. IAGOD Quadrennial Symposium, London, 22-25.9.1999. 177–180.

Korsman, K., Koistinen, T., Kohonen, J., Wennerström, M., Ekdahl, E., Honkamo, M., Idman, H., Pekkala, Y., eds., 1997, Suomen kallioperäkartta – Berggrundskarta över Finland – Bedrock Map of Finland. 1:1 000 000. Geological Survey of Finland, Espoo.

Lahtinen, R., Korja, A., Nironen, M., 2005, Paleoproterozoic tectonic evolution of the Fennoscandian Shield – a plate tectonic model. In: Lehtinen, M., Nurmi, P., Rämö, O.T. eds., Precambrian Geology of Finland – Key to the Evolution of the Fennoscandia Shield. Elsevier Science B.V., Amsterdam, 483–504.

Luukkonen, A., 1994, Main geological features, metallogeny and hydrothermal alteration phenomena of certain gold and gold-tin-tungsten prospects in southern Finland. Geological Survey of Finland, Bulletin 377, 153 p.

Mäkelä, K., 1980, Geochemistry and origin of Haveri and Kiipu, Proterozoic strata-bound volcanogenic gold-copper and zinc mineralizations from southwestern Finland. Geological Survey of Finland, Bulletin 310, 79 p.

Mänttäri, I., Luukkonen, A., Grönholm, P., 1997, Isotopic studies on the Kutemajärvi gold deposit, Orivesi, Southern Finland. In: S. Autio ed., Geological Survey of Finland, Current Research 1995–1996. Geological Survey of Finland, Special Paper 23, 55–58.

Mouri, H., Korsman, K., Huhma, H., 1999, Tectono-metamorphic evolution and timing of the melting processes in the Svecofennian Tonalite-Trondhjemite Migmatite Belt: An example from Luopioinen, Tampere Area, southern Finland. Bulletin of the Geological Society of Finland 71, 31–56.

Nironen, M., 1989, Emplacement and structural setting of granitoids in the early Proterozoic Tampere and Savo Schist Belts, Finland – implications for contrasting crustal evolution. Geological Survey of Finland, Bulletin 346, 83 p.

Nironen, M., Lahtinen, R., Koistinen, T., 2002, Suomen geologiset aluenimet – yhtenäisempään nimikäytäntöön!. Summary: Subdivision of Finnish bedrock – an attempt to harmonize terminology. Geologi 54, 8–14.

Nurmi, P.A., Front. K., Lampio, E., Nironen, M., 1984, Etelä-Suomen svekokarjalaiset porfyyrityyppiset molybdeeni- ja kupariesiintymät, niiden granitoidi-isäntäkivet ja litogeokemiallinen etsintä. Svecokarelian porphyry-type molybdenum and copper occurrences in southern Finland: their granitoid host rocks and lithogeochemical exploration. Geological Survey of Finland, Report of Investigations 67, 88 p.

Ojakangas, R.W., 1986, An Early Proterozoic metagaywacke-slate turbidite sequence: The Tampere schist belt, southwestern Finland. Bulletin of the Geological Society of Finland 58, 241–261.

Poutiainen, M., Grönholm, P., 1996, Hydrothermal fluid evolution of the Paleoproterozoic Kutemajärvi gold-telluride deposits, SW Finland. Economic Geology 91, 1335–1353.

Poutiainen, M., Ristolainen, J., Grönholm, P., Luukkonen, A., 1999, Retrograde metamorphic H_2O-NaCl-CO_2-CH_4-N_2 fluid inclusions in orogenic lode-gold deposits of the Paleoproterozoic volcanic-sedimentary Tampere Schist Belt (TSB), southern Finland. In: Cook, N.J. & Sundblad eds., Precambrian gold in the Fennoscandian and Ukrainian Shields and related areas. Gold '99 Trondheim, Norway, 4-6 May 1999. Geological Survey of Norway, Trondheim, 129–130.

Seitsaari, J., 1951, The Tampere schist belt northeast of Tampere in Finland. Bulletin de la Commission Geologique de Finlande 153, 120 p.

Talikka, M., 2003, Pukalan porfyyri ja sen yhteys hydrotermiseen muuttumiseen Orivedellä. M.Sc. Thesis, University of Helsinki, Finland, 119 p.

Talikka, M., Mänttäri, I., 2005, Pukala intrusion, its age and connection hydrothermal alteration in Orivesi, southwestern Finland. Bulletin of the Geological Society of Finland 77, 165–180.

Gold-silver tellurides and bismuth sulfosalts in the high-intermediate sulfidation Perama Hill deposit, western Thrace (NE Greece)

Panagiotis VOUDOURIS — Dept. Mineralogy-Petrology, University of Athens, 15784 Athens, Greece, voudouris@geol.uoa.gr
Constantinos PAPAVASSILIOU — Dept. Economic Geology & Geochemistry; University of Athens, 15784 Athens, Greece
Dimitrios ALFIERIS — S&B Industrial minerals S.A., 15A Metaxa str. 14564 Kifissia, Athens, Greece
George FALALAKIS — Thracean Gold Mining S.A., 123 Democratias Ave., 68100 Alexandroupolis

Summary: Telluride-bearing quartz-barite base metal veins at the Perama Hill Au-Ag deposit (W. Thrace, Greece), overprint earlier pyrite-enargite-bearing mineralization hosted in an advanced argillic altered andesitic breccia. The tellurides sylvanite, krennerite, petzite, hessite, stützite and altaite are associated with tennantite, galena and sphalerite. Bismuthinite derivatives, lillianite homologues show contact relations to enargite and Bi-tennantite. Tellurides were deposited from intermediate-high sulfidation fluids under logfS_2 values between -9.7 and -11.2 and at logfTe_2 values between -7.3 and 10.5 (at 275°C). This study suggests that the Perama Hill deposit has been developed at the transition between a shallow submarine to subaerial environment, showing thus considerable similarities with the mineralization at the Western part of Milos island.

Key Words: Gold ores, silver ores, ore minerals, tellurides, sulfosalts, bismuth, sulfides, electron probe data, Perama Hill, Thrace, Greece

1. INTRODUCTION

Tellurides occur throughout high-intermediate sulfidation epithermal assemblages in the Tertiary precious metal mineralization in W. Thrace, Greece: the Viper-St Demetrios-Kassiteres, Perama Hill and Pefka (Dimou et al., 1994; Voudouris and Arikas, 1994; Michael et al., 1995; Arikas and Voudouris, 1998; Border et al., 1999; Mc Alister et al., 1999; Skarpelis et al., 1999; Lescuyer et al., 2003; Melfos et al., 2003; Voudouris et al., 2006; Voudouris, 2006). Tellurides were also recently described from the porphyry-type Pagoni Rachi deposit (Voudouris & Melfos, 2006). The mineralization was formed during orogenic collapse, which led to block faulting and Oligocene-Miocene silicic to intermediate magmatism (Marchev et al., 2005). Plutonic, subvolcanic and volcanic rocks include basic to intermediate mantle-derived members as well as felsic crustal anatectic products, and show calc-alkaline, high-K calc-alkaline, and shoshonitic affinities (Christofides et al., 2004). This work presents a mineralogical description of the deep sulfide-sulfosalt rich ores of Perama Hill deposit, emphasizing the presence of bismuth sulfosalts and tellurides and discussing their genetic significance in relationship to the adjacent epithermal-porphyry prospects in western Thrace.

2. GEOLOGY OF THE AREA

The Perama Hill Au-Ag deposit is located on the northeastern part of the Petrota graben, which represents a tectonic depression within the metamorphic rocks of the Circum-Rhodope belt (Papadopoulos, 1982). Transtensional opening of the Petrota graben during the Late Eocene-Oligocene was succeeded by Oligocene NW-SE shortening with sinistral strike-slip reactivation of the submeridian basement faults and graben margins into which the NNE-trending Perama fault is included (Lescuyer et al., 2003). This movement was synchronous with the hydrothermal activity along mineralized NW-trending tension gashes. The graben of Petrota is mainly covered by calc-alkaline and shoshonitic volcanic rocks (Fig. 1). Petrographic and geochemical studies indicate the presence of high-

K calc-alkaline andesites to dacites, shoshonitic andesites, trachytic lavas, rhyodacitic ignimbrites and rhyolites (Arikas and Voudouris, 1998). The Perama Hill deposit is mainly hosted by a felsic volcanic sandstone (Perama sandstone) overlying a sequence of andesitic volcanic breccias including subaqueous andesite flows, in-situ and reworked hyaloclastites, intercalated beds of andesite bearing conglomerates and finely bedded reworked tuff. A basal conglomerate unit containing reworked andesite volcanic clasts marks the transition from the andesitic breccia to sandstone (Lescuyer et al., 2003). The Perama sandstone is coeval to the subaerial felsic eruptions in the western part of the graben and it is considered to be indicative of a palustrine environment (Lescuyer et al., 2003). To the north, the Perama sandstones grade to shallow water sandy biomicrite (Early Oligocene), and are capped by opaline deposits, which are considered to be contemporaneous to the Perama Hill hydrothermal event (Lescuyer et al., 2003). In the same graben occurs also the Mavrokoryfi high-sulfidation epithermal prospect, which is hosted in andesitic hyaloclastites (Voudouris and Skarpelis, 1998; Skarpelis et al., 1999; Voudouris, 2005).

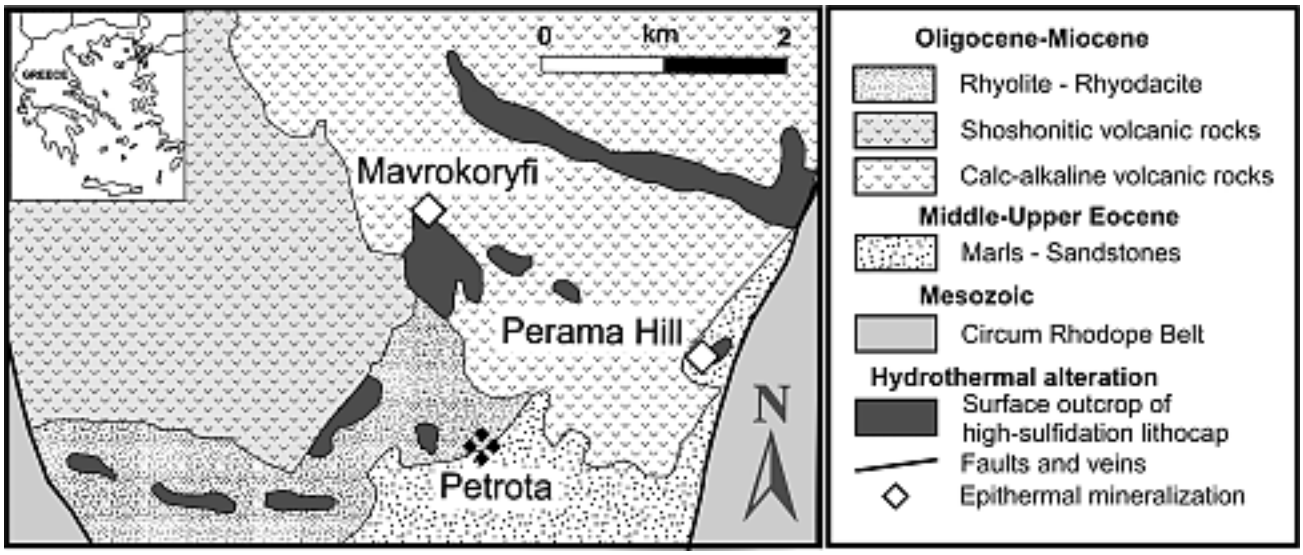

Fig. 1: (a) Simplified geological map of the northeastern part of Petrota Graben showing epithermal Au-(±Ag) deposits and prospects (after Arikas and Voudouris 1998; Voudouris 2006)

3. MINERALIZATION AND ALTERATION

The Perama Hill deposit can be described as an initial high-sulfidation epithermal system overprinted by intermediate sulfidation banded quartz-chalcedony-barite veins and stockworks. Two different styles of mineralization are present, a structurally controlled sulfide-bearing vein-type mineralization, in the andesites and a stratabound oxidized mineralization in the overlying sandstones (McAlister et al., 1999; Lescuyer et al., 2003; Evans, 2004). The mineralization took place initially through structurally controlled feeders, located inside the andesitic volcanic breccia, and then it has been disseminated into the porous sandstones. Beneath the oxidized ore, the deposit consists of sulfide mineralization that contains stannite, bornite, Au-Ag tellurides, native gold, pyrite, galena, tetrahedrite-group minerals, bismuthinite, enargite and luzonite (Lescuyer et al., 2003; Skarpelis et al., 2006). Gold is found in association with very fine pyrite and as inclusions in enargite. In the upper, mainly oxidized parts of the deposit, native gold is associated with quartz-barite veins cutting through silicic, sericitic-argillic altered and hematitized sandstones (McAlister et al., 1999; Voudouris and Skarpelis, 1998; Skarpelis et al., 1999). Paragenetic relationships during the present study suggest three stages of ore deposition, an early deposition of marcasite and pyrite, followed by an assemblage composed of enargite, very low-Fe sphalerite, covellite and bismuthinite and then by an intermediate sulfidation association including tennantite, galena, bismuthinite, lillianite homologues and the tellurides hessite, petzite,

stützite, sylvanite, krennerite and altaite. Native gold has not been observed. The early pyrite and marcasite show textural features that are indicative for a deposition on a seafloor environment. The presence of framboidal pyrite and microchimney-similar structrures composed of either pyrite or various sulfide combinations (Fig. 2) is very similar to those described from western Milos, and suggest rapid deposition on the seafloor environment (Alfieris & Voudouris, 2006a,b).

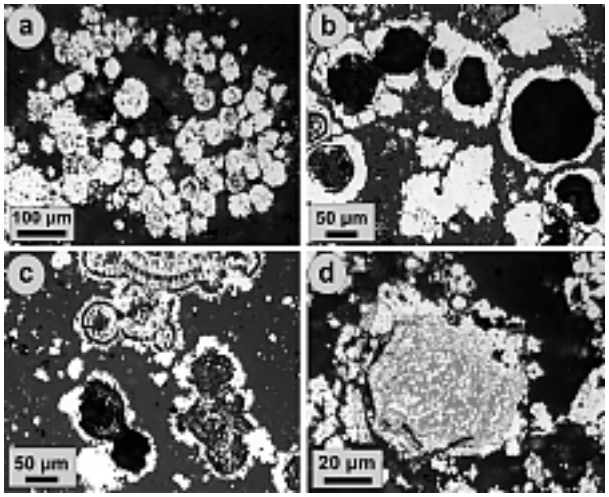

Fig. 2. Microphotographs (reflected light) demonstrating ore paragenesis in Perama Hill: (a) Framboidal pyrite within silicified matrix (b) Micro-chimney composed of pyrite; (c) early colloidal pyrite and late marcasite in silicified matrix; (d) Tennantite and pyrite intergrowth in a chimney-similar structure surrounded by pyrite.

4. ORE MINERALOGY

Electron microprobe analyses (EPMA) were obtained using a Cameca-SX 100 microprobe at the Institute of Mineralogy-Petrology, University of Hamburg.

Tennantite represents an important constituent of the mineralization, since it is intimately associated with precious metal tellurides (Fig. 3f, g). Representative EPMA of tennantite are given in Table 1. Three types of tennantite are distinguished: Fe-rich tennantite, zincian tennantite and bismuth-zincian tennantite. Fe-tennanite associated with enargite contains up to 6.9 wt.% Fe and no Zn. Up to 3.96 wt.% Bi has been detected in the bismuth-zincian tennantite. The later is associated with bismuthinite and lillianite homologues. In the zincian tennantite variety, values up to 7.9 wt.% Zn, 0.11 wt.% Bi, 0.14 wt.% Te and < 1.0 wt.% Fe were detected (Table 1). Zn-tennantite contains up to 0.5 wt.% Au and up to 1.1 wt.% Ag that are likely due to the presence of submicroscopic inclusions of native gold/electrum.

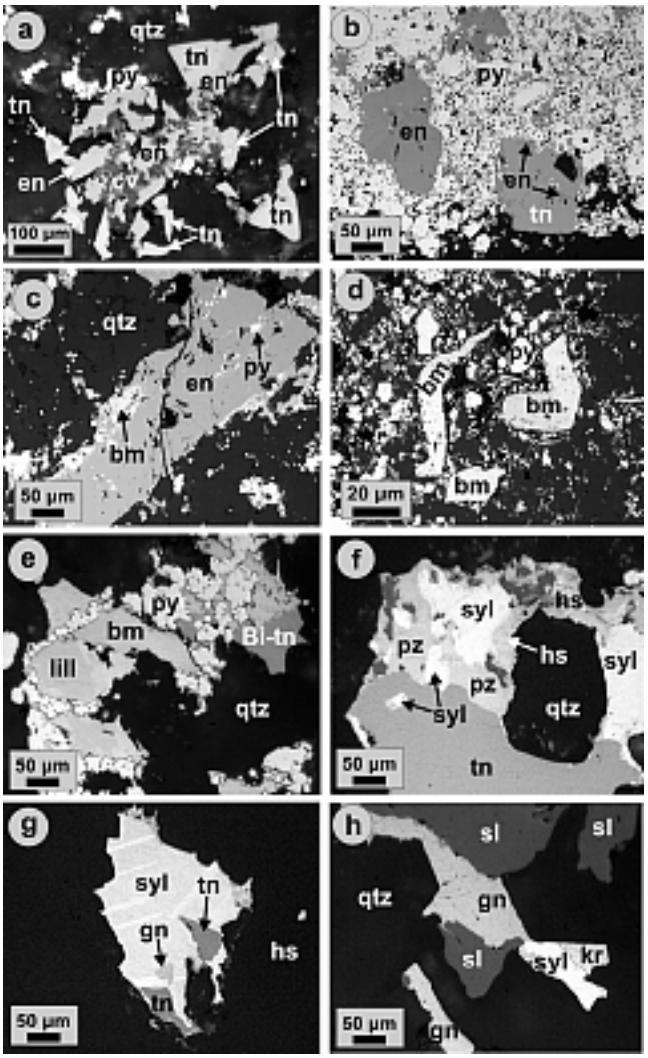

Fig. 3. (a) Early pyrite (py), enargite (en) and covellite (cv) surrounded by tennantite (tn); (b) Early pyrite (py) replaced by enargite (en) and late tennantite (tn); (c) Bismuthinite (bm) associated with enargite (en) including pyrite (py); (d) Bismuthinite (bm) postdating early pyrite (py); (e) Intergrowth of pyrite (py) bismuthinite (bm), lillianite homologue (lill) and Bi-rich tennantite (tn); (f) Sylvanite (syl), petzite (pz) and hessite (hs) in association with tennantite (tn); (g) Sylvanite (syl) including galena (gn) and tennantite (tn);(h) Galena (gn), sylvanite (syl) and krennerite (kr) postdating sphalerite (sl). Quartz (qtz) is present in the matrix.

Enargite and its tetragonal polymorph, luzonite, are intergrown with bismuthinite and Fe-rich tennantite. EPMA data shows that enargite

contains elevated Au contents (up to 0.3 wt.%), similarly to tennantite, probably as a result of the submicroscopic inclusions of native gold (Table 1). Enargite has elevated contents in Sn (up to 1.2 wt %) and minor amounts in Te (<0.2 wt.%).

Covellite is a primary mineral in Perama Hill and it is associated with enargite.

Table 1. EPMA data of tennantite, enargite and stannite

	1	2	3	4	5	6
Cu	40.20	40.32	39.17	45.52	46.01	29.71
Ag	0.32	0.15	0.12	0.00	0.32	0.00
Au	0.31	0.09	0.00	0.00	0.10	0.00
Fe	0.12	0.78	0.56	0.30	0.10	1.46
Zn	7.88	6.83	6.69	0.16	0.01	6.61
Sb	2.37	2.61	2.00	0.30	0.05	0.00
As	20.38	17.80	18.01	18.15	21.88	0.31
Bi	0.00	1.02	2.79	0.00	0.00	0.00
Sn	0.00	0.18	0.00	1.22	0.00	26.72
Te	0.14	0.000	0.11	0.16	0.00	0.00
Se	0.09	0.09	0.11	0.12	0.00	0.15
S	27.56	27.67	26.94	32.38	32.46	29.53
Total	99.37	97.53	96.49	98.30	100.93	94.50
Cu	9.589	9.766	9.702	2.877	2.847	2.141
Ag	0.045	0.021	0.018	0.000	0.012	0.000
Au	0.023	0.007	0.000	0.000	0.002	0.000
Fe	0.032	0.215	0.157	0.022	0.007	0.120
Zn	1.827	1.607	1.611	0.010	0.001	0.463
Sb	0.295	0.329	0.259	0.010	0.002	0.000
As	4.123	3.656	3.782	0.973	1.148	0.019
Bi	0.000	0.075	0.210	0.000	0.000	0.000
Sn	0.000	0.023	0.000	0.041	0.000	1.031
Te	0.017	0.000	0.013	0.005	0.000	0.000
Se	0.017	0.017	0.022	0.006	0.000	0.009
S	13.031	13.282	13.226	4.056	3.981	4.218

1,2: Zincian tennantite; 3: Bismuth-zincian tennantite; 4,5: Enargite; 6: stannite.

A stannite-similar phase with a composition approximating $(Cu,Zn,Fe)_3SnS_4$ (Table 1) is found in the form of small grains included in Fe-tennantite.

Sphalerite replaced by zincian tennantite and predating the telluride mineralization it is of the very-low iron variery. It contains up to 0.1 mole % FeS.

Galena replaces zincian tennantite in the barite ± quartz veins and it is closely related to the tellurides (Fig. 3 g, h). The Ag content reaches a maximum of 0.48 wt %; Sb and Bi contents are below detection limit. Se substituting for S has been detected in amounts up to 2.5 wt. % (Table 2).

Bismutinite is an abundant mineral phase in the Perama Hill deposit. It is included into enargite, either intergrown with it, or occurs disseminated in the silicified matrix (Fig. 3d). Selected microprobe analyses are presented in Table 2. Sb (up to 0.66 wt.%) substituting for Bi and Ag (<0.2 wt.%) substituting for Cu (<0.5 wt.%) were also detected. Bismuthinite contains up to 1.4 wt.% Se substituting for S.

Lillianite homologues form irregular grains included in tennantite and galena. They are associated with bismuthinite (Fig. 3e). Representative microprobe analyses are given in Table 2. The lillianite homologues can be divided into Cu-free varieties (nuffieldites), into Cu-bearing varieties ("schirmerites") and into heyrovskyite (according to the definitions of Makovicky & Karup-Møller, 1977; Cook, 1997). The Ag-content reach values up to 6.6 wt.%. Sb substituting for Bi ranges between 0.02 and 0.51 wt%. The lillianite homologues contain appreciable amounts of Se substituting for S (up to 3.9 wt.%) and Te up to 0.4 wt%.

Table 2. EPMA data of bismuthinite, lillianite homologues and galena

	1	2	3	4	5	6
Bi	79.76	80.32	33.79	21.44	46.38	0.00
Pb	0.00	0.00	43.10	60.63	26.88	83.03
Sb	0.31	0.27	0.04	0.00	0.25	0.00
Ag	0.07	0.01	6.03	3.51	6.55	0.37
Cu	1.67	0.00	0.00	0.02	0.98	0.03
Fe	0.23	0.23	0.03	0.00	0.07	0.00
S	17.95	18.82	13.42	13.13	15.29	11.22
Te	0.00	0.00	0.40	0.17	0.13	0.12
Se	1.25	0.14	3.90	3.71	1.70	2.49
Total	101.69	99.92	100.75	102.63	98.44	97.75
Bi	7.727	7.999	1.899	1.198	2.554	0.000
Pb	0.000	0.000	2.443	3.418	1.493	1.014
Sb	0.051	0.046	0.003	0.000	0.024	0.000
Ag	0.014	0.002	0.657	0.380	0.699	0.009
Cu	0.533	0.000	0.000	0.003	0.177	0.001
Fe	0.083	0.085	0.007	0.000	0.014	0.000
S	11.335	12.217	4.917	4.783	5.490	0.886
Te	0.000	0.000	0.037	0.016	0.012	0.002
Se	0.321	0.037	0.580	0.549	0.247	0.080

1,2: Bismuthinite, formula to (Cu+Ag+Pb)/2 +Bi = 8.00 atoms); 3-5: Lillianite homologues, formula to 5 (Cu+Ag+Pb+Bi); 6: Galena.

Tellurium-bearing minerals

Six tellurides (hessite, stützite, petzite, altaite, sylvanite and krennerite) were identified in this

study and representative microprobe analyses are given in Table 3. They occur in the following contact assemblages: sylvanite-altaite, sylvanite-petzite, sylvanite-krennerite, sylvanite-hessite and petzite-hessite. The intergrowths between sylvanite-petzite and sylvanite-hessite may be breakdown products of the γ-phase or x-phase below 120 °C (Cabri, 1965). However Ciobanu et al. (2004) and Cook et al. (2004) reported co-crystallization of petzite with sylvanite and krennerite at Săcărîmb deposit (Golden Quadrilateral, Romania).

Hessite (Ag_2Te) is intimately associated with petzite, and sylvanite (Fig. 3f). The Au content of hessite is up to 0.66 wt%.

Petzite (Ag_3AuTe_2) is commonly observed at Perama Hill where it is intergrown with sylvanite and hessite (Fig. 3f). EPMA reveal Au contents between 16.6 and 18.1 wt%, most probably as a result of melting of the grains during analysis (Rucklidge and Stumpfl, 1968).

Tab. 3. EPMA data on sylvanite (1,2), krennerite (3), petzite (4), hessite (5), stützite (6)

	1	2	3	4	5	6
Ag	10.10	8.62	3.84	44.36	63.01	55.33
Au	28.49	30.00	35.46	18.00	0.66	1.54
Cu	0.01	0.00	0.08	0.57	0.32	2.79
Bi	0.11	0.22	0.14	0.08	0.01	0.09
Te	61.76	61.42	59.44	34.24	40.90	37.87
S	0.00	0.02	0.01	0.11	0.04	0.63
Total	100.87	100.71	100.75	98.64	105.83	101.84
Atoms	6	6	3	6	3	8
Ag	0.777	0.516	0.156	3.098	1.917	4.655
Au	1.201	1.795	0.790	0.689	0.011	0.071
Cu	0.001	0.000	0.006	0.067	0.016	0.398
Bi	0.005	0.013	0.003	0.003	0.000	0.004
Te	4.017	3.745	2.043	2.022	1.051	2.694
S	0.000	0.001	0.002	0.026	0.005	0.177

na: not analyzed; <bdl: below detection limit

Sylvanite ($AgAuTe_4$) is the most abundant telluride in Perama Hill and occurs in complex intergrowths with galena, and other tellurides replacing tennantite (Fig. 3f to h). Sylvanite-petzite intergrowths are very common and probably the result of decomposition of γ-phase. The Au content in sylvanite ranges between 26.9 and 30.0 wt% and Ag between 8.6 and 12.5 wt%. Sylvanite in association with krennerite is presented Ag-poor, whereas in contact with petzite it is Ag-rich. Sylvanite contains up to 0.4 wt% Sb and 0.26 wt% Bi.

Krennerite ($AuAgTe_2$) is found in contact with sylvanite and in association with galena (Fig. 3h). To our knowledge it is the second occurrene of this mineral in Greece, after that of Panormos bay in Tinos island (Spry et al., 2006). A single analysis is presented in Table 3.

Stützite ($Ag_{5-x}Te_3$) is a rare phase at Perama Hill occuring rather as inclusions in tennantite. It contains up to 1.5 wt% Au (Table 3).

Altaite (PbTe) is found in complex intergrowths with sylvanite, galena, hessite and petzite and forms irregular grains (up to 100 μm in length). Altaite contains up to 0.35 wt% Au, 0.31 wt % Ag, 0.94 wt% Sb and 0.82 wt% Se.

DISCUSSION-CONCLUSIONS

Bismuth sulfosalts and tellurides are common constituents of porphyry-epithermal ores in northeastern Greece, where they are found in association with both intermediate and high sulfidation ore assemblages (Voudouris, 2006): The tellurides hessite, petzite, sylvanite, stützite, altaite, coloradoite and tetradymite accompany aikinite/friedrichite, hammarite/lindströmite and lillianite homologues in the Kassiteres, St Demetrios, Pefka and Pagoni Rachi prospects/deposits. In addition, calaverite was reported, but not quantitatively documented, from the Viper deposit/Sappes area (Shawh and Constantinides, 2001). This study demonstrates an abundance of precious metal tellurides in the Perama Hill deposit. They accompany bismuthinite derivatives (bismuthinite/pekoite) and lillianite homologues similarly to the above mentioned occurrences. Textural relationships suggest that introduction of tellurides in Perama Hill postdate formation of enargite/luzonite and it is closely related to the introduction of tennantite and galena in the system. This is in accordance with previous observations that suggest deposition of most tellurides in western Thrace by intermediate sulfidation fluids and in the stability field of tennantite/tetrahedrite.

The telluride and sulfide mineralogy, as well as the composition of sphalerite are used to constrain fTe_2 and fS_2 values of the hydrothermal solutions

(Fig. 4). On the absence of fluid inclusion data the coexistance of enargite and luzonite in the sulfide mineralization suggests temperatures near 280ºC (Pósfai and Buseck, 1998). However the assemblage sylvanite-petzite indicates an upper temperature limit of 170 ºC, as based on the experimental studies of Cabri (1965). Thermodynamic data for sulfides and tellurides used for calculating fTe_2 and fS_2 were derived from Mills (1974), Barton and Skinner (1979) and Afifi et al. (1988).

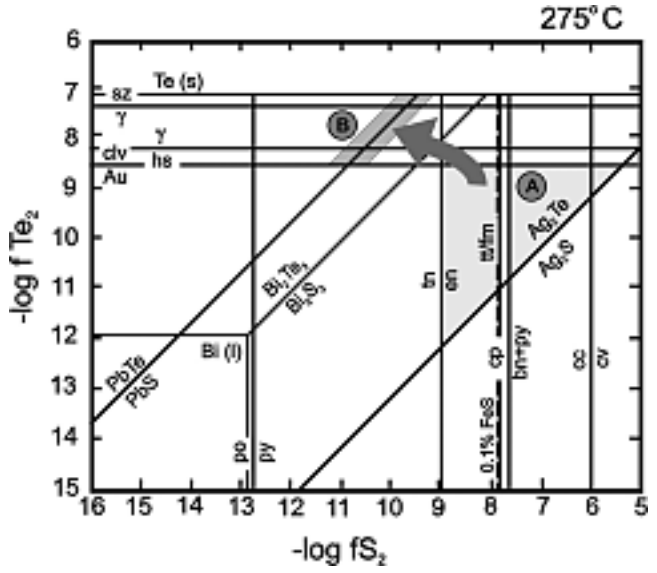

Fig. 4. LogfTe_2 vs logfS_2 diagram indicating equilibria between tellurides and sulfides, at 275°C, at vapor saturation. The shaded area indicates approximate conditions of telluride and Bi-sulfosalts deposition at Perama Hill deposit. Abbreviations: clv = calaverite, hs = hessite, sz = stützite, γ = gamma-phase, tn = tennantite, td = tetrahedrite, fm = famatinite, en = enargite, cp = chalcopyrite, bn = bornite, py = pyrite, po = pyrrhotite, cc = chalcocite, cv = covellite.

Early deposition of enargite, very low-Fe sphalerite, covellite and native gold took place (at 275 °C) under logfS_2 values between -9 and -6 and logfTe_2 from -8.5 and -12 and in the stability field for bismuthinite and hessite (area A, Fig. 4). The telluride deposition occurred under logfS_2 values between -9 and -11 consistent with the presence of tennanite. The logfTe_2 values were constrained by the galena/altaite boundary and the stability field of γ-phase at about -7.3 and -8.2. The above data indicate a shift towards higher logfTe_2 and lower logfS_2 values for the mineralizing fluids during telluride deposition in Perama Hill, probably due to the tellurium contribution in the form of magmatic vapors (Jensen and Barton, 2000). Cooling of the mineralizing fluids during their ascent resulted in a saturation in silica and in a near-surface deposition of gold-bearing quartz-chalcedony veins by low salinity fluids (2.3 to 3.2 wt.% NaCl equiv) at 176º to 191 °C (Skarpelis et al., 1999).

Based on geological and mineralogical information it is suggested that the Perama Hill mineralization was formed under shallow submarine to subaerial conditions. Early framboidal pyrite and marcasite microchimney structures in the deeper levels of the deposit are indicative for a formation at a seafloor/sub-seafloor environment and at relatively low temperatures. Subsequent high sulfidation (enargitic) ore and base metal sulfides took place as replacements and intergrowths in the earlier microchimney structures. Later telluride-bearing quartz-barite-base metals and/or quartz-barite veins crosscut the deep pyrite/marcasite-enargite-covellite ore and have been emplaced into the subaerial sandstones. The extreme abundance of barite, compared to other epithermal mineralization in western Thrace it is an additional mineralogical evidence of seawater contribution to the mineralizing fluids. The Perama Hill mineralization has many similarities to the transitional submarine to subaerial high sulfidation epithermal Pueblo Viejo/Dominican Republic deposit (Kesler et al., 2005). Finally it can be compared to the western Milos high-intermediate sulfidation epithermal system, considered to have been formed in a transitional submarine to subaerial setting (Plimer, 2000; Stewart and McPhie, 2003; Alfieris et al., 2204; Naden et al., 2005; Alfieris, 2006).

REFERENCES

Afifi, A.M., Kelly, W.C. and Essene, E.J., 1988, Phase relations among tellurides, sulfides and oxides: I. Thermochemical data and calculated equilibria. Econ. Geol. 83: p.377-394.

Alfieris, D., 2006, Geological, geochemical and mineralogical studies of shallow submarine epithermal mineralizations in an emergent volcanic edifice, W. Milos island, Greece. Unpubl. PhD thesis, Univ. Hamburg, 211pp.

Alfieris, D., Kilias, S., Naden, J. and Voudouris, P., 2004, Spatially coincident low- and high-suldidation epithermal mineralization in an emerging volcanic edifice, W. Milos, Greece. 5th Int. Symp. Eastern Mediteranean Geology, 4pp.

Alfieris, D. and Voudouris, P., 2006, First occurrence of tellurides in the epithermal Profitis Ilias deposit, Milos Island, Greece, 12th IAGOD, Moskow, CD-ROM.

Alfieris, D. and Voudouris, P., 2006, Tellurides and sulfosalts in the shallow submarine epithermal deposits of Milos Island, Greece. In: N.G. Cook, I. Özgenc and T. Oyman. IGCP-486 Field workshop, Izmir 24-29 September 2006, Proc. 6-14.

Arikas, K. and Voudouris, P., 1998, Hydrothermal alterations and mineralizations of magmatic rocks in the southern Rhodope Massiv. Acta Vulcanol. 10: p.353-365.

Barton, P.B.Jr. and Skinner, B.J., 1979, Sulfide mineral stabilities. In: Barnes H.L. (ed), Geochemistry of hydrothermal ore deposits. Wiley Interscience, New York, p278-403.

Border, A., Constantinides, D. and Michael, C., 1999, Discovery and evaluation of the Sappes gold deposit, Northeastern Greece. In: Currie D. and Nielsen K. (eds). New generation gold mines '99, Case histories of discovery. Austral. Min. Found. Conf. Proc. 29-38.

Cabri, L.J. 1965, Phase relations in the Au-Ag-Te system and their mineralogical significance. Econ. Geol. 60: 1569-1606.

Christofides, G., Pecskay, Z., Soldatos, T., Eleftheriadis, G. and Koroneos, A., 2004, The Tertiary Evros volcanic rocks (Greece): Petrology, K/Ar geochronology and volcanism evolution. Geol. Carp. 55: p.397-409.

Ciobanu, C.L., Cook, N.J., Damian, G., Damian, F., 2004, Telluride and sulfosalt associations at Săcărîmb. In: Cook N.J. and Ciobanu C.L. (eds) Au-Ag-telluride deposits of the Golden Quadrilateral, Apuseni Mts., Romania, IAGOD Guidebook Ser. 12: 145-186.

Cook, N., 1997, Bismuth and bismuth-antimony sulphosalts from Neogene vein mineralization, Baia Borşa area, Maramureş, Romania, Mineral. Mag. 61: 387-409.

Cook, N.J., Ciobanu, C.L., Damian, G. and Damian, F., 2004, Tellurides and sulfosalts from deposits in the Golden Quadrilateral. In: Cook N.J. and Ciobanu C.L. (eds), Au-Ag-telluride deposits of the Golden Quadrilateral, Apuseni Mts., Romania, IAGOD Guidebook Ser. 12: 111-144.

Dimou, E., Michael, K. and Serment, R., 1994, Mineralogical composition of the epithermal polymetallic mineralization at Pefka area, Rhodope district. Bull. Geol. Soc. Greece 30: 533-550 (in Greek)

Evans, L., 2004, Report on Perama Hill gold deposit, Mineral resource estimate, Greece, www.frontierpacific.com/pdf/report_perama.pdf

Jensen, E.P. and Barton, M.D., 2000, Gold deposits related to alkaline magmatism. Rev. Econ. Geol. 13: 279-314.

Kesler, S.E., Campbell, I.H., Smith, C.N., Hall, C.M. and Allen, C.M., 2005, Age of the Pueblo Viejo gold-silver deposit and its significance to models for high-sulfidation epithermal mineralization. Econ. Geol. 100: 253-272.

Lescuyer, J.L., Bailly, L., Cassard, D., Lips, A.L.W., Piantone, P. and McAlister, M., 2003, Sediment-hosted gold in south-eastern Europe: the epithermal deposit of Perama, Thrace, Greece In: Eliopoulos D.G. et al. (eds), Mineral exploration and sustainable development. Millpress, Rotterdam, 499-502.

Makovicky, E., and Karup-Møller, S., 1977, Chemistry and crystallography of the lillianite homologous series (Part II: Definition of new minerals: eskimoite, vikingite, ourayite and treasureite. Redefinition of schirmerite and new data on the lillianite-gustavite solid-solution series). N. Jb. Mineral. Abh. 131: 56-82.

Marchev, P., Kaiser-Rohrmeier, M., Heinrich, Ch., Ovtcharova, M., von Quadt, A. and Raicheva, R., 2005, Hydrothermal ore deposits related to post-orogenic extentional magmatism and core complex formation: The Rhodope Massif of Bulgaria and Greece. Ore Geol. Rev. 27: 53-89.

McAlister, M., Hammond, J.M., Normand, D. and Kampasakalis, M., 1999, Discovery case history for the Perama Hill gold deposit, Greece. In: Currie D. and Nielsen K. (eds), New generation gold mines '99, Case Histories of Discovery. Austral. Min. Found. Conf. Proc., Perth, 39-49.

Melfos, V., Vavelidis, M. and Bogdanov, K., 2003, Occurrence, mineralogy and chemical composition of primary gold from Tertiary ore mineralisations in the Rhodope massif (Greece-Bulgaria). In: D.G. Eliopoulos et al. (eds), Mineral exploration and sustainable development. Millpress, Rotterdam, 1201-1204.

Michael, C., Perdikatsis, V., Dimou, E. and Marantos, I., 1995, Hydrotherma1 a1teration and ore deposition in epitherma1 precious metal deposit of Agios Demetrios, Konos area, Northern Greece. Geo1. Soc. Greece, Special Pub1. 4: 778-782.

Mills, K.C., 1974, Thermodynamic data for inorganic sulfides, selenides and tellurides. Butterworths, London, 925pp.

Naden, J., Kilias, S. and Darbyshire, D.B.F., 2005, Active geothermal systems with entrained seawater as analogues for transitional continental magmato-hydrothermal and volcanic-hosted massive sulfide mineralization-the example of Milos Island, Greece: Geology 33: 541-544.

Papadopoulos, P., 1982, Geological map of Greece, Maronia sheet, scale 1:50.000, I.G.M.E., Athens.

Plimer, I., 2000, Milos Geologic history. KOAN Publishing House, Athens, 262pp.

Pósfai, M. and Buseck, P.R., 1998, Relationships between microstructure and composition in enargite and luzonite. Amer. Mineral. 83: 373-382.

Rucklidge, J. and Stumpfl, E.F., 1968, Changes in the composition of petzite (Ag_3AuTe_2) during analysis by electron microprobe. N. Jb. Mineral. Monatsh. 61-68.

Shawh, A.J. and Constantinides, D.C., 2001, The Sappes gold project. Bull. Geol. Soc. Greece. 34: 1073-1080.

Skarpelis, N., Voudouris, P. and Arikas, K., 1999, Exploration for epithermal gold in SW Thrace, Greece: New target areas. In: Stanley C.J. et al. (eds), Mineral deposits: Processes to processing, Balkema, Rotterdam, 589-592.

Skarpelis, N., Triantafyllidis, S. and Falalakis G., 2006, The Perama intermediate sulfidation epithermal Au system (Thrace, Greece): Hypogene mineralogy and supergene alteration. Abstract Volume of the Conference "International magmatism of the Central Aegean and adjacent areas: Petrology, tectonics, geodynamics, mineral resources and environment, Milos.

Spry, P.G, Tombros, S.F., Seymour, K.St. and Zouzias, D.P., 2006, Geology, mineralogy and geochemistry of granite-hosted gold telluride mineralization at Panormos Bay, Tinos island, Greece. Geol. Soc. Amer. Abstr. Prog. 38: 55.

Stewart, A.L. and McPhie, J., 2003, Setting of epithermal Au deposits in a modern volcanic island arc setting, Milos, Greece: Implications for mineral exploration. In: Eliopoulos D et al. (eds) Mineral Exploration and Sustainable Development, Millpress, Rotterdam, 533-536.

Voudouris, P., 2005, Mineralogy of the high-sulfidation Cu-Sb-Te Mavrokoryfi prospect (western Thrace/Greece). In: J.W. Mao and F.P. Bierlein (eds) Mineral deposit research: Meeting the global challenge. Springer, Berlin, 1435-1438.

Voudouris, P., 2006, A comparative mineralogical study of Te-rich magmatic-hydrothermal systems in northeastern Greece. Mineral. Petrol. 87: 241-275.

Voudouris, P. and Arikas, K., 1994, Epithermal Au-Ag mineralizations at Kassiteres-Sappes, NE-Greece: Mineralogical, geological and microthermometric studies. Bull. Geol. Soc. Greece 30: 427-443 (in German)

Voudouris, P. and Skarpelis, N., 1998, Epithermal gold-silver mineralization in Perama (Thrace) and Lemnos areas. Bull. Geol. Soc. Greece. 32: 125-135

Voudouris, P. and Melfos, V., 2006, Bismuth sulfosalts and silver tellurides in the Pagoni Rachi porphyry-Cu-Mo prospect, western Thrace (NE Greece). In: N.G. Cook, I. Özgenc and T. Oyman. Field workshop, Izmir 24-29 September 2006, Proc. 159-166.

Voudouris, P., Tarkian, M. and Arikas, K., 2006, Mineralogy of telluride-bearing epithermal ores in Kassiteres-Sappes area, western Thrace, Greece. Mineral. Petrol. 87: p.31-52.

Tellurides and bismuth sulfosalts in gold occurrences of Greece: mineralogical and genetic considerations

P. VOUDOURIS — Dept. Mineralogy-Petrology, University of Athens, 15784 Athens, Greece, voudouris@geol.uoa.gr
P.G. SPRY — Department of Geological and Atmospheric Sciences, Iowa States University, 253 Science Hall I, Ames IA 50011-3212, USA
V. MELFOS — Dept. Mineralogy-Petrology-Economic Geology, Aristotle University of Thessaloniki, 54124, Thessaloniki, Greece
D. ALFIERIS — S&B Industrial minerals S.A., 15A Metaxa str. 14564 Kifissia, Athens, Greece

Summary: Pre-Tertiary to Tertiary gold deposits in Greece occur in a wide range of genetic types including volcanic massive sulfides, orogenic, intrusion-hosted, skarn, manto-, porphyry- and epithermal-type ores. Almost all of the gold mineralization hosts various Bi-tellurides and Bi-sulfosalts, which in addition to Au-Ag-tellurides, are indicators of specific physicochemical conditions of ore formation. The Bi-bearing mineralization can be subdivided into three groups regarding their spatial relationship to gold: (a) mineralization which lacks tellurides but includes Bi-sulfosalts and native gold, (b) mineralization where Bi-tellurides of the reduced-type (joseite-A, joseite-B, pilsenite) accompany Bi-sulfosalts, native bismuth and native gold, (c) deposits/prospects where Au-Ag-tellurides are abundant and Bi-tellurides and Bi-sulfosalts are absent. Bi-telluride and -sulfosalt mineralization in Greece underwent several stages of remobilization during successive accretionary episodes in active continental margins and arc terranes during the Carboniferous to Pleistocene.

Key Words: Gold ores, tellurides, gold, silver, sulfosalts, bismuth, Greece

1. INTRODUCTION

Primary gold deposits in Greece occur in a wide range of genetic types, comprising VMS deposits of pre-Tertiary age, those related to metamorphic or deformation processes, ores related to Mesozoic-Miocene shearing, and deposits related to Tertiary-Quaternary magmatic activity (skarn and manto-type, porphyry-type, vein-type, epithermal-type) (Eliopoulos and Kalogeropoulos, 1985; Bitsios, 1989; Skarpelis, 2002; Arvanitidis, 2003). The Rhodope metallogenic ore province (Melfos et al., 2002) including the Servomacedonian-Rhodope massifs (Mposkos and Krohe, 2001, Reischmann and Kostopoulos, 2007) host porphyry Cu-Mo-Au and epithermal Au deposits, Pb-Zn (Ag-Au) carbonate replacement, skarn and vein deposits of Late Eocene to Oligocene age, epithermal Au-Ag deposits and shear zone hosted mesothermal to low sulfidation epithermal gold-silver deposits not related to intrusive activity (e.g. Ada Tepe in Bulgaria) (Ashworth et al., 1988; Nesbitt et al., 1988; Arvanitidis and Constantinides, 1989; Hellingwerf et al., 1994; Arvanitidis et al., 1996; Marchev et al., 2005; Eliopoulos and Chryssoulis, 2005). Both the shear zone Au-Ag deposits and the low sulfidation epithermal Au-Ag deposits lie close to or within metamorphic domes and may be related to post collision orogenic collapse and exhumation of these structures (Marchev et al., 2005). The Attico-Cycladic metamorphic belt comprises a number of types of mineralization, which are in part genetically related to arc-related magmatic rocks, and in part controlled by exhumation structures of high-pressure units in a back-arc setting (Skarpelis, 2002; Neubauer, 2005). The Attico-Cycladic Massif (Okrusch andd Bröcker, 1990) contains base- and precious-metal skarn, intrusion-related, orogenic and epithermal mineralization in south Evia, Sifnos, Mykonos, Tinos and Kythnos Islands (Alexouli-Livaditi, 1978; Vavelidis, 1997; Tombros et al., 2004; Neubauer, 2005; Spry et al., 2006). At Sifnos Island, orogenic ore formation occurred during extensional kinematic conditions, when the Sifnos metamorphic core complex reached a near-surface level (Neubauer, 2005).

Despite several mineralogical studies of gold mineralization in Greece, an integrated

documentation of telluride and Bi-sulfosalt bearing ores has yet to be done. The aim of the present study is to review all mineralogical data concering tellurides and Bi-sulfosalts from various gold deposits/prospects in Greece (Fig. 1), to present new information concerning the location of bismuth sulfosalts and tellurides, and to discuss their origin.

Fig. 1. Location map of tellurides and Bi-sulfosalts occurrences in Greece

2. Bi SULFOSALTS AND NATIVE BISMUTH

Bismuth sulfosalts are widespread in almost all the gold deposits in Greece. In the Oligocene porphyry-type mineralization of Pagoni Rachi/W. Thrace, Bi-sulfosalts spatially associated with tellurides are enriched in late-stage quartz-carbonate veins, which overprinted chalcopyrite-molybdenite-bearing quartz stockworks (Voudouris and Arikas, 2003; Voudouris and Melfos, 2006). The bismuthinite derivatives (aikinite to lindströmite) and lillianite homologues are closely related to hessite and stützite and occur as tiny inclusions within chalcopyrite, galena, sphalerite and tennantite. New observations in Pagoni Rachi indicate intergrowths between wittichenite $(Cu_{2.92}Ag_{0.06})_{2.97}Bi_{0.99}S_{3.02}$, a berryite-like sulfosalt, $(Cu_{1.33}Ag_{0.66})_{1.99}Bi_{2.29}Pb_{0.96}S_{5.41}$, hessite, bornite and galena (Figs. 2a,b). Bismuthinite was reported by Melfos et al. (1996, 2002) from the adjacent Miocene(?) microgranite-hosted porphyry Cu-Mo system of Maronia/W. Thrace. Intrusion-hosted sheeted quartz veins and stockworks, rich in molybdenite and scheelite from the Kimmeria Oligocene granodioritic body, which outcrop east of Xanthi/Rhodope massif, contain minor emplectite, wittichenite and aikinite (Walenta and Pantzartzis, 1969). The Stypsi prospect, a newly discovered porphyry Cu±Mo mineralization on Lesvos Island contains bismuthinite (Voudouris and Alfieris, 2005). Bismuthinite, galenobismutite, cosalite and aikinite were reported from the Oligocene skarn-carbonate replacement polymetallic Madem Lakkos sulfide deposit, Chalkidiki/northern Greece, in marbles of the Servomacedonian massif (Nebel et al., 1991; Gilg 1993). In a similar style of mineralization, at Kamariza mines in the Lavrion area (Attika), a close spatial association exists among native gold, native bismuth and bismuthinite (Fig. 2c) (Voudouris, 2005). Several other Bi-Cu-Pb-Ag sulfosalts, including bismuthinite, lillianite homologues, Cu-matildite, aikinite, Ag-aikinite, mummeite, emplectite and wittichenite occur as inclusions in chalcopyrite (Voudouris and Economou-Eliopoulos, 2003). In the high-intermediate sulfidation epithermal assemblages of St Philippos, St Demetrios and Pefka in W. Thrace/Greece, the Bi-sulfosalts kirkiite, bismuthinite, cosalite, aikinite and hammarite have been reported (Dimou, 1993; Voudouris et al., 2006; Voudouris, 2006). New paragenetic relationships from the Perama Hill high-intermediate sulfidation epithermal system (Voudouris et al., 2007, this volume) demonstrates the presence of bismuthinite related to enargite and covellite, as well as of lillianite homologues associated with tennantite, galena and precious metal tellurides. Bismuth sulfosalts spatially associated with Bi-tellurides, native bismuth and native gold have been reported from several pre-Tertiary to Tertiary shear-zone-controlled (orogenic according to Groves et al., 1998) and/or metamorphosed gold deposits/mineralization in northern Greece. The ore occurs in both folded/deformed and undeformed varieties as replacement-type, irregular pods or as lenses developed in marble-gneiss contacts, in gneisses, amphibolites, marbles, and as quartz veins

crosscutting the above lithologies of the Rhodope-Servomacedonian massifs (Mposkos, 1983; Kalogeropoulos et al., 1986, 1991; Vavelidis, 1994; Hellingwerf et al., 1994; Thymiatis, 1995; Chatzikirkou, 2003; Eliopoulos and Chryssoulis, 2005). Folded and deformed massive to disseminated mineralization is associated with quartz segregations and pegmatoid bodies crosscutting at low angles, or are parallel, to the schistosity of mica gneisses, schists and amphibolites, at Paliomilos, Chalkoma and Paliopyrgos/Stanos areas in Chalkidiki, at Koronouda, Paliomylos and Laodikino in Kilkis. In the Stanos/Chalkidiki area, the Paliomilos and Chalkoma mineralization contains bismuthinite, cosalite, gladite, pavonite and emplectite associated with native gold, as well as native bismuth, native gold and an intergrowth of cosalite/joseite-A included in late chalcopyrite (Kalogeropoulos et al., 1991). Investigations during the present study from Chalkoma mineralization indicated a close spatial relationship between electrum, native bismuth and gustavite ($Ag_{0.92}Cu_{0.05}Pb_{1.20}Bi_{2.82}S_{5.34}$) in chalcopyrite veinlets crosscutting pyrite (Fig. 2i). Our study of mineralization at Paliomilos indicates complex intergrowths among lillianite homologues ($Ag_{0.69}Pb_{1.70}Bi_{2.60}S_{5.26}$), galena and native bismuth (Fig. 2g). Electrum is associated with lillianite homologues (Fig. 2h). In Au-Ag bearing mineralization in the Paliopyrgos area, aikinite is intergrown with native gold, friedrichite, and galena, the latter two minerals being included in chalcopyrite (Vavelidis and Tarkian, 1995). In the Koronouda and Paliomylos areas, quartz segregations and pegmatoid bodies, hosted within gneisses and schists of the Vertiskos series, contain bismuthinite, aikinite and native bismuth in addition to Bi-tellurides and Au-Ag-tellurides as inclusions in chalcopyrite (Vavelidis 1994; Vavelidis et al., 1996; Melfos et al., 2001). During the present study at Koronouda mineralization, tiny inclusions of native Bi occur in galena and hessite and along their grain boundaries (Fig. 2k, l). Bi-sulfosalts are also common constituents in several gold-bearing post-metamorphic quartz veins throughout the Servomacedonian-Rhodope massif: bismuthinite, cosalite and native gold included in chalcopyrite were reported at Palea Kavala (Vavelidis et al., 1997), bismuthinite intergrown with tetradymite and isolated grains of hessite are included in chalcopyrite from a Bi-Te-Ag-bearing Cu prospect in the Panagia area (Thasos island) (Vavelidis et al., 1995) and bismuthinite, native bismuth, cosalite, joseite $Bi_4(S,Te)_3$, and lillianite from Angistron Mt (W. Rhodope massif) (Katirtzoglou et al., 1994). Recently studied samples from Palea Kavala (Chalkero locality), revealed a close spatial association among tetradymite, pyrite and bismuthinite ($Bi_{2.06}Sb_{0.04}S_{2.87}Te_{0.02}Se_{0.01}$) in milky quartz from detachment-related mineralization. Finally, bismuthinite, emplectite, aikinite and wittichenite accompanying tetradymite and hessite, are described from shear zone-hosted ores at the Eptadendron (Aberdeen)-Rachi areas in eastern Rhodope massif (Chatzikirkou, 2003; Chatzikirkou and Michailidis, 2004).

3. Bi TELLURIDES

Bi-tellurides are common in the pre-Tertiary to Tertiary orogenic and metamorphosed gold deposits/mineralization in northern Greece. Joseite-A is intergrown with cosalite from Paliomilos and Chalkoma Stanos/Chalkidiki (Kalogeropoulos et al., 1991), pilsenite-galena-hessite intergrowths and tellurobismuthinite, werhlite are included in chalcopyrite in the Koronouda area (Mposkos, 1983; Vavelidis 1994, Vavelidis et al., 1996), tetradymite is intergrown with bismuthinite and hessite at Panagia area (Thasos island) (Vavelidis et al., 1995), joseite $Bi_4(S,Te)_3$ occurs at Mt. Angistron (Katirtzoglou et al. 1994) and tetradymite occurs in the Eptadendron-Rachi areas in eastern Rhodope Massif (Chatzikirkou, 2003; Chatzikirkou and Michailidis, 2004). In addition, the following Bi-tellurides were identified in the present study: tetradymite ($Bi_{2.06}Te_{1.88}S_{1.03}$) in the Chalkero/Palea Kavala (Fig. 2j), pilsenite ($Bi_{3.97}Te_{3.03}$) included in chalcopyrite (Fig. 2e) in Laodikino, joseite-B ($Bi_{3.92}Au_{0.05}Te_{1.93}Se_{0.04}S_{0.98}$) associated with pilsenite ($Bi_{3.80}Te_{2.85}S_{0.35}$) and tellurobismuthite ($Bi_{2.05}Te_{2.78}S_{0.17}$) surrounding hessite in the Koronouda, area (Fig. 2k).

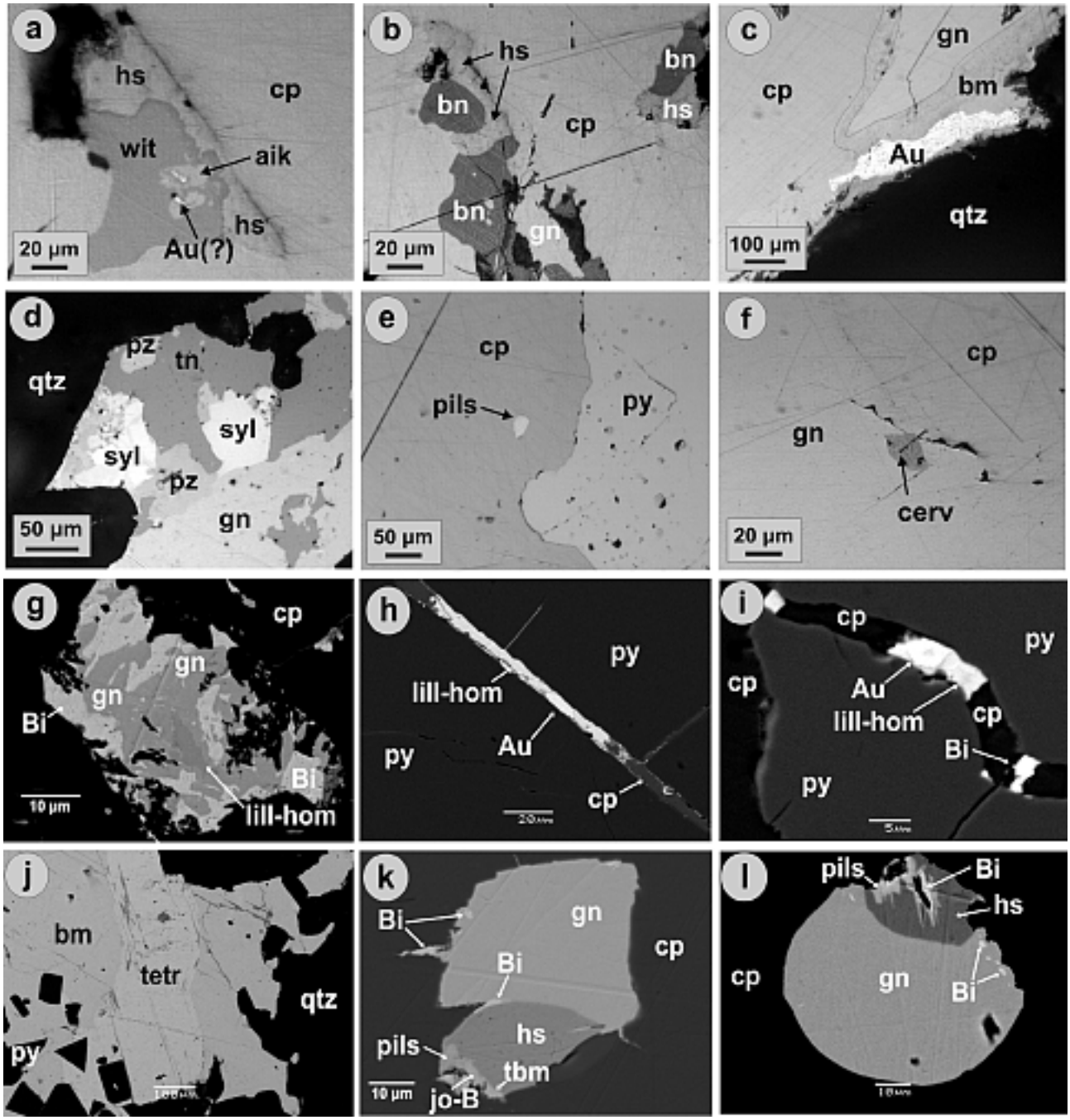

Fig. 2. Photomicrographs demonstrating the ore paragenesis of various telluride-Bi sulfosalt bearing mineralization in Greece: (a, b) Intregrowth of wittichenite (wit), aikinite (aik), hessite (hs), bornite (bn), galena (gn) and native gold (Au?) included in chalcopyrite (cp), Pagoni Rachi porphyry Cu-Mo; (c) native gold (Au) associated with bismuthinite (bm), galena (gn) and chalcopyrite (cp) from the Kamariza/Lavrion carbonate replacement deposit; (d) petzite (pz), sylvanite (syl) intergrowths with tennantite (tn) and galena (gn), Perama Hill epithermal deposit; (e) Pilsenite (pils) included in chalcopyrite (cp); pyrite (py) is also present, Laodikino metamorphosed VMS-orogenic deposit; (f) Cervelleite (cerv) included in galena (gn) at the grain boundaries to chalcopyrite (cp), Kallianou orogenic gold deposit; (g) lillianite homologue (lill-hom), galena (gn) and native bismuth (Bi) included in chalcopyrite (cp), Paliomylos metamorphosed VMS-orogenic deposit; (h) lillianite homologue (lill-hom), native gold (Au) and chalcopyrite (cp) filling a fissure in pyrite (py), Paliomylos metamorphosed VMS-orogenic deposit; (i) lillianite homologue (lill-hom), native gold (Au), native bismuth (Bi) and chalcopyrite (cp) filling a fissure in pyrite (py), Chalkoma metamorphosed VMS-orogenic deposit; (j) tetradymite (tetr) and bismuthinite (bm) surrounding pyrite (py) and included in quartz (qtz), Chalkero orogenic mineralization; (k,l) Blebs of galena (gn) within chalcopyrite (cp) spatially associated with hessite (hs), native bismuth (Bi), pilsenite (pils), joseite-B (jos-B) and tellurobismuthite (tbm), Koronouda metamorphosed VMS-orogenic deposit (a to f: reflected light, g to l: BSE images)

Tellurobismuthite has previously been described in the syenite-hosted porphyry Au-PGE system at Skouries, in addition to gold-silver tellurides and the Pd-telluride merenskyite (Eliopoulos and Economou-Eliopoulos, 1991; Tarkian et al., 1991; Economou-Eliopoulos and Eliopoulos, 2005). Tellurobismuthite and tetradymite occur in association with bismuth sulfosalts and Au-Ag-tellurides in the porphyry-epithermal assemblages of St Demetrios and Pefka prospects in W. Thrace, Greece (Dimou et al., 1994; Voudouris and Arikas, 1994; Voudouris et al., 2006; Voudouris, 2006). Finally, Leleu et al. (1973) reported the presence of tetradymite and native Bi from the Plaka skarn deposit at Lavrion (Attika).

4. Au-Ag TELLURIDES AND Ag SULFO-TELLURIDES

The potassic alteration core of the Skouries porphyry deposit in NE Chalkidiki contains the tellurides hessite, sylvanite and calaverite in association with native gold at grain boundaries between chalcopyrite and bornite (Tarkian at al., 1991). Hessite and stützite in the Pagoni Rachi/W. Thrace, porphyry-Cu-Mo system, occur in contact with Bi-sulfosalts, bornite and galena (Fig. 2a, b) in late-stage veins (Voudouris and Arikas, 2003; Voudouris and Melfos, 2006, this study). In the Fakos porphyry Cu±Mo prospect, on Limnos island, electrum, hessite, petzite and an unnamed Ag-sulfotelluride, occur in late quartz-carbonate veins overprinting tourmaline-sericite veins, as well as quartz stockworks hosted within a Miocene monzonitic body (Voudouris and Alfieris, 2005; Voudouris 2006). Hessite, altaite and electrum were identified as inclusions in galena from the Thermes ore-field, which represents the southward extension of the Madan deposit (Bulgaria) and comprises both fault-controlled vein-type Pb-Zn and stratabound mineralization within marbles of the Rhodope metamorphic complex (Arvanitidis and Dimou, 1990). Au-Ag-tellurides occur throughout the Tertiary precious metal high-intermediate sulfidation epithermal assemblages in W. Thrace, Greece (Dimou et al., 1994; Voudouris and Arikas, 1994; Michael et al., 1995; Arikas and Voudouris, 1998; Border et al., 1999; Mc Alister et al., 1999; Skarpelis et al., 1999; Lescuyer et al., 2003; Melfos et al., 2003; Voudouris et al., 2006; Voudouris, 2006). Hessite, petzite, sylvanite and stützite in association with altaite, coloradoite, native tellurium and goldfieldite, accompany Bi-tellurides and Bi-sulfosalts in the St Demetrios, Pefka, Mavrokoryfi and Kassiteres prospects/deposits. Calaverite was reported, but not quantitatively documented, from the Viper deposit/Sappes area (Shawh and Constantinides, 2001). New paragenetic relationships from the Perama Hill high-intermediate sulfidation epithermal system (Voudouris et al., 2007, this volume) suggest the abundance of hessite, petzite, stützite, sylvanite, krennerite and altaite (Fig. 2d) with late-stage barite-tennantite-galena veins crosscutting earlier high sulfidation enargite-pyrite ores. In the orogenic Au-Ag bearing mineralization in the Paliopyrgos area, Vavelidis and Tarkian (1995) identified hessite intergrown with gold and aikinite as small inclusions in chalcopyrite. The mineralization at Koronouda area contains galena-hessite-pilsenite intergrowths and hessite, petzite, sylvanite and native gold included in chalcopyrite (Mposkos, 1983; Vavelidis, 1994, Vavelidis et al., 1996). However, during the current study only hessite, showing curvilinear boundaries to galena, was detected (Fig. 2k, l). Similarly, in the Paliomylos/Kilkis area, hessite is reported in association with bismuthinite derivatives and with galena in chalcopyrite (Melfos et al., 2001). Isolated grains of hessite included in chalcopyrite occur in the Bi-Te-Ag-bearing Cu mineralization at Panagia (Thasos island) (Vavelidis et al., 1995). Chatzikirkou (2003) and Chatzikirkou and Michailidis (2004), reported on the presence of hessite intergrown with tetradymite and included in chalcopyrite from the Eptadendron-Rachi areas in eastern Rhodope massif.

In the submarine epithermal mineralization of Profitis Ilias (Milos island) at the active south Aegean volcanic arc, Alfieris and Voudouris (2006) and Alfieris (2006) documented the presence of a hessite-petzite-altaite association with native gold/electrum within veinlets crosscutting the Upper Pliocene Profitis Ilias rhyodacitic cryptodome. An extremely rich suite of tellurides, was reported by Tombros (2001) and

Spry et al. (2006), from the orogenic Au-Ag-Te mineralization at Panormos Bay (Tinos island) The marble-hosted Panormos Bay vein system, is characterized by hessite, sylvanite, altaite, native tellurium, stützite, Cu-bearing cervelleite, melonite, rickardite, vulcanite, weissite, native tellurium, rickardite, kostovite, krennerite, petzite, and calaverite. A similar style of Te-rich mineralization is present further to the north in orogenic quartz veins hosted in metamorphic rocks of the Blueschist Unit of the Kallianou area (S. Evia Island). Alexouli-Livaditi (1978) was the first person to describe the presence of sylvanite as small inclusions in pyrite from that area, and new investigations (Voudouris and Spry in prep.) indicate the presence of silver sulfotellurides in association with hessite. These are minerals of the cervelleite-group as well as unnamed minerals with composition approximating the chemical formula Ag_2CuTeS and $(Ag,Cu)_2TeS$. The sulfotellurides are enclosed in galena and occur in proximity to electrum.

5. DISCUSSION AND CONCLUSIONS

Bismuth sulfosalts and tellurides are abundant in several types ore deposits in Greece. They can be considered as pathfinder minerals for gold since they are intimately associated with gold bearing ores. The mineralization studied can be subdivided into three groups based on their association with gold: (a) deposits which lack tellurides but include Bi-sulfosalts and native gold. In this category, belong the Lavrion (manto-type), Maronia (porphyry-Cu-Mo), Kimmeria (intrusion-hosted Cu-Mo), Stypsi/Lesvos (porphyry-Cu-Mo) and some orogenic mineralization in northern Greece. (b) The second category includes mineralization where Bi-tellurides of the reduced-type (joseite-A, joseite-B, pilsenite, where Bi:X>1, X=Te, S, Se) accompany Bi-sulfosalts, native bismuth and native gold. Examples are the VMS-orogenic mineralization in Serbo-Macedonian Massif (Koronouda and Laodikino at Kilkis, Paliomilos and Chalkoma at Stanos/Chalkidiki) whereas at the Agerdeen prospect in the Rhodope massif and at the orogenic Chalkero/Palea Kavala mineralization, the tetradymite (with Bi:X<1) is present. The calcalkaline-alkaline-hosted porphyry and epithermal deposits/prospects in the Chalkidiki and W. Thrace areas contain Bi-tellurides with Bi:X<1 (tetradymite, tellurobismuthite) in association with Bi-sulfosalts and Au-Ag-tellurides, consistent with oxidizing conditions during ore formation (see Cook and Ciobanu 2002, 2004).
(c) The third category includes deposits/prospects where Au-Ag-tellurides are abundant but Bi-tellurides and Bi-sulfosalts are absent. Such deposits include the orogenic Panormos, Kallianou and the epithermal Profitis Ilias mineralization in southern Greece. However a Bi signature in Kallianou is recorded by the elevated Bi-content of electrum (up to 0.5 wt%).
The hypothesis of gold that is scavenged by a Bi-melt may be important in mineralization where formation conditions exceeded those necessary for the generation of such melts (Ciobanu et al. 2005, 2006a,b). This may the case for mineralization at Kamariza (Lavrion district), the Pagoni Rachi prospect, and the VMS-orogenic mineralization in northern Greece. The last occurrence is considered to have formed during metamorphism and/or to be post-metamorphic, which are conditions favourable for the formation of metallic melts (Tomkins et al., 2007). According to Kalogeropoulos et al. (1991) at Paliomilos and Chalkoma/Chalkidiki, the introduction of Au-Bi-Te-Cu-bearing fluids was contemporaneous with retrograde greenschist metamorphism. Based on arsenopyrite and sphalerite geothermometry-geobarometry and fluid inclusion data, Kalogeropoulos et al. (1991), Thymiatis (1995) and Vavelidis et al. (1995, 1997) concluded that the mineralization formed at 460-510 ºC/5.6 ± 0.8kb (Paliomilos and Chalkoma/Stanos), at 500 to 600 ºC/5kb (Koronouda), at 360-450 ºC/4.5-5.7kb (Laodikino). In all of the above occurrences, early VMS sulfide mineralization was affected by deformation and retrograde greenschist metamorphism. A multiple-stage model for the ore occurrences of the Eptadendron-Rachi areas in the Rhodope massif has been proposed by Chatzikirkou (2003) and Chatzikirkou and Michailidis (2004). For the Kallianou mineralization, Theophilopoulos and Vakondios (1978) proposed a remobilization of metals from

earlier volcano-sedimentary ores during retrograde greenschist facies metamorphism. The abundance of sulfotellurides in the Kallianou veins may suggest a deficiency in fTe_2 necessary for the deposition of most common Au-Ag-tellurides. The Panormos system started in much the same way as Kallianou but evolved through time towards more Te and Au rich minerals.

There is higher proportion of silver tellurides relative to gold-bearing tellurides in Greece. Exceptions represent the porphyry-epithermal Viper and Perama Hill deposits in Thrace and the Panormos system in Attico-Cycladic belt. The recent discovery of tellurides in the deeper levels of Profitis Ilias deposit may suggest that arc related rhyodacitic magmas in south Aegean area are enriched in tellurium from their source regions. In general, Greece is highly enriched in tellurides, which contrasts to their paucity (but not complete absence) in neighbouring Turkey and southern Bulgaria where similar Tertiary magma generating and metallogenetic processes occurred. However tellurides and Bi-sulfosalts are abundant in the Late Cretaceous Srednogorie-Pontides belt, which host significant porphyry and VMS-epithermal ores (Bogdanov et al., 2004; Kouzmanov et al., 2005; Bogdanov and Filipov, 2006). Telluride mineralization in Greece underwent several stages of remobilization from earlier pre-Tertiary to Tertiary events during successive accretion episodes in active continental margins and arc terranes from the Carboniferous to the Pleistocene.

REFERENCES

Alexouli-Livaditi, K.A., 1978, The mixed-sulfide ores at Kallianou area, south Evia. Unpubl. PhD thesis Techn. Univ. Athens, 122pp.

Alfieris, D., 2006, Geological, geochemical and mineralogical studies of shallow submarine epithermal mineralization in an emergent volvanic edifice, at western Milos island, Greece. Unpubl. PhD thesis, Univ. Hamburg, 211pp.

Alfieris, D. and Voudouris, P., 2006, First occurrence of tellurides in the epithermal Profitis Ilias deposit, Milos Island, Greece, 12th IAGOD, Moskow, CD-ROM.

Arikas, K. and Voudouris, P., 1998, Hydrothermal alterations and mineralizations of magmatic rocks in the southern Rhodope Massiv. Acta Vulcanol. 10: p.353-365.

Arvanitidis, N.D. and Constantinides, D., 1989, Base and precious metal sulfide mineralization of the Greek Rhodope Massif. Geol. Rhodopica, 1: 298-305.

Arvanitidis, N., Constantinides, D.C., Ashworth, K.L., Baker, J.H., Hellingwerf, R.H. and Epitropou, N., 1996, Regional and local metallogenetic concepts, in the Servo-Macedonian and Rhodope Massifs, northern Greece, In: Pasava et al. (eds), Mineral deposits, Balkema, Rotterdam, 27-30.

Arvanitidis, N. and Dimou, E., 1990, Electrum and silver telluride occurrences in the polymetallic sulfide mineralization of the Thermes orefield, N. Greece. Geol. Rhodop., 2: 309-325.

Arvanitidis, N.D., 2003, Gold deposits in Greece: genetic types and economic perspectives. In: Eliopoulos D.G. et al. (eds), Mineral exploration and sustainable development. Millpress, Rotterdam, 941-943.

Ashworth KL, Billet MF, Constantinides D, Demetriades A, Katirtzoglou C, Michael C (1988) Base metal mineralization in the Evros region, N.E. Greece. In: Friedrich GH, Herzig PM (eds) Base metal sulfide deposits. Springer, Berlin, pp 169-181

Bitsios, D., 1989, Types of primary gold deposits in Greece: metallogenetic data, metallogenetic map, and target areas. Unpubl. Report, I.G.M.E, 39-65 (in Greek).

Bogdanov, K., Ciobanu, C.L. and Cook, N.J., 2004, Porphyry-epithermal Bi-Te-Se assemblages as a guide for gold ore enrichment. In: Cook N.J. and Ciobanu C.L. (eds), Au-Ag-telluride deposits of the Golden Quadrilateral, Apuseni Mts., Romania, IAGOD Guidebook Ser. 12: 211-214.

Bogdanov, K. and Filipov A., 2006, Bi-Te mineral assemblages of gold in porphyry-epithermal systems: examples from the western segment of the Tethian-Eurasian copper belt. In: Cook, N.J., Özgenc, I., and Oyman. T. IGCP-486 field workshop, Izmir 24-29 September 2006, Proc. 15-22.

Border, A., Constantinides, D. and Michael, C., 1999, Discovery and evaluation of the Sappes gold deposit, Northeastern Greece. In: Currie D. and Nielsen K. (eds) New generation gold mines '99, Case histories of discovery. Austral. Min. Found. Conf. Proc. 29-38.

Chatzikirkou, A., 2003, Study of the sulfide mineralization at Eptadendron and Rachi, Eastern Rhodope, Greece. Unpubl. PhD thesis, University of Thessaloniki, 233p.

Chatzikirkou, A. and Michailidis K., 2004, The Eptadendron and Rachi sulfide mineralization, Eastern Rhodope, Greece. Bull. Geol. Soc. Greece. 36: 397-405 (in Greek).

Ciobanu, C.L., Cook, N.J. and Pring, A., 2005, Bismuth tellurides as gold scavengers. In: Mao J.W. and Bierlein F.P. (eds) Mineral deposit research: Meeting the global challenge. Springer, Berlin, 1383-1386.

Ciobanu, C.L., Cook, N.J., Damian, G. and Damian, F., 2006a, Gold scavenged by bismuth melts: An example from Alpine shear-remobilisates in the Highiş Massif, Romania. Mineral. Petrol. 87: 351-384.

Ciobanu, C.L., Cook, N.J., Damian, G. and Damian, F., 2006b, A review of recent data on occurrences of Bi-sulphosalts and –tellurides in Romania and genetic implications for gold deposition. In: Cook, N.G., Özgenc I. and Oyman, T. IGCP-486 field workshop, Izmir 24-29 September 2006, Proc. 30-41.

Cook, N.J. and Ciobanu, C.L., 2002, Tellurides: more than mineralogical curiosities, but also markers of fS_2-fO_2 evolution in zoned hydrothermal systems. IMA, 18th General Meeting, Programm with Abstracts, Edinburg, Scotland, 283.

Cook, N.J. and Ciobanu, C.L., 2004, Bismuth tellurides and sulfosalts from the Larga hydrothermal system, Metaliferi Mts, Romania: Paragenesis and genetic significance Mineral. Mag. 68: 301-321.

Cook, N.J. and Ciobanu, C.L., 2005, Tellurides in Au deposits: Implications for modeling. In: Mao J.W. and Bierlein F.P. (eds) Mineral deposit research: Meeting the global challenge. Springer, Berlin, 1387-1390.

Dimou, E. 1993, A correlative mineralogical study of Achla Tarla and St Philippos mineralization, Kirki are (NE Greece). Bull Geol Soc Greece, 28, 37-54.

Dimou, E., Michael, K. and Serment, R., 1994, Mineralogical composition of the epithermal polymetallic mineralization at Pefka area, Rhodope district. Bull. Geol. Soc. Greece 30: p. 533-550 (in Greek)

Economou-Eliopoulos, M. and Eliopoulos D.G., 2005, Mineralogical and geochemical characteristics of the Skouries porphyry Cu-Au-Pd-Pt deposit (Greece): Evidence for the precious metal. In: Mao, J. and Bierlein F.P. (eds) Mineral deposit research: Meeting the global challenge. Springer, Berlin, 395-398.

Eliopoulos, D.G. and Kalogeropoulos, S., 1986, Preliminary priority rating of the known primary gold occurrences in Greece and exploration methodology. Miner. Dep. Research, I.G.M.E. publ. 18: 1-31.

Eliopoulos, D.G. and Economou-Eliopoulos, M., 1991, Platinum-group element and gold contents in the Skouries porphyry copper deposit, Chalkidiki peninsula, Northern Greece. Econ. Geol. 86: 740-749.

Eliopoulos, D.G. and Chryssoulis, S.L., 2005, Gold deportation in the Asympotrypes carbonate-hosted mesothermal Au deposit, Greece: Mineralogical sitting, distribution and conditions of deposition. In: Mao, J. and Bierlein F.P. (eds) Mineral deposit research: Meeting the global challenge. Springer, Berlin, 931-934.

Gilg, H.A., 1993, Geochronology (K-Ar), fluid inclusion, and stable isotope (C,H,O) studies of skarn, porphyry copper, and carbonate-hosted Pb-Zn-(Ag,Au) replacement deposits in the Kassandra mining district (Eastern Chalkidiki, Greece). Unpub. PhD thesis, ETH Zurich, 152 p.

Groves, D.I., Goldfarb, R.J.,Gebre-Mariam, M., Hagemann, S.G. and Robert, F., 1998, Orogenic gold deposits: A proposed classification in the context of their crystal distribution and relationship to other gold deposit types. Ore Geol. Rev. 13: 7-27.

Hellingwerf, R., Arvanitidis, N. and Constantinides, D., 1994, Ores, exploration tools and new target areas in the eastern Chalkidiki Peninsula, Northern Greece. Bull. Geol. Soc. Greece, 30: 457-467.

Kalogeropoulos, S., Veranis, N. and Kougoulis, C., 1986, Composition of arsenopyrite as temperature indicator in sulfide mineralizations from Laodikino, Kilkis province and asimitrypes Pageo, Kavala Province, N. Greece. Geol. Geoph. Res., I.G.M.E., 161-167.

Kalogeropoulos, S., Constantinidou, H. and Simos, E., 1991, Mineralogy and mineral chemistry of sulfide mineralization with gold in the Stanos area, Vertiskos Formation, Chalkidiki. Bull. Geol. Soc. Greece, 25: 225-243 (in Greek).

Katirtzoglou, K., Chatzikirkou, A. and Dimitroula, M., 1994, Mineralizations of the Menikion-Vrontou-Angistron mountain chain (Macedonia, N. Greece). Bull. Geol. Soc. Greece, 30: 497-505 (in Greek).

Kouzmanov, K., Bogdanov, K., Ramboz, C., 2005, Te- and Bi-bearing minerals in the Elshitsa and Radka epithermal deposits, Central Srednogorie, Bulgaria: Mineralogy and genetical features. In: Cook N. and Bonev I. (eds), Au-Ag-Te-Se deposits, Geochem. Mineral. Petrol. 43: 108-112.

Leleu, M., Morikis, A. and Picot, P., 1973, Sur des mineralisations de type skarn au Laurium (Grece). Miner. Deposita, 8: 259-263.

Lescuyer J.L., Bailly, L., Cassard, D., Lips, A.L.W., Piantone, P. and McAlister, M., 2003, Sediment-hosted gold in south-eastern Europe: the epithermal deposit of Perama, Thrace, Greece. In: Eliopoulos D.G. et al. (eds), Mineral exploration and sustainable development. Millpress, Rotterdam, 499-502.

Marchev, P., Kaiser-Rohrmeier, M., Heinrich, Ch., Ovtcharova, M., von Quadt, A. and Raicheva, R., 2005, Hydrothermal ore deposits related to post-orogenic extentional magmatism and core complex formation: The Rhodope Massif of Bulgaria and Greece. Ore Geol. Rev. 27: 53-89.

McAlister, M., Hammond, J.M., Normand, D. and Kampasakalis, M., 1999, Discovery case history for the Perama Hill gold deposit, Greece. In: Currie D. and Nielsen K. (eds), New generation gold mines '99, Case Histories of Discovery. Austral. Min. Found. Conf. Proc., Perth, 39-49.

Melfos, V., Vavelidis, M. and Christofides, G., 1996, Cu-Pb-(Sb+As) sulphosalts from the porphyry type Cu-Mo(±Au) mineralization in Maronia area, Thrace county, Greece. In: Knežević, V. and Kristić, B. (eds). Terranes of Servia, 305-310.

Melfos, V., Vavelidis, M. and Arikas K., 2001, A new occurrence of argentopentlandite and gold from the Au-Ag-rich copper mineralisation in the Paliomylos area, Serbomacedonian massif, Central Macedonia, Greece. Bull Geol Soc Greece 34: 1065-1072.

Melfos, V., Vavelidis, M., Christofides, G. and Seidel, E., 2002, Origin and evolution of the Tertiary Maronia porphyry copper-molybdenum deposit, Thrace, Greece. Miner. Deposita 37: 648-668

Melfos, V., Vavelidis, M. and Bogdanov, K., 2003, Occurrence, mineralogy and chemical composition of primary gold from Tertiary ore mineralisations in the Rhodope massif (Greece-Bulgaria). In: Eliopoulos D.G. et al. (eds), Mineral exploration and sustainable development. Millpress, Rotterdam, p.1201-1204.

Michael, C., 2004, Epithermal systems and gold mineralization in western Thrace (North Greece). Bull .Geol. Soc. Greece, 36: 416-423.

Michael, C., Perdikatsis, V., Dimou, E. and Marantos, I., 1995, Hydrotherma1 a1teration and ore deposition in epitherma1 precious metal deposit of Agios Demetrios, Konos area, Northern Greece. Geo1. Soc. Greece, Special Pub1. 4: p.778-782.

Mposkos, E., 1983, A mineralogical study of the Au-Ag-Bi-Te-Cu-Co-Ni-As-S ore mineralization in Macedonia, Greece. Chem. Erde, 281-296.

Mposkos, E. and Krohe, A., 2001, Structural evolution and exhumation history of the Rhodope UHP-HP metamorphic province (Northern Greece). Bull. Geol. Soc. Greece, 35: 75-82.

Nebel, M.L., Hutchinson R.W. and Zartman, R.E. 1991, Metamorphism and polygenesis of the Madem Lakkos polymetallic sulfide deposit, Chalkidiki, Greece. Econ. Geol. 86: 81-105.

Nesbitt, R.W., Billet, M.F., Ashworth, K.L., Deniel, C., Constantinides, D., Demetriades, A., Katirtzoglou, C., Michael, C., Mposkos, E., Zachos, S. and Sanderson, D., 1988, The geological setting of base metal mineralization in the Rhodope region, Northern Greece, In: Boissonnas J. and Omenetto P. (eds), Mineral deposits within the European Community, 499-514.

Neubauer, F., 2005, Structural control of mineralization in metamorphic core complexes. In: Mao J, Bierlein FP (eds): Mineral Deposit Research: Meeting the Global Challenge, Springer, Berlin-Heidelberg, pp 561-564

Okrusch, M. and Bröcker, M., 1990, Eclogites associated with high-grade blueschists in the Cyclades archipelago, Greece: a review. Eur. Jour. Miner., 2: 451-478.

Reischmann, T. and Kostopoulos, D., 2007, Terrane accretion in the internal Hellenides. Geoph. Res. Abstrs. 9, 05337.

Shaw, A.J. and Constantinides, D.C., 2001, The Sappes gold project. Bull. Geol. Soc. Greece, 34: 1073-1080

Skarpelis, N., 2002, Geodynamics and evolution of the Miocene mineralization in the Cycladic-Pelagonian belt, Hellenides. Bull. Geol. Soc. Greece, 34: 2191-2206.

Skarpelis, N., Voudouris, P. and Arikas, K., 1999, Exploration for epithermal gold in SW Thrace, Greece: New target areas. In: Stanley C.J. et al. (eds), Mineral deposits: Processes to processing, Balkema, Rotterdam, p.589-592.

Spry, P.G, Tombros, S.F., Seymour, K.St. and Zouzias, D.P., 2006, Geology, mineralogy and geochemistry of granite-hosted gold telluride mineralization at Panormos Bay, Tinos island, Greece. Geol. Soc. Amer. Abstr. Prog. 38: 55.

Tarkian, M., Eliopoulos, D.G. and Economou-Eliopoulos, M., 1991, Mineralogy of precious metals in the Skouries porphyry copper deposit, Northern Greece. N. Jb. Miner. Mh. 12: 529-537.

Theophilopoulos, D. and Vakondios, I., 1982, Geological and metallogenetic studies at Kallianou area, SE. Evia, Miner. Wealth, 19: 27-50 (in Greek).

Thymiatis, G.E., 1995, Metallogenesis of Laodikino-Lipsidrio area, Kilkis/Mecedonia, Northern Greece.

Unpubl. PhD thesis, University of Thessaloniki, 240pp.

Tombros, S., 2001, The Au-Ag-Te polymetallic mineralization of Tinos Island, Cyclades, Aegean. Unpubl. PhD thesis, Univ. Patras, 450p.

Tombros, S., Seymour, K.St. and Spry, P.G., 2004, Description and conditions of formation of new unnamed Ag-Cu and Ag-Cu-Au sulfotellurides in epithermal polymetallic Ag-Au-Te mineralization, Tinos Island, Hellas. N. Jb. Miner. Abh., 179: 295-310.

Tomkins A.G., Pattison, D.R.M. and Frost, B.R., 2007, On the initiation of metamorphic sulfide anatexis, J. Petrol. 48: 511-535.

Vavelidis M., 1994, Au-Ag-bearing mineralizations in the Servomacedonian massif, Northern Greece. Ber. Deutch. Mineral. Gesell., Beih. 1, 292.

Vavelidis, M., 1997, Au-bearing quartz veins and placer gold on Sifnos Island, Aegean Sea, Greece. In: Papunen H (ed), Mineral Deposits: Research and Exploration Where do They Meet? 335-338.

Vavelidis M. and Tarkian, M., 1995, Mineralogy of the gold-silver-bearing copper mineralized zones in the Paliopyrgos (Nea Madytos-Stanos) area, Northern Greece. N. Jb. Miner. Mh., 3: 133-143.

Vavelidis, M., Melfos, V., Sklavounos, S., Bogdanov, K. and Driesner, Th., 1995, Bi-Te-Ag-bearing Cu mineralization in the Panagia area, Thasos island (Northern Greece). In: Pašava J. et al. (eds), Mineral deposits. Balkema, Rotterdam, 393-396.

Vavelidis, M., Kilias, A., Melfos, V. and Schmidt-Mumm, A., 1996, New investigations in the Au-Ag-bearing Cu mineralization and its structural control in the Koronouda area, central Macedonia, Northern Greece. In: Knežević, V. and Krstić, B. (eds). Terranes of Serbia, 317-322.

Vavelidis, M., Melfos, V. and Eleftheriadis, G., 1997, Minerlaogy and microthermometric investigations in the Au-bearing sulphide mineralization of Palea Kavala (Macedonia, Greece). In: Papunen H. (ed). Mineral deposits: Research and exploration, where do they meet? Balkema, Rotterdam, 343-346.

Voudouris, P., 2006, A comparative mineralogical study of Te-rich magmatic-hydrothermal systems in northeastern Greece. Mineral. Petrol. 87: 241-275.

Voudouris, P. and Arikas, K., 1994, Epithermal Au-Ag mineralizations at Kassiteres-Sappes, NE-Greece: Mineralogical, geological and microthermometric studies. Bull. Geol. Soc. Greece 30: 427-443 (in German).

Voudouris, P. and Arikas, K., 2003, The Pagoni Rachi and Kassiteres porphyry Cu-(±Mo) occurences on Thrace: Ore mineralogy of late-stage veins. In: Eliopoulos D.G. et al. (eds), Mineral exploration and sustainable development. Millpress, Rotterdam, p.411-414.

Voudouris, P. and Economou-Eliopoulos, M., 2003, Mineralogy and chemistry of Cu-rich ores from the Kamariza carbonate-hosted deposit (Lavrion), Greece. In: Eliopoulos D. et al. (eds). Mineral Exploration and Sustainable Development, Millpress, Rotterdam, 499-502.

Voudouris, P. and Alfieris, D., 2005, New porphyry-Cu±Mo occurrences in northeastern Aegean/Greece: Ore mineralogy and transition to epithermal environment. In: Mao, J. and Bierlein F.P. (eds) Mineral deposit research: Meeting the global challenge. Springer, Berlin, 473-476.

Voudouris, P. and Melfos, V., 2006, Bismuth sulfosalts and silver tellurides in the Pagoni Rachi porphyry-Cu-Mo prospect, western Thrace (NE Greece). In: N.G. Cook, I. Özgenc and T. Oyman. IGCP 486 field workshop, Izmir 24-29 September 2006, Proc. 159-166.

Voudouris, P., 2005, Gold and silver mineralogy of the Lavrion deposit Attika/Greece. In: Mao J.W. and Bierlein F.P. (eds) Mineral deposit research: Meeting the global challenge. Springer, Berlin, 1089-1092.

Voudouris, P., Tarkian, M. and Arikas, K., 2006, Mineralogy of telluride-bearing epithermal ores in Kassiteres-Sappes area, western Thrace, Greece. Mineral. Petrol. 87: p.31-52.

Walenta K. and Pantzartzis P., 1969, The molybdenite deposit of Kimmeria, Xanthi, northern Greece. Erzmetall, 22:272-278.

www.gtk.fi
info@gtk.fi

ISBN 978-952-217-002-6
ISSN 0781-643X